Assessment and Contributions to Local Hybrid Functionals

vorgelegt von

A Seshaditya

M.Sc.

aus Hyderabad, Indien

von der Fakultät II - Mathematik und Naturwissenschaften

der Technischen Universität Berlin

zur Erlangung des akademischen Grades

Doktor der Naturwissenschaften

- Dr. rer. nat. -

genehmigte Dissertation

Promotionsausschuss:

Vorsitzender: Prof. Dr. Andreas Grohmann

Gutachterin: Prof. Dr. Beate Paulus

Gutachter: Prof. Dr. Martin Kaupp

Tag der wissenschaftlichen Aussprache: 30. Mai 2018

Berlin 2018

Abstract

A Seshaditya,

Assessment and Contributions to Local Hybrid Functionals

The exchange-correlation energy functional (XC) is the most important ingredient of Kohn-Sham density-functional theory (KS-DFT). Unfortunately this quantity has to be approximated as the exact functional form is not known. But many mathematical studies on density functionals have demonstrated conditions to hold for the exact XC functional. The most important conditions are the stepwise-linearity of the energy (fractional charges), derivative discontinuity (DD) of XC potential, and spin-constancy condition (fractional spins). The development of XC functionals which satisfy most of these exact behaviours is highly desirable for the computation of a wide range of properties with good accuracy at feasible computational cost. Extensive studies carried out reveal that approximations developed so far do not satisfy the rigorous set of conditions mentioned above resulting in poor performance for properties such as enthalpies, band gaps, charge-transfer excitations, and Rydberg excitations etc.

Local hybrid functionals are a new class of XC approximations where the constant exact-exchange (EXX) admixture of global hybrid functionals is replaced by a position-dependent admixture in real space, governed by a local mixing function (LMF). A local hybrid functional is defined by the choice of local mixing function (LMF) as well as by the choice of density functional exchange-energy density and the correlation contribution. Those local hybrids developed so far-, have been tested for various atomic/molecular properties, and promising results have been obtained. Therefore, it is very important to carry out studies related to the exact conditions for currently available local hybrid functionals.

In this work, computations have been performed using different local hybrid functionals on atomic and molecular systems for testing the fractional charge- and fractional spin-behaviour. A strongly-correlated local hybrid functional has been constructed along the lines of Becke's strong correlation model (B13 + strgC) and evaluated for the strong-correlation test set. *s*-*d* Transfer energies of 3*d*-transition metal atoms have been computed using two different formalisms (namely Furche-Perdew and broken-symmetry approaches) for studying the performance of different local hybrids. These studies will aid in the refinement of the local hybrid functionals and should provide a basis for their further development.

Zussammenfassung

A Seshaditya,
Beurteilung und Beiträge zur lokalen Hybridfunktionalen

In der Dichtefunktionaltheorie (DFT) ist das Austausch-Korrelations ('exchange-correlation', XC) Energiefunktional von größter Bedeutung. Leider muss das XC-Funktional angenähert werden, da seine genaue Form nicht bekannt ist. In einer großen Anzahl mathematischer Arbeiten über Dichtefunktionale sind exakte Eigenschaften des XC-Funktionals ergründet worden. Zu den ziemlich strengen Eigenschaften gehören die stufenweise Linearität der Energie ('fraktionale Ladungen'), die Unstetigkeit der Ableitung des XC-Funktionals, und die Bedingung der 'Spin-Konstanz' ('fraktionale Spins'). Um eine breite Palette von Eigenschaften mit guter Genauigkeit und vertretbarem Aufwand zu berechnen, ist die Entwicklung von XC-Funktionalen, die die meisten dieser exakten Bedingungen erfüllen, höchst wünschenswert. Umfangreiche Studien zeigen, dass bisher entwickelte Näherungen nicht die genannten strengen Bedingungen erfüllen, was eine schlechte Beschreibung von Eigenschaften wie Enthalpien, Bandlücken, Charge-Transfer-Anregungen und Rydberg-Anregungen zur Folge hat.

Lokale Hybridfunktionale stellen eine neue Klasse von XC-Näherungen dar. Der Ansatz besteht hier darin, die Beimischung exakten Austauschs ('exact-exchange', EXX) im globalen Hybridfunktional durch eine von einer lokalen Mischfunktion (LMF) bestimmte ortsabhängige Beimischung zu ersetzen. Definiert wird ein lokales Hybridfunktional durch die LMF, die Wahl der Austausch-Energiedichte sowie der Korrelationsbeiträge zum Dichtefunktional. Die bisher entwickelten lokalen Hybride wurden für verschiedene atomare/molekulare Eigenschaften getestet, und erzielten vielversprechende Ergebnisse. Daher ist es sehr wichtig, bezüglich der derzeit verfügbaren lokalen Hybridfunktionale Untersuchungen zu den exakten Bedingungen durchzuführen.

Hier werden Berechnungen mit verschiedenen lokalen Hybridfunktionalen an atomaren und molekularen Systemen durchgeführt, um das Verhalten bezüglich der Frage fraktionaler Ladungen und fraktionaler Spins zu testen. Die Konstruktion eines stark korrelierten lokalen Hybridfunktionals nach dem Vorbild von Beckes Modell für starke Korrelation ('B13 + strgC') und Tests für fraktionales Spin-Verhalten werden ebenfalls durchgeführt. *s-d* Transferenergien von 3*d*-Übergangsmetallatomen werden unter Verwendung zweier verschiedenener Formalismen berechnet ('Furche-Perdew' und 'gebrochene Symmetrie'), um die Leistung der unterschiedlichen lokalen Hybride zu prüfen. Diese Untersuchungen werden die Verfeinerung von lokalen Hybridfunktionalen unterstützen und sollten auch eine Grundlage für deren weitere Entwicklung darstellen.

List of Abbreviations

AC Adiabatic connection

AO Atomic orbital

BH Barrier height

DFT Density functional theory

DFA Density functional approximation

XC Exchange-correlation

FDO Functional derivative with respect to the orbitals

GGA Generalized gradient approximation

HK Hohenberg-Kohn

LDA Local density approximation

LMF Local mixing function

LSDA Local spin-density approximation

KS Kohn-Sham

MAE Mean absolute error

MSE Mean signed error

MO Molecular orbital

OEP Optimised effective potential

RI Resolution of the identity

SCF Self-consistent field

DE Delocalisation error

TM Transition metal

DD Derivative discontinuity

HOMO Highest occupied molecular orbital

LUMO Lowest unoccupied molecular orbital

IP Ionisation potential

EA Electron affinity

SIE Self-interaction error

SIR/SIF Self-interaction reduction/free

FP Furche-Perdew

Contents

Chapter 1

Introduction

Kohn-Sham density functional theory (KS-DFT) has been widely used for electronic structure calculations of ground-state properties in atoms, molecules and solid state systems. The important ingredient of this methodology is the exchange-correlation (XC) functional, which not only accounts for the difference between the classical and quantum mechanical electron-electron interaction, but also includes the difference in kinetic energy between a fictitious non-interacting system and the real system [1–3]. Unfortunately this XC term has to be approximated as the exact functional form is not known. Early developments include the local density approximation (LDA) which is based on the density at that point in space, whereas generalized gradient approximations (GGA) [4] take into account the spatially varying density effects through the gradient of the density. The LDA approximation produces very good results for solid-state systems, but is not satisfactory for atoms and molecules: atomisation energies are very poor and band gaps are underestimated [5, 6]. GGA functionals show significant improvement over LDA for total energies, atomisation energies, and reaction barriers, but typically fail for ionisation potentials (IP) and electron affinities (EA) [4, 7]. Hybrid density functional methods combine the exchange-correlation contributions of a conventional LDA/GGA with some part of Hartree-Fock (HF) exchange [8]. Global hybrid functionals (which have a constant amount of HF exchange and the popular B3LYP [7] belongs to this class) have been very successful in lowering errors for heats of formation, barrier heights, and molecular structures mainly due to reduction in self-interaction error (SIE). But these functionals still exhibit problems for *s-d* transfer energies in transition-metal atoms, modelling radicals, charge-transfer complexes, Rydberg excitations, and van der Waals complexes [9–11]. This suggests that the global hybrid functionals may be at their limit in providing a flexible compromise between minimi-

sation of self-interaction errors and adequate simulation of non-dynamical correlation [9, 12]. Local hybrids are the next generation of hybrid functionals, where the constant exact-exchange (EXX) admixture is replaced by a position-dependent admixture in real space, governed by a local mixing function (LMF) [13]. A local hybrid functional is defined by the choice of local mixing function (LMF) as well as by the choice of density functional exchange-energy density and correlation contributions [14, 15]. They are conceptually/mathematically rigorous, highly flexible, and computationally efficient (with the recent semi-numerical implementation [16]).

Along-side the development of XC approximations, many mathematical studies on density functionals have demonstrated conditions to hold for the exact XC functional. The basic set of conditions are coordinate-scaling, spin-scaling, viral theorem, and uniform electron gas (UEG) limit [3, 9]. The next set of conditions which are quite rigorous are the stepwise linearity of the energy, derivative discontinuities, absence of self-interaction error, spin constancy (fractional spins), and non-uniform density scaling [5, 17–20]. Development of XC functionals which satisfy most of these exact conditions is highly desirable for the computation of a wide range of properties with good accuracy at a feasible computational cost. So far the XC approximations (Jacob's ladder to heaven of chemical accuracy [21]) developed such as LDA, GGA, meta-GGA, and hybrid functionals gave rather good results for thermochemistry, structures, and molecular properties. Extensive studies reveal that these approximations do not satisfy the rigorous set of conditions mentioned above, resulting in the poor performance for properties such as band gaps, charge-transfer excitations, and Rydberg excited states etc. Thus, it is very important to carry out similar kinds of studies related to the exact conditions on the so-far developed local hybrid functionals. Based upon on these studies, refinement of local hybrid functionals and improvement upon the results obtained for thermochemical, kinetic, and molecular properties can be carried out further.

The structure of the thesis is outlined as follows. Firstly in Chapter 2, a brief description of known exact conditions for density functionals, starting with the stepwise linearity of the total energy from an ensemble formulation, the derivative discontinuity (DD) and the band gap problem, the fractional occupation approach in DFT, self-interaction errors, and static correlation error (the spin-constancy condition) are discussed. Further, the concepts of local hybrid functionals, common local mixing functions (LMF), and range-separated correlation functionals are also introduced. The idea of strong correlation in DFT and Becke's B13

model [22] with strong-correlation correction are discussed. *s*-*d* Transfer energies of 3*d*-transition metals serve as a good benchmark for testing the performance of XC functionals. This becomes even more challenging when states with near-degeneracy are involved. Therefore, a detailed introduction to the formalisms (Furche-Perdew formalism [23] and broken-symmetry approaches from the Truhlar group [24]) used for the computation of *s*-*d* transfer energies is provided.

In Chapter 3, the self-consistent (SCF) implementation of the common *t*-LMF and a post-SCF implementation of Kümmel's *z*-LMF are discussed [25]. The first steps towards the construction of a strongly correlated local hybrid functional on the basis of Becke's correlation model with strong-correlation correction (B13 + strgC) [22, 26] are also presented in detail.

In Chapter 4, *s*-*d* transfer energies of the 3*d*-transition metal atoms have been computed using the formalisms discussed in Chapter 2. Detailed analyses of the results obtained are carried out for understanding the performance of local hybrid functionals.

In Chapter 5, an assessment of local hybrid functionals for the stepwise linearity of the total energy in the ground-state and low-energy excited states for atomic and molecular systems is performed. Studies related to the fundamental band gap problem and the ionisation potential (IP) theorem are also discussed in detail [27, 28].

Finally in Chapter 6, results obtained for a strong-correlation test-set using the strongly correlated local hybrid along with other functionals are presented. Preliminary results clearly show a poor performance of the strongly correlated local hybrid functional in comparison to B13 + strgC model. This is mainly attributed to the positive static correlation energy density in some regions of space resulting in a divergence of the ratio of static correlation energy to the total correlation energy. In this regard, a construction of strongly correlated local hybrid functional with calibrated exchange-energy densities (developed by Alexei Arbuznikov [29]) has been carried out and subsequent results obtained are discussed.

Chapter 2

Theoretical Background

Many problems in non-relativistic quantum chemistry rely on finding solutions to the time-independent Schrödinger equation [30]

$$\hat{H}\Psi = E\Psi, \tag{2.1}$$

where $\hat{H}$ is the Hamilton operator of the system and Ψ is wave function of the system. The electronic Hamilton operator for a system consisting of A nuclei and N electrons, in atomic units, takes the form (within the Born-Oppenheimer approximation [31]):

$$\hat{H}_{ee} = \hat{T} + \hat{V}_{ne} + \hat{V}_{ee}, \tag{2.2}$$

where $\hat{T}$ is the kinetic energy, $\hat{V}_{ne}$ is the nuclear-electron interaction, and $\hat{V}_{ee}$ is the electron-electron interaction. The kinetic energy is given by

$$\hat{T} = \sum_{i=1}^{N} \left(-\frac{1}{2}\nabla_i^2 \right), \tag{2.3}$$

where the index i sums over all N electrons of the system. The nuclear-electron attraction is expressed as

$$\hat{V}_{ne} = -\sum_{i=1,\alpha=1}^{N,A} \frac{Z_\alpha}{\mathbf{r}_{i\alpha}}, \tag{2.4}$$

and the electron-electron interaction is given by

$$\hat{V}_{ee} = \sum_{i=1<j}^{N,A} \frac{1}{\mathbf{r}_{ij}}. \tag{2.5}$$

The wave function Ψ is a complicated 3N-dimensional function of space coordinates. Solving for the exact solution of an N-electron system analytically and numerically is

impossible, except in the case of one-electron systems. To swim across this great ocean of impossibilities, various mean-field approximations have been developed. Two of these approximations, that have achieved tremendous success in quantum chemistry, are the Hartree-Fock (HF) method and Kohn-Sham density functional theory (KS-DFT).

2.1 Hartree-Fock method

In the Hartree-Fock method, the wave function is approximated with a single Slater determinant made up of one spin-orbital per electron. The anti-symmetry of the Slater determinant ensures that the Pauli principle is satisfied with respect to the exchange of electrons. The expression for Hartree-Fock energy is given by

$$E_{HF}[\{\phi_i\}] = T_S[\{\phi_i\}] + V_{ne}[\{\phi_i\}] + J[\{\phi_i\}] + E_X[\{\phi_i\}], \tag{2.6}$$

where the exchange-energy interaction is

$$E_X^{HF}[\{\phi_i\}] = -\frac{1}{2}\sum_{ij}\int\int \frac{\phi_i(\mathbf{r}_1)\phi_j(\mathbf{r}_1)\phi_i^*(\mathbf{r}_2)\phi_j^*(\mathbf{r}_2)}{\mathbf{r}_{12}}\mathrm{d}\mathbf{r}_1\mathrm{d}\mathbf{r}_2. \tag{2.7}$$

But the largest drawback of the HF method is the complete neglect of electron correlation. The term correlation energy, coined by Löwdin [32] is expressed as

$$E_C = E_{exact} - E_{HF}. \tag{2.8}$$

To overcome this drawback, many correlated methods beyond HF such as perturbation theory (MP2, MP4), coupled cluster theory (CC), configuration interaction (CI), and many other multireference methods have been developed [33–37]. These methods are rigorous and can be improved systematically, but are computationally extensive.

2.2 Kohn-Sham density functional theory

The fundamental formulation of DFT lies in the Hohenberg-Kohn theorem [2], which demonstrates that the ground-state energy of a many-electron system is the functional of the its density ρ. However the energy functional has to be approximated as the explicit form is not known. Kohn and Sham [38] came up with an idea of a fictitious non-interacting reference system of N-electrons (the KS system), with the same density as the interacting one. The total energy functional is now expressed as

$$E_{KS} = T_S[\phi_i^{KS}] + V_{ne}[\rho] + J[\rho] + E_{XC}[\rho], \tag{2.9}$$

where the terms are the non-interacting kinetic energy (with KS-orbitals), nuclear-electron attraction, Coulomb electron-electron repulsion, and finally the exchange-correlation (XC) energy term. Among all these quantities, only the exchange-correlation energy has to be approximated as no exact functional forms are available. However, many physical and mathematical constraints have been formulated for the development of these approximations. These constraints are known as the exact conditions for density functionals and will be discussed further in detail [1, 3, 39, 40].

2.3 Exchange-correlation (XC) approximations

The exchange-correlation energy (E_{XC}) is separated into two entities, an exchange term E_X and a correlation term E_C,

$$E_{XC}[\rho] = E_X[\rho] + E_C[\rho]. \tag{2.10}$$

The exchange term invokes the interactions between the electrons of same spin and is usually an approximation to the HF exchange energy. The correlation energy (E_C) is the remaining interaction which contains both kinetic and potential-energy contributions expressed as,

$$E_C = (T - T_S) + (V_{ee} - J - E_X). \tag{2.11}$$

The main success/failure of KS-DFT depends squarely on the quality of the XC approximations and the error cancellation between the approximate exchange and correlation contributions.

2.3.1 From LDA to GGA

The local-density approximation (LDA) is the simplest approach to represent the exchange-correlation functional. The only input information employed within the LDA is the electron density distribution, $\rho(\mathbf{r})$. The general form is expressed as

$$E_{XC}^{LDA}[\rho] = \int \varepsilon_{XC}(\mathbf{r})\rho(\mathbf{r})\mathrm{d}\mathbf{r}. \tag{2.12}$$

An analytical expression for the uniform electron gas (UEG) exchange energy functional was derived significantly earlier by Dirac [41]:

$$E_X^{LDP}[\rho] = -\frac{3}{4}\left(\frac{3}{\pi}\right)^{\frac{1}{3}} \int \rho^{\frac{4}{3}}(\mathbf{r})\mathrm{d}\mathbf{r}. \tag{2.13}$$

The correlation energy cannot be expressed analytically, therefore Monte-Carlo simulations of the UEG correlation energy have been performed [42] that allow one to construct an analytical ansatz. The widely used ones are the parameterizations of the LDA approach provided by Vosko, Wilk, and Nusair (VWN) [43] and Perdew-Wang (PW92) [44]. The spin-polarized extension of LDA, the local spin density approximation (LSDA) is applied for the description of open-shell systems. The LDA/LSDA approximations provide reasonable results for systems with slowly varying densities and typically LDA/LSDA underestimates E_X but overestimates E_C, resulting in unexpectedly reasonable E_{XC} values. Usually the LDA approximation overestimates bond strengths, resulting in too short bond lengths. The generalized gradient approximation (GGA) construction is carried out by expanding exchange and correlation energies in terms of the density and its gradient followed by an appropriate real-space cut-off procedure. The GGA exchange-correlation energy is expressed as

$$E_{XC}^{GGA}[\rho] = \int f(\rho_\alpha, \rho_\beta, \nabla\rho_\alpha, \nabla\rho_\beta)\mathrm{d}\mathbf{r}. \tag{2.14}$$

The exchange part of a GGA is given by

$$E_{X,\sigma}^{GGA}[\rho] = \int \varepsilon_{X,\sigma}(\mathbf{r})F(s_\sigma)\rho_\sigma(\mathbf{r})\mathrm{d}\mathbf{r} \tag{2.15}$$

where $F(s_\sigma)$ is a function of the reduced density gradient s_σ,

$$s_\sigma = \frac{|\nabla\rho_\sigma(r)|}{2(3\pi^2)^{\frac{1}{3}}\rho_\sigma^{\frac{4}{3}}(r)} \tag{2.16}$$

Popular GGA functionals are the Becke exchange (B88) [45] and PBE (Perdew, Burke, and Ernzerhof) exchange and correlation functionals [4]. In general, GGA methods represent a significant improvement over the LDA for thermochemistry, activation barriers, total energies, electric and magnetic properties. But in case of solid-state computations, GGA functionals do not yield significantly better results than LDA, nor in the calculation of ionisation potentials and electron affinities. They also suffer from self-interaction errors (SIE) [46, 47] which limits their applicability.

2.3.2 Global hybrid functionals

These methods combine the exchange-correlation of a conventional GGA/LDA method with some constant amount of exact-exchange admixture [7, 8]. The global hybrid exchange-correlation energy is given by

$$E_{XC}^{Hybrid} = a_0 E_X^{exx} + (1 - a_0) E_X^{DFT} + E_C^{DFT}, \tag{2.17}$$

where E_X^{exx} is the exact-exchange energy in the Kohn-Sham formalism obtained by inserting KS orbitals into the HF exchange energy expression. The most popular global hybrid is the B3LYP functional [7] which contains 20 admixture of exact-exchange. Global hybrid functionals have been very successful in predicting thermochemistry, molecular structures, and response properties. However, global hybrids are not flexible enough to describe different aspects of electronic structure simultaneously (for example in case of energy barriers high amounts of exact-exchange admixture are needed). Incomplete elimination of self-interaction errors leads to errors in describing polarizabilities of long chains, charge-transfer complexes, and Rydberg excitations [47]. Therefore advanced developments have been proposed which offer flexibility by range-separation of the exchange interaction (range-separated hybrids) as well as introducing a position-dependent exact-exchange admixture (local hybrid functionals).

2.3.3 Range-separated hybrid functionals

In this scheme, the electron-electron interaction is partioned into short-range (SR) and long-range (LR) components:

$$\frac{1}{r_{12}} = \frac{erf(\omega r_{12})}{r_{12}} + \frac{erfc(\omega r_{12})}{r_{12}}, \tag{2.18}$$

where ω is the screening or range-separation parameter whereas the erf and erfc are the error function and its complimentary respectively [48, 49]. Based on this idea, the exchange energies are split as:

$$E_X^{DFT} = E_X^{SR,DFT} + E_X^{LR,DFT}, \tag{2.19}$$

$$E_X^{exx} = E_X^{SR,exx} + E_X^{LR,exx}. \tag{2.20}$$

Two different classes of range-separated hybrids have been developed: long-range corrected hybrids and screened hybrids. The long-range corrected hybrids have exact-exchange in long range- and short-range DFT exchange [50]. The long-range corrected PBE (LC-ωPBE) functional is given by

$$E_{XC}^{LC-\omega PBE}(\omega) = E_X^{exx,LR}(\omega) + E_X^{PBE,SR}(\omega) + E_C^{PBE}, \tag{2.21}$$

where ω = 0.40 $bohr^{-1}$, is the screening or range-separation parameter. They perform substanially well for long-range charge transfer, Rydberg excitations, and properties related to the asymptotic nature of the XC potential [51] .

The other class, screened hybrid functionals retain only the short-range part of exact-exchange which allows to reduce the computational cost, especially for periodic systems. The screened hybrid functional of Heyd, Scuseria, and Ernzerhof (HSE) [52] has the following form:

$$E_{XC}^{HSE}(\omega) = a_{exx}E_X^{exx,SR}(\omega) + (1 - a_{exx})E_X^{PBE,SR}(\omega) + E_X^{PBE,LR}(\omega) + E_C^{PBE}. \quad (2.22)$$

where a is the mixing parameter and ω, the range-separation parameter. The value of the screening parameter ω, determined by fitting to experimental band gap values in order to achieve the best possible accuracy for the problem of interest. Therefore, the HSE hybrid functional predicts much more accurate lattice constants and band gaps than any standard semilocal functionals [53, 54].

2.4 Local hybrid functionals

Local hybrids are the next level of hybrid functional developments in DFT [13]. Here the global exact-exchange (EXX) admixture is replaced by a position-dependent admixture in real space, governed by a local mixing function (LMF) $a(r)$. The general form for local hybrid functional is given as

$$E_{XC}^{lh} = \sum_{\sigma=\alpha,\beta} \int [a_\sigma(\mathbf{r})\varepsilon_{X,\sigma}^{exx}(\mathbf{r}) + (1 - a_\sigma(\mathbf{r}))\varepsilon_{X,\sigma}^{DFT}(\mathbf{r})]\mathrm{d}\mathbf{r} + E_C^{DFT}. \quad (2.23)$$

The quantity $\varepsilon_{X,\sigma}^{exx}$, is the exact-exchange energy density defined as

$$\varepsilon_{X,\sigma}^{exx} = -\frac{1}{2}\sum_{i_\sigma,j_\sigma}^{occ} \phi_i(\mathbf{r})\phi_j\mathbf{r} \int \frac{\phi_i^*(\mathbf{r}')\phi_j^*\mathbf{r}'}{|\mathbf{r} - \mathbf{r}'|}\mathrm{d}\mathbf{r} \quad (2.24)$$

and the other quantity $\varepsilon_{X,\sigma}^{DFT}$, is the conventional DFT exchange-energy density. Most of the currently studied local hybrids are based on local exchange (Slater-Dirac exchange [55]) combined with the semi-local correlation [56],[57].

2.4.1 Local mixing function (LMF)

As stated above, the amount of exact-exchange admixture is made spatially dependent using a local mixing function. This can give more flexibility than global hybrid functionals

which in turn are expected to improve the accuracy and applicability range [15, 58–60]. The basic variables that enter the LMFs are the density (ρ), gradient of density ($\nabla\rho$), local kinetic energy density (τ), von Weizsäcker kinetic energy density (τ_W), and spin polarisation $\zeta(\mathbf{r}) = \frac{\rho_\alpha(\mathbf{r})-\rho_\beta(\mathbf{r})}{\rho_\alpha(\mathbf{r})+\rho_\beta(\mathbf{r})}$. The most popular LMF is the one constructed based on the ratio of von Weizsäcker kinetic energy density to the local kinetic energy density, the so-called *t*-LMF given by

$$a_\sigma(\mathbf{r}) = bt_\sigma(\mathbf{r}), \text{ where } \quad t_\sigma(\mathbf{r}) = \tau_{w,\sigma}(\mathbf{r})/\tau_\sigma(\mathbf{r}). \tag{2.25}$$

The optimised value (for atomisation energies of the small G2-1 test set) of the LMF parameter, b = 0.48 [56]. Due to the scaling down of the mixing parameter from 1 to 0.48 the asymptotic behaviour is lost and self-interaction elimination is not complete. Another type of local mixing function namely *s*-LMF has been constructed based on the dimensionless gradient of electron density [57, 61]. The form of *s*-LMF is given by

$$a_\sigma(\mathbf{r}) = erf(cs_\sigma(\mathbf{r})), \quad s_\sigma = \frac{|\nabla\rho_\sigma(r)|}{2(3\pi^2)^{\frac{1}{3}}\rho_\sigma^{\frac{4}{3}}(r)}, \tag{2.26}$$

where 'c' is the adjustable parameter. The optimal value of 'c' is 0.22 (obtained for atomisation energies of G2 test sets). A new LMF construction (denoted as *r*-LMF) [62], formulated as

$$a_\sigma(\mathbf{r}) = [1 - exp(-bt_\sigma - c\rho(r)^{\frac{5}{3}})]^2 \tag{2.27}$$

where b and c are parameters with values 1.1275 and 0.01625 respectively. Apart from the spin-resolved LMFs, the idea of common LMFs for both spin channels is also considered. This idea is instigated from the construction of LMFs using first principles, the adiabatic connection (AC) formalism [59]. The AC-LMFs constructed are completely determined by the uniform scaling properties of the correlation functional. This suggested the existence of a principal interdependence between exchange and correlation functional used in local hybrids. The exchange-correlation functional expression with common LMF is given as

$$E_{XC}^{lh} = \int \left[a(\mathbf{r}) \sum_{\sigma=\alpha,\beta} \varepsilon_{X,\sigma}^{exx}(\mathbf{r}) + (1 - a(\mathbf{r})) \sum_{\sigma=\alpha,\beta} \varepsilon_{X,\sigma}^{DFT}(\mathbf{r}) \right] \mathrm{d}\mathbf{r} + E_C^{DFT} \tag{2.28}$$

where $a(\mathbf{r})$ is the common LMF reformulated from simple *t*-LMF by including total quantities, given by

$$a(\mathbf{r}) = bt(\mathbf{r}), \text{ where } \quad t(\mathbf{r}) = \tau_W(\mathbf{r})/\tau(\mathbf{r}), \text{ and } \tau_W(\mathbf{r}) = \frac{|\nabla\rho(\mathbf{r})|^2}{8\rho(\mathbf{r})}. \tag{2.29}$$

Here the local kinetic energy density is an additive quantity,

$$\rho(\mathbf{r}) = \rho_\alpha(\mathbf{r}) + \rho_\beta(\mathbf{r});\ \tau(\mathbf{r}) = \tau_\alpha(\mathbf{r}) + \tau_\beta(\mathbf{r}), \tag{2.30}$$

whereas von Weizsäcker kinetic energy density is non-additve. For closed shell systems, the common LMF is same as the spin-resolved *t*-LMF. The optimal value obtained for the common *t*-LMF parameter is 0.534 (on the AE6/BH6 test set). The idea of separation of the correlation energy into dynamical and non-dynamical parts (similar to B05 model [63]) is also considered. Therefore, the expression for local hybrids can be rewritten as

$$\begin{aligned} E_{XC}^{lh} &= \int \left[\sum_{\sigma=\alpha,\beta} \varepsilon_{X,\sigma}^{exx}(\mathbf{r}) + (1 - a(\mathbf{r})) \sum_{\sigma=\alpha,\beta} (\varepsilon_{X,\sigma}^{DFT}(\mathbf{r}) - \varepsilon_{X,\sigma}^{exx}(\mathbf{r})) \right] \mathrm{d}\mathbf{r} + E_C^{DFT} \\ &= E_X^{exx} + E_{NDC}^{lh} + E_{DC}, \end{aligned} \tag{2.31}$$

where the second term is the non-dynamical correlation energy (NDC). The idea of common LMFs for both spin channels is a way to mimic part of the non-dynamical correlation arising from the opposite spins.

2.4.2 Newer correlation functionals for local hybrids: range separation and self-interaction reduction (SIR)

The separation of correlation energy into dynamical (DC) and non-dynamical (NDC) contributions is considerably non-trivial. So, a natural way towards a DC-NDC separation of the correlation energy is by separating the local spin density approximation (LSDA) correlation functional into long- and short-range parts along the inter-electronic coordinate r_{12}. The most widely used range separation schemes are Gaussian error function "erf", its complement "erfc", and the "erfgau" interaction [49]. The long-range LSDA correlation is associated with the non-dynamical correlations whereas the short-range LSDA takes care of the dynamical correlations [58]. Spurious self-interaction errors (SIE) are one of the main problems of semi-local exchange-correlation functionals, particularly LSDA. In LSDA correlation, the parameterisation of Perdew and Wang (PW92) [64] has been used. Only a part of the self-interaction error is removed from the short-range(SR) LSDA. The self-interaction reduced short-range LSDA (SIR-SR-LSDA) correlation is expressed as

$$\begin{aligned} E_{C;\mu\lambda}^{SIR-SR-SDA} = \int \big[&\rho e_{C,\mu}^{SR-LSDA}[\rho_\alpha, \rho_\beta] - \lambda(\tau_{w,\alpha}/\tau_\alpha)\rho_\alpha e_{C,\mu}^{SR-LSDA}[\rho_\alpha, 0] \\ &-\lambda(\tau_{w,\beta}/\tau_\beta)\rho_\beta e_{C,\mu}^{SR-LSDA}[0, \rho_\beta] \big] \mathrm{d}\mathbf{r}, \end{aligned} \tag{2.32}$$

where $e_C^{SR-LSDA} = e_C^{LSDA}(\mathbf{r}_s, \zeta)/(1 + c_1(\mathbf{r}_s)\mu + c_2(\mathbf{r}_s)\mu^2)$, and $0 \leq \lambda \leq 1$.

Depending on the range separation scheme, range separation parameter (μ), self-interaction reduction parameter (λ) and the common *t*-LMF parameter (b), three different local hybrid functionals have been considered [58]. They are

LRSR1: Local hybrid with LSDA exchange and SIR-SR-LSDA correlation, eq.2.31 with range separation scheme erfgau, μ = 0.8, λ = 0.646, and b = 0.646.

LRSR2: Local hybrid with LSDA exchange and SIR-SR-LSDA correlation, eq.2.31 with range separation scheme erf, μ = 0.5, λ = 0.622, and b = 0.622.

LRSR3: Local hybrid with LSDA exchange and SIF-SR-LSDA correlation, eq.2.31 with range separation scheme erfgau, μ = 0.8, λ = 1.0, and b = 0.709.

Results obtained using these functionals clearly indicate significant improvement of reaction barriers, atomisation energies, binding energies of odd-electron radical cations, and electron response properties of hydrogen chains [58]. This can be attributed to the large exact-exchange admixture which reduces the LSDA exchange contributions. More discussions on the local hybrid potential and local mixing functions (LMF) will be discussed in coming chapters.

2.5 Exact conditions for density functionals

2.5.1 Stepwise linearity of ground-state energy from ensemble-DFT formalism

The discussion on this topic starts with the question, whether the total energy density functional is defined only for the densities integrating to an integer number of electrons or is defined over all densities integrating to a fractional number of electrons. To understand the concept of fractional electron numbers one can consider an open system which can exchange electrons with its environment, thus the number of electrons can be fractional on time average. Fractional electron numbers can be found in systems and processes where delocalization of an electron occurs over spatially separated fragments. Mermin formulated an extension of the zero-temperature to the finite-temperature case [65]. This was followed by the extension of DFT for fractional electron numbers by Perdew, Parr, Levy, and Balduz [17] using the grand canonical ensemble construction. In the above ensemble method, the orbital occupation numbers of the standard KS theory remain integer but an ensemble

is introduced where a fraction of the fragments have N+1 electrons while the rest have N electrons, where N is an integer. In this formalism the ground-state energy of such an open system varies linearly when the electron number is varied between two integers with derivative discontinuities at each integer. The ground-state density and energy of the system with N+q number of electrons is expressed as,

$$\rho_{N+q} = q\rho_{N+1} + (1-q)\rho_N; \quad E[\rho_{N+q}] = qE[\rho_{N+1}] + (1-q)E[\rho_N]. \tag{2.33}$$

This extension is a mathematical formulation which makes a continuous link between N-1, N, and N+1 number of electrons leading to a relationship between ionisation potential (I), electron affinity (A), and the DFT energy levels. The derivatives of the energy functional with respect to the number of electrons are given by,

$$\mu[\rho_{N+q}] = \frac{\partial E(N)}{\partial(N)}\Big|_{N+q} = -A(N), \tag{2.34}$$

$$\mu[\rho_{N-q}] = [\frac{\partial E(N)}{\partial(N)}]_{N-q} = -I(N). \tag{2.35}$$

The above equations shows that the chemical potential is constant between the integers and exhibits a jump on passing through the integer number of electrons [19],[66].

2.5.2 Extension of stepwise linearity to low-energy excited states of different spin/spatial symmetry

The stepwise linearity condition for the exact functional has also been extended by Yang and his co-workers [66, 67] to systems in the lowest energy state of a given spin or spatial symmetry different from the ground-state. Consider a system which is constructed using an N-electron degenerate lowest energy system with symmetry S and an (N+1)-electron degenerate lowest energy system with symmetry S', where these two symmetry states S and S' are connected by addition/removal of an electron. The density of such a system is given by

$$\rho_{qN+p} = \sum_{i=1}^{g_N} c_i \rho^S_{N,i} + \sum_{j=1}^{g_{N+1}} d_j \rho^{S'}_{N+1,i} \tag{2.36}$$

where c_i and d_j are positive and finite integers which satisfy the normalization condition. Then the exact energy functional is shown to satisfy the following equation

$$E[\frac{1}{q}\sum_{i=1}^{g_N} c_i \rho^S_{N,i} + \frac{1}{q}\sum_{j=1}^{g_{N+1}} d_j \rho^{S'}_{N+1,i}] = \frac{p-q}{q}E[\rho^S_N] + \frac{p}{q}E[\rho^{S'}_{N+1}], \tag{2.37}$$

where $q = \sum_{i=1}^{g_N} c_i + \sum_{j=1}^{g_{N+1}} d_j$, $p = \sum_{j=1}^{g_{N+1}} d_j$, and $q - p = \sum_{i=1}^{g_N} c_i$. This piecewise constraint implies that for the exact functional the total energy is a sum of the HOMO eigenvalues of the system with 1,2,3,..N electrons. The direct consequence of this is the rigorous connection between the experimental ionisation potential and electron affinity to the HOMO and LUMO values [68]. This extension also serves as an initial step for the combination of fractional charge and fractional spins giving rise to the flat-plane condition for strongly correlated systems.

2.5.3 Derivative discontinuity and the band gap problem

The linearity condition for the ground-state energy means that the fundamental band gap of an N-electron system is given as the difference between the ionisation energy (I) and electron affinity(A),

$$E_{gap} = [E(N-1) - E(N)] - [E(N) - E(N+1)] = I(N) - A(N). \tag{2.38}$$

The Perdew-Levy formulation of the band gap [69] in terms of the energy functional derivatives is

$$E_{gap} = \lim_{q \to 0} (\mu_{(N+q)} - \mu_{(N-q)}), \tag{2.39}$$

$$E_{gap} = \lim_{q \to 0} \left\{ \left[\frac{\delta T_s[\rho]}{\delta \rho(r)} \right]_{N+q} - \left[\frac{\delta T_s[\rho]}{\delta \rho(r)} \right]_{N-q} + \left[\frac{\delta E_{XC}[\rho]}{\delta \rho(r)} \right]_{N+q} - \left[\frac{\delta E_{XC}[\rho]}{\delta \rho(r)} \right]_{N-q} \right\}. \tag{2.40}$$

As the above expression shows that only the non-interacting kinetic energy and the exchange-correlation energy contributes to the discontinuity of the energy functional derivative. The final expression for the band gap is

$$E_{gap} = \varepsilon_{N+1}(N) - \varepsilon_N(N) + \Delta_{XC}, \tag{2.41}$$

where the term Δ_{XC} is the most important discontinuity of the XC potential. The derivative discontinuity is expressed as the difference in the potentials,

$$\Delta_{XC} = \nu_{N+q}(\mathbf{r}) - \nu_{N-q}(\mathbf{r}). \tag{2.42}$$

Unfortunately this term is absent in all the explicit density functionals, thus resulting in underestimated band gap values. Alternative realisations of DFT, the generalized Kohn-Sham (GKS) schemes [28, 70] introduce an interacting model system which incorporates electron-electron interaction to a certain extent and still can be represented by a single

Slater determinant. Usually a fraction of the Hartree-Fock exchange (a_{HF}) is incorporated into the XC functional. The fundamental band gap within the GKS formalism is given by

$$I - A = \varepsilon_{gap}^{KS} + \Delta_{XC}^{KS} = \varepsilon_{gap}^{GKS} + (1 - a_{HF})\Delta_X^{KS} + \Delta_C^{KS}. \tag{2.43}$$

Another implication of the piecewise-linearity condition is the IP theorem [71] which gives the relation between the highest occupied orbital energy (HOMO) and the ionisation potential (IP):

$$\varepsilon_{HOMO} = -I. \tag{2.44}$$

Satisfaction of the IP theorem also invokes the closely related fundamental property of the derivative discontinuity (DD) of the exchange correlation energy. Violation of the IP theorem is related to the central problem in DFT, the self-interaction error (SIE) [47, 72, 73]. It is also related to the wrong asymptotic behaviour of the KS-potential, and affects not just the asymptotes but even the shape of the potential in the non-asymptotic regions [27, 74].

The ensemble approach is a meaningful one from a physical point of view as no reference to a fractional number of electrons is made. It also serves as a practical approach to the problem of open systems as the exchange-correlation energy is defined over the whole domain of ensemble densities, including fractional number of electrons. However, there are some objections to this formalism: firstly the ensemble describes a physical admixture of two non-interacting stable systems rather than one dynamical system of interest. Secondly, the vanishing chemical hardness between integers renders the concept of chemical hardness useless for chemistry. Finally this formalism, very much practical for calculations, but not a favorable methodology for the development of density functionals, paved the way for the fractional occupation approach in DFT [18, 72, 75].

2.5.4 Fractional occupations in DFT

Another approach for treating fractional electron numbers is by having fractional occupations in DFT. In this approach the usual Kohn-Sham equation, which was derived only for integer occupation number, is considered. But the orbital occupation numbers (f_i) entering into the total-energy expression through the kinetic energy and the charge density, are allowed to be fractional. The energy expression is given by,

$$E = -\frac{1}{2}\sum_i f_i \langle\phi_i|\nabla^2|\phi_i\rangle + \int \nu(\mathbf{r})\rho(\mathbf{r})\mathrm{d}\mathbf{r} + \frac{1}{2}\int\int \frac{\rho(\mathbf{r}_1)\rho(\mathbf{r}_2)}{|\mathbf{r}_1 - \mathbf{r}_2|}\mathrm{d}\mathbf{r}_1\mathrm{d}\mathbf{r}_2 + E_{XC}[\rho(\mathbf{r})], \tag{2.45}$$

where the density is given by

$$\rho(\mathbf{r}) = \sum_i f_i |\phi|^2. \tag{2.46}$$

Here the Kohn-Sham system is no longer a single determinant, but instead a linear combination of Kohn-Sham Slater determinants. The importance of choosing the occupation numbers that minimize the total energy is given by Janak's theorem [76] which states that the change in total energy with respect to orbital occupation is given as

$$\frac{\partial E[\rho]}{\partial f_i} = \epsilon_i, \tag{2.47}$$

where ϵ_i is the orbital energy with f_i occupation number. By allowing the occupation numbers to be fractional, lowering of energy of the system can be achieved by transfering an infinitesimal amount of charge from higher energy orbitals to those with lower energy. This is purely a mathematical approach that allows properties of functionals to be studied in the vicinity of integer particle number thereby giving information about the physical picture of an integer number of electrons [18].

2.5.5 Self-interaction error in DFT

Self-interaction errors (SIE) plays a crucial role in DFT with approximate XC functionals. This is mainly due to the spurious interaction of an electron with itself [46]. The SIE leads to wrong dissociation limits, low reaction barriers and overestimation of intermolecular interaction of some charge-transfer complexes . For a one-electron system the electron-electron interaction should be exactly zero

$$J[\rho] + E_{XC}[\rho] = 0. \tag{2.48}$$

Unfortunately most of the approximate XC functionals violate this condition and for systems with more than one electron the SIE definition is quite complicated. Using the scaling relations, Yang and Zhang [12] have shown that the SIE increases in case of a fractional number of electrons. For a q-electron system the electron density in terms of the one-electron density is given as,

$$\rho_q = q\rho_1, \quad \text{where } 0 \leq q \leq 1. \tag{2.49}$$

Now the new scaling relation for the SIE free exchange-correlation energy is given as

$$E_{XC}[q\rho_1] = q^2 E_{XC}[\rho_1]. \tag{2.50}$$

But most of the approximate functionals do not obey this relation. The exchange functionals in LDA and BLYP instead follow the inequality

$$E_X[q\rho_1] < q^2 E_X[\rho_1]. \tag{2.51}$$

Since the negative exchange term dominates the exchange-correlation energy, the SIE would be even more negative according to the above relation for a fractional number of electrons. Therefore in general, SIE increases for systems with a fractional number of electrons. This erroneous behaviour of DFAs results in energies which are too low for any system [66, 72].

2.5.6 Static correlation error

Static correlation in DFT mainly arises due to the mixing of near degenerate and absolute degenerate states with the reference Slater determinant. Treatment of such systems within KS-DFT is believed to be a task cut out for the exchange-correlation functional and can be understood using fractional spins. The extension of DFT to fractional-spin states and the derivation of the spin-constancy condition for exact energy functional has been carried out by Yang and his co-workers [20]. Similar to fractional electron numbers, fractional-spin states can arise when ensembles of degenerate states with integer spins are considered. For an N-electron system with g-fold degenerate densities ($\rho_i,\ i = 1, 2, ..g$), the ensemble density is given by

$$\rho = \sum_{i=1}^{g} C_i \rho_i, \quad \text{where} \quad 0 \leq C_i \leq 1 \text{ and } \sum_{i=1}^{g} C_i = 1. \tag{2.52}$$

The spin constancy condition is expressed as,

$$E\left[\sum_{i=1}^{g} C_i \rho_i\right] = E[\rho_j] = E^0(N), \quad j = 1, 2, \ldots, g, \tag{2.53}$$

which means that the energy of the exact functional for fractional-spin states is equal to the degenerate pure-spin state energies and is a constant. For example, in the case of an H-atom with two degenerate spin states α ($m_s = +1/2$) and β ($m_s = -1/2$), the spin constancy condition is written as

$$E\left[\rho(1,0)\right] = E\left[\rho(0,1)\right] = E\left[\rho(\frac{1}{2},\frac{1}{2})\right] = E\left[\rho(\gamma, 1-\gamma)\right], \quad 0 < \gamma \leq \frac{1}{2}. \tag{2.54}$$

Even though this seems to be a very trivial condition, all density functional approximations produces fractional-spin errors. These failures are very much apparent in systems such as

a stretched H_2 molecule. This fractional-spin error (or the static correlation error) plays an important role in the physics of strong correlation which will be discussed next.

2.6 Strong correlation in DFT

The ability to describe dissociating chemical systems using spin- and spatially symmetric single Slater determinants is considered as the hallmark of strongly correlated DFT methods. Consider the dissociation of an H_2 molecule using spin-unrestricted and spin-restricted formalisms. For the unrestricted case each dissociated hydrogen atom has one electron in the H1s atomic orbitals with either up or down spin causing undesirable symmetry breaking. In case of spin restricted orbitals, each dissociated hydrogen atom has half an electron with spin up and another half with spin down in the H1s atomic orbital. The electronic states with fractional spins are attributed to the large static correlation (strong correlations) in DFT. These systems require multi-determinant reference states in order to describe the dissociating behavior using symmetry restricted orbitals. The exact density functional should give identical energies for both spin restricted and unrestricted cases. In fact, the exact ground-state energy functional for any given linear combination of degenerate ground-state densities should result in the same energy (flat-plane behavior). This is a very stringent condition not satisfied by the conventional density functionals (nor by HF theory). Therefore, it is of great importance to develop exchange-correlation functionals which can also describe strongly correlated systems. Becke has recently proposed a model based on his previous B05 model which includes static, dynamic, and strong-correlation contributions combined with exact-exchange. In this new model (B13) [22, 26], the exchange-correlation functional is composed of exact-exchange and a specifically tailored correlation functional

$$E_{XC}^{B13} = E_X^{exx} + E_C^{B13}. \tag{2.55}$$

The correlation energy (E_C^{B13}) is composed of the static (B05 model) and a modified B88 dynamic correlation energy [63],

$$E_C^{B13} = E_{B05}^{statC} + E_{B88}^{dynC}. \tag{2.56}$$

Both terms can be further separated as parallel-spin and opposite-spin correlations

$$\begin{aligned} E_{statC}^{B05} =& a_{statC}^{opp} U_{statC}^{opp} + a_{statC}^{par} U_{statC}^{par}, \\ E_{dynC}^{B88} =& a_{dynC}^{opp} U_{dynC}^{opp} + a_{dynC}^{par} U_{dynC}^{par}. \end{aligned} \tag{2.57}$$

In the above equation the correlation functional is made up of purely potential energy terms and the semi-empirical fitting coefficients a^{opp}_{statC}, a^{par}_{statC}, a^{opp}_{dynC}, and a^{par}_{dynC}. The potential energy terms are given by

$$\begin{aligned} U^{opp}_{statC} &= \int u^{opp}_{statC}(\mathbf{r})\mathrm{d}\mathbf{r}, \\ U^{par}_{statC} &= \int u^{par}_{statC}(\mathbf{r})\mathrm{d}\mathbf{r}, \\ U^{opp}_{dynC} &= \int u^{opp}_{dynC}(\mathbf{r})\mathrm{d}\mathbf{r}, \\ &\text{and} \\ U^{par}_{dynC} &= \int u^{par}_{dynC}(\mathbf{r})\mathrm{d}\mathbf{r}. \end{aligned} \tag{2.58}$$

The B13 correlation model is very good to describe static correlations in molecules at equilibrium, but cannot handle dissociating molecules with restricted (symmetry adapted) orbitals. To capture these strong correlations a simple correction term was introduced into the B13 model [22],

$$E^{B13}_{XstrgC} = E^{ex}_{X} + E^{B13}_{C} + \Delta E^{B13}_{strgC}. \tag{2.59}$$

Usually, the strong-correlation energy functional is given by the expression

$$E^{B13}_{strgC} = \int \alpha_C(\mathbf{r}) u_C(\mathbf{r})\mathrm{d}\mathbf{r}, \tag{2.60}$$

where the term α_C can be expressed as a polynomial

$$\begin{aligned} \alpha_c(\mathbf{r}) &\cong \sum_{n=0}^{N} c_n x^n(\mathbf{r}),\ x(\mathbf{r}) = \frac{u^{opp}_{statC}(\mathbf{r}) + u^{par}_{statC}(\mathbf{r})}{u_C(\mathbf{r})}, \\ u_C(\mathbf{r}) &= u^{opp}_{statC}(\mathbf{r}) + u^{par}_{statC}(\mathbf{r}) + u^{opp}_{dynC}(\mathbf{r}) + u^{par}_{dynC}(\mathbf{r}). \end{aligned} \tag{2.61}$$

The strength of the correlation depends on the term $x(r)$, a dimensionless parameter measuring the relative importance of the static correlation potential-energy density to the total correlation potential-energy density. The first two terms of the expression [Eq.2.59] are the total potential-energy contributions to the correlation with different coefficients, so the strong-correlation correction begins at second order

$$E^{B13}_{strgC} = E^{B13}_{C} + \Delta E^{B13}_{strgC}, \tag{2.62}$$

where the correction term is given as

$$\Delta E^{B13}_{strgC} = \sum_{n=2}^{N} c_n \int x^n(\mathbf{r}) u_c(\mathbf{r})\mathrm{d}\mathbf{r}. \tag{2.63}$$

In general one or two correction terms are sufficient to capture the strong-correlation effects (i.e., N=2,3). The testing of this model has been carried out on a stringent strong-correlation test set using numerical (post-LSDA) computations [22, 26]. The strong-correlation test set is that for each open-shell atom, two cases are considered, spin-depolarised (SDP) and free atom (FA). For a carbon atom with an open $2p$ shell, the two cases are

Free-atom occupancies	:	$(2p_x\alpha)^1(2p_y\alpha)^1(2p_z\alpha)^0(2p_x\beta)^0(2p_y\beta)^0(2p_z\beta)^0$
Spin-depolarised occupancies	:	$(2p_x\alpha)^{\frac{1}{2}}(2p_y\alpha)^{\frac{1}{2}}(2p_z\alpha)^0(2p_x\beta)^{\frac{1}{2}}(2p_y\beta)^{\frac{1}{2}}(2p_z\beta)^0$

For the exact functional the spin-depolarised (SDP) energy should be equal to the free-atom (FA) energy and the value of ΔE should be zero

$$\Delta E = E^{spin-depolarised} - E^{free-atom}. \tag{2.64}$$

By considering a balanced set of G2/97 atomization energies of Curtiss, Raghavachari, and Pople [11] and strong-correlation test set of 28 atoms (H-Br), the best-fit coefficients obtained for the static correlation, dynamic correlation and the strong-correlation correction terms are of the order 0.5-0.7. Results (mean errors (ME) and mean absolute errors (MAE)) have been obtained for HF, GGA, B13, and B13 with strong-correlation correction (two strong-correlation correction terms (N=2,3)) approaches. Mean errors and mean average errors obtained by B13 (XstrgC) model are six times better than for GGA functionals and an order of magnitude better than for the B13 model [26]. Construction of a local hybrid functional with strong-correlation correction along these lines has been considered and will be discussed in detail in Chapter 3.

2.7 *s-d* Transfer energies

s-d Transfer energies have been considered an excellent qualitative benchmark for computational models in transition-metal (TM) chemistry. For the example of $3d$-elements, the accuracy of the methods employed depends mainly on the balanced description of the $4s$ and $3d$ one-electron states [77–79]. Unfortunately, an accurate prediction of these atomic excitations for transition-metal atoms becomes very complicated, especially in the open-shell cases [80–82]. This is mainly due to the presence of several low-lying electronic states with different spin/orbital occupancy close to the reference Slater determinant. In general, HF gives good results for the atomic systems Sc-Cr, but fails miserably for later

3*d*-series atoms due to strong differential correlation effects. Therefore DFT methodologies come in handy as they cover these correlation effects to a certain extent. Harris and Jones [83], in their early work using the LSDA, recognised that the *s-d* transfer energies have been underestimated by an average of -1.0 eV. Computations using GGA and meta-GGA functionals have worsened the results for atoms Sc-Fe, but the errors remained constant for other atoms [82]. Global hybrids tend to give less negative mean signed errors (MSE) and lower mean average errors (MAE), due to the exact-exchange admixture shifting the excitation energies to larger values. The source of errors for the functionals are mainly due to the problems with the simulation of non-dynamical correlation (NDC) and the presence of self-interaction errors (SIE) [84–87]. There is also a general tendency of all XC approximations to favour one configuration over the other which results in errors for *s-d* transfer energies. Therefore, it is of great importance to test the performance of local hybrid functionals for these difficult cases. Here, two different approaches have been used for the computation of *s-d* transfer energies. The first is the formalism proposed by Furche and Perdew [23] which uses a symmetry-constrained procedure for multi-determinant states. In the other formalism given by Truhlar and his co-workers [24], broken-symmetry approaches are used for states with multi-determinant character.

2.7.1 Furche-Perdew formalism

The protocol for the Furche-Perdew formalism consists of two steps [23]. In the first step calculations are performed self-consistently using O_h symmetry. In the second step, whenever fractional occupations are present (due to degenerate orbitals in higher symmetry), transformation of the orbitals from O_h to C_1 symmetry and then averaging the non-self-consistent energies of the multiplet components are performed. This procedure allows for a maximum symmetry breaking without mixing of *s* and *d* states. In general, e_g orbitals are used for fractional occupations.

2.7.2 Broken-symmetry approaches

It has been common knowledge that open-shell KS-DFT calculation features spatial and spin symmetry breaking which results in the mixing of s and d orbitals for 3*d*-transition-metal atoms. Recently extensive studies on 3*d*-transition metals have been carried out by Truhlar and coworkers [24] using broken-symmetry approaches. In those studies, the

closed shell atomic states have been computed using the Kohn-Sham approach for the lowest energy solutions. But in the case of open-shell states which have a partially filled sub-shell, there can be several low-energy states with different spin multiplicities, and the lowest-energy solutions to the unrestricted-KS equations are often the broken-symmetry solutions. These electronic states are classified into nominally single-determinant (NSD) states and intrinsically multi-determinant (IMD) states. The NSD states are those with total spin equal to half the number of nominally single occupied orbitals ($S = \frac{n_{SO}}{2}$) (nominally means orbitals in an unrestricted computation where α and β of an electron pair are not identical). The energy of NSD state is always the SCF energy of the state with $M_s = S$. The IMD states are those with total spin less than half the number of nominally single occupied orbitals ($S < \frac{n_{SO}}{2}$). For example, consider the Fe atom with states Fe($^5F, 4s^1 3d^7$) and Fe($^3F, 4s^1 3d^7$). In the state Fe(^5F) all the four unpaired electrons occupy the α-orbitals whereas the state Fe(^3F) has three $d\alpha$ and one $s\beta$ electrons. The possible IMD and their corresponding NSD states considered for each atom are shown in Table 2.1. Out of all possible IMD states, experimental data are available only for four atomic systems, namely Cr, Fe, Co, and Ni. For obtaining the energy of an IMD state three different ways have been used, namely the variational method, the weight-average broken-symmetry (WABS) method, and the reinterpreted broken-symmetry (RBS) method [24, 88].

Atom	IMD states	corresponding NSD states
Ca	$d^1s^1(^1D)$	$d^1s^1(^3D)$
Sc	$d^2s^1(^2F)$	$d^2s^1(^4F)$
Ti	$d^3s^1(^3F)$	$d^3s^1(^5F)$
V	$d^4s^1(^4D)$	$d^4s^1(^6D)$
Cr	$d^5s^1(^5S)$	$d^5s^1(^7S)$
Mn	$d^6s^1(^4D)$	$d^6s^1(^6D)/d^5s^2(^6S)$
Fe	$d^7s^1(^3F)$	$d^7s^1(^5F)/d^6s^2(^5D)$
Co	$d^8s^1(^2F)$	$d^8s^1(^4F)/d^7s^2(^4F)$
Ni	$d^9s^1(^1D)$	$d^9s^1(^3D)/d^8s^2(^3F)$

Table 2.1: The IMD and NSD states

Variational method

In this approach the energy of the IMD state is computed as the energy of the stably optimised SCF computation of the state with $M_s = S$,

$$E^{Var}_{IMD}(n_{SO}, S, M_S) = E^{SCF}_{IMD}(n_{SO}, S, M_S = S). \tag{2.65}$$

For example, consider the Co atom IMD state with configuration $3d^8 4s^1(^2F)$. The stably optimised SCF energy of the IMD state Co($^2F, 3d^8 4s^1$) is taken as the variational energy.

Weighted-average broken-symmetry approach (WABS)

The main aspect of this method is that the states which are intrinsically multi-determinantal (IMD) are actually considered to be a mixture of states with different multiplicities. In the NSD state all single (unpaired) electrons are filled into the α-orbitals whereas in the IMD state one or more unpaired electrons occupy the β-orbital. The energy for the IMD state in generalization to other multiplicities is

$$\begin{aligned} E_{IMD}^{WABS}(n_{SO}, S, M_S) =& E_{NSD}^{SCF}(n_{SO}, S = \frac{n_{SO}}{2}, M_S = \frac{n_{SO}}{2}) \\ & - k[E_{NSD}^{SCF}(n_{SO}, S = \frac{n_{SO}}{2}, M_S = \frac{n_{SO}}{2}) \\ & - E_{IMD}^{SCF}(n_{SO}, S, M_S = S)], \end{aligned} \tag{2.66}$$

where $k = \frac{2S_{HS}}{(\langle S^2\rangle_{HS} - \langle S^2\rangle_{BS})}$. The above formula, given by Yamaguchi [88], has been popular for broken-symmetry calculations. The IMD states for each atom are given in Table 2.1. For certain atomic configurations such as Mn($^6D, 4s^1 3d^6$), Fe($^3F, 4s^1 3d^7$), Co($^4F, 4s^1 3d^8$), and Ni($^3D, 4s^1 3d^9$) there are two possible NSD states with the same number of unpaired electrons. In the case of Fe($^3F, 4s^1 3d^7$), the IMD state has three $d\alpha$ electrons and one $s\beta$ electron. There are two possibilities for the NSD state, Fe($^5D, 4s^2 3d^6$) and Fe($^5F, 4s^1 3d^7$). Here the Fe($^5D, 4s^2 3d^6$) state is considered for NSD as it is lower in energy than Fe($^5F, 4s^1 3d^7$). Similarly for the Co atom, computations are carried out using Co($^4F, 4s^2 3d^7$) as the NSD state. For the Ni atom there are two possible NSD states, $d^9 s^1(^3D)$ or $d^8 s^2(^3F)$ of which (^3D) is considered as the NSD state due its relative stability. Still there is an underlying issue about the spatial orbitals being the same for both the NSD and the IMD states as there are cases stated for Fe and Co, where this is not true.

Reinterpreted broken-symmetry approach (RBS)

In this method, for each IMD state an artificial NSD state (post-SCF state labelled as PSCF) is obtained using the same orbitals as in the IMD state. The RBS approach is more physically justified as it makes sure that both the IMD and NSD states considered have the same spatial orbitals [24]. For example, in the case of Fe($^3F, 4s^1 3d^7$) IMD state, the corresponding NSD state considered is the stabilized quintet, Fe($^5D, 4s^2 3d^6$). But using the same orbitals as in the Fe(^3F) state, an artificial NSD state (PSCF) can be obtained

by flipping the spin of one or more singly occupied orbitals. The spin flipping is carried out by identifying the virtual orbital of other spin that is most similar in energy to the spin orbital intended to flip. Thus the PSCF state obtained have the same spatial orbitals as the IMD state. The equations for the RBS are given as

$$\begin{aligned} E_{IMD}^{RBS}(n_{SO}, S, M_S) =& E_{NSD}^{PSCF}(n_{SO}, S = \frac{n_{SO}}{2}, M_S = \frac{n_{SO}}{2}) \\ & - k[E_{NSD}^{PSCF}(n_{SO}, S = \frac{n_{SO}}{2}, M_S = \frac{n_{SO}}{2}) \\ & - E_{IMD}^{SCF}(n_{SO}, S, M_S = S)], \end{aligned} \tag{2.67}$$

where $k = \frac{2S_{HS}}{(\langle S^2\rangle_{HS} - \langle S^2\rangle_{BS})}$. There are cases where the PSCF state in RBS approach has different orbitals to the NSD state in the WABS approach. In the case of Fe($^3F, 4s^1 3d^7$) the PSCF state is obtained by flipping the spin of the $s\beta$ electron and for the Co($^2F, 4s^1 3d^8$) the PSCF state is obtained by flipping the $d\beta$ electron in the IMD state. In case of Co($^2F, 4s^1 3d^8$) and Ni($^1D, 4s^1 3d^9$), some functionals on spin flipping can give a PSCF state with energy higher than the unflipped state in order of 100 kcal/mol [89]. This is due to very different highest-energy occupied orbitals for α and β electrons. In such cases broken-symmetry approaches must not be used. Detailed discussions on the results obtained for *s-d* transfer energies using the above formalisms are carried out in Chapter 4.

Chapter 3

Implementation

3.1 Self-consistent implementation of common LMFs

The idea of local hybrid functionals using common LMFs for both the spin channels, has been proposed for the simulation of some of the non-dynamic correlation (NDC) arising from opposite-spin electrons [Sec.2.4.1]. Previously, spin-polarized *t*-LMFs and *s*-LMFs have been constructed to obtain the cross terms between the two spin channels [15]. Also, to achieve separation of the correlation energy into dynamical (DC) and non-dynamical (NDC) contributions, construction of local hybrids with range-separated correlation functionals have been done [58]. Self-consistent (SCF) implementations of these developments are very important for the computation of properties. Local hybrids with the spin-channel *t*-LMF, *s*-LMFs, *r*-LMFs, and range-separated correlation functionals had already been implemented self-consistently (in a local version of Turbomole program) [56–58]. Along similar lines, the SCF implementation of common *t*-LMFs has been carried out here.

In the KS scheme, the XC potential is defined as a functional derivative:

$$\nu_{XC}(\mathbf{r}) = \frac{\delta E_{XC}}{\delta \rho(\mathbf{r})}. \tag{3.1}$$

For LDA/GGA functionals the functional derivative is obtained in a straightforward way, whereas for the hybrid functional, due to the orbital-based exact-exchange term, it is not so trivial. The local hybrid functional comprises an orbital-based exact-exchange term and the density-dependent DFT exchange-correlation term [Eq.2.23]. Due to the orbital-dependent term, the KS potential is evaluated using functional derivatives with

respect to the orbitals (FDOs). The substitution relation between the functional derivatives and KS-potential is given as

$$\nu^{lh}_{XC,\sigma}(\mathbf{r})\phi_{i,\sigma}(\mathbf{r}) \leftarrow \frac{1}{2}\frac{\delta E^{lh}_{XC}}{\delta\phi_{i,\sigma}(\mathbf{r})}. \tag{3.2}$$

This substitution generates a non-local and non-multiplicative exchange contribution to the local hybrid potential defined by its operation on a particular orbital whose form is:

$$\hat{\nu}^{exx}_{X,\sigma}\phi_{i,\sigma}(\mathbf{r}) = -\sum_{j\sigma}^{occ}\phi_{j,\sigma}(\mathbf{r})\int\frac{\phi_{j,\sigma}(\mathbf{r}')\phi_{i,\sigma}(\mathbf{r}')}{|\mathbf{r}-\mathbf{r}'|}d\mathbf{r}'. \tag{3.3}$$

The non-local potential implies that electrons in different orbitals move in different potentials. Direct use of this non-local and non-multiplicative exchange potential represents a step outside the KS formalism (the GKS formalism [70]). The expression for the exchange-correlation part of the local hybrid KS-potential is given as:

$$\begin{aligned}\frac{1}{2}\frac{\delta E^{lh}_{XC}}{\delta\phi_{i,\sigma}(\mathbf{r})} &= \frac{1}{2}[a(\mathbf{r})\hat{\nu}^{exx}_{X,\sigma}\phi_{i,\sigma} + \hat{\nu}^{exx}_{X,\sigma}(a(\mathbf{r})\phi_{i,\sigma})] + [(1-a(\mathbf{r}))\nu^{DFT}_{X,\sigma} + \nu^{DFT}_{C,\sigma}(\mathbf{r})]\phi_{i,\sigma}(\mathbf{r}) \\ &+ \frac{1}{2}\Delta\varepsilon_X\frac{\partial a(\mathbf{r})}{\partial\phi_{i,\sigma}(\mathbf{r})} - \frac{1}{2}\nabla\left[\Delta\varepsilon_X\frac{\partial a(\mathbf{r})}{\partial\nabla\phi_{i,\sigma}(\mathbf{r})}\right] + \nabla a(\mathbf{r}).\frac{\partial\varepsilon^{DFT}_{X,\sigma}}{\partial\nabla\rho_\sigma}\phi_{i,\sigma}(\mathbf{r}) \\ &- \frac{1}{2}\left[\left(\nabla\frac{\partial\varepsilon^{lh}_{X,\sigma}}{\partial\tau_\sigma}\right).\nabla + \frac{\partial\varepsilon^{lh}_{X,\sigma}}{\partial\tau_\sigma\nabla^2}\right]\phi_{i,\sigma}(\mathbf{r}),\end{aligned} \tag{3.4}$$

where $\Delta\varepsilon^\sigma_X = \varepsilon^{exx}_{\sigma,X} - \varepsilon^{DFT}_{\sigma,X}$, and $\Delta\varepsilon_X = \sum_{\sigma=\alpha,\beta}\Delta\varepsilon^\sigma_X$.

The first two terms in the above expression are the non-local exact-exchange terms (evaluated numerically on the grid or analytically by using the resolution of the identity (RI) [90]). The next two terms include the local exchange potential weighted by the common LMF and the local correlation potential. The other three terms are the derivatives of the LMF multiplied by semi-local exchange energy densities. The last two terms in the expression are the derivatives with respect to τ (while the LSDA exchange and correlation energy densities do not depend on τ, but the LMF does). The Fock matrix element for the exchange in a given atomic basis is given by

$$\mathrm{F}^{X,\sigma}_{\mu\nu} = \int\chi_\mu\,\hat{\nu}_{X,\sigma}\,\chi_\nu\,d\mathbf{r}. \tag{3.5}$$

The partial derivatives of the common *t*-LMF with respect to the density ρ, to the absolute

square of the density gradient $|\nabla\rho|^2$, and to the local kinetic energy density τ:

$$\begin{aligned}
\frac{\partial a}{\partial \phi_i} &= \frac{\partial a}{\partial \rho}\frac{\partial \rho}{\partial \rho_i} + \frac{\partial a}{\partial |\nabla\rho|^2}\frac{\partial |\nabla|^2}{\partial \phi_i} = 2\frac{\partial a}{\partial \rho}\phi_i + 4\frac{\partial a}{\partial |\nabla\rho|^2}\nabla\rho.\nabla\rho_i, \\
\frac{\partial a}{\nabla \phi_i} &= \frac{\partial a}{\partial |\nabla\rho|^2}\frac{\partial |\nabla\rho|^2}{\partial \rho_i} + \frac{\partial a}{\partial \tau}\frac{\partial \tau}{\partial \nabla\phi_i} = \frac{\partial a}{\partial \rho}\nabla\phi_i + 4\frac{\partial a}{\partial |\nabla\rho|^2}(\nabla\rho)\phi_i, \\
\frac{\partial a}{\partial \rho} &= -\frac{a}{\rho}, \\
\frac{\partial a}{\partial |\nabla\rho|^2} &= \frac{a}{|\nabla\rho|^2}, \\
\frac{\partial a}{\partial \tau} &= -\frac{a}{\tau}.
\end{aligned} \tag{3.6}$$

Applying the partial integration technique and gradients of the LMF or the DFT exchange-energy density, the Fock matrix element for the exchange is expressed as

$$\begin{aligned}
\mathrm{F}_{\mu\nu}^{X,\sigma} = \frac{1}{2}\Big[\int \chi_\mu \, \mathrm{a} \, \hat{\nu}_{X,\sigma}^{exx} \, \chi_\nu + \int \chi_\mu \, \hat{\nu}_{X,\sigma}^{exx}(\mathrm{a} \, \chi_\nu)\Big] + \int \chi_\mu \Delta\varepsilon_X \frac{\partial \mathrm{a}}{\partial \rho}\chi_\nu \\
+2\int [1-\mathrm{a}]\frac{\partial \varepsilon_{X,\sigma}^{DFT}}{\partial |\nabla\rho_\sigma|^2}\nabla\rho_\sigma.\nabla(\chi_\mu\chi_\nu) + 2\int \Delta\varepsilon_X \frac{\partial \mathrm{a}}{\partial |\nabla\rho|^2}\nabla\rho.\nabla(\chi_\mu\chi_\nu) \\
+\int \chi_\mu [1-\mathrm{a}]\frac{\partial \varepsilon_{X,\sigma}^{DFT}}{\partial \rho_\sigma}\chi_\nu + \frac{1}{2}\int \Delta\varepsilon_X \frac{\partial \mathrm{a}}{\partial \tau}\nabla\chi_\mu.\nabla\chi_\nu.
\end{aligned} \tag{3.7}$$

The Fock matrix elements for the common LMF differ from those of the spin-channel LMF only in the LMF and its derivatives. This implementation has been carried out in a local version of the Turbomole program (TBM5.10 local version developed for local hybrids) [56, 91].

Implementation procedure

The required changes have been made to the Turbomole/dftlib directory.

Step 1: the first set of changes made for setting the common LMF as an input for the calculations. The file modified for this purpose is gridin.f.

Step 2: the next set of changes are for the evaluation of common LMF and its derivatives on the grid. the files modified for this purpose are lmfscf_r1.f and lmfscf_ u1.f.

Step 3: Fock matrix evaluation: in case of closed shell system the common *t*-LMF is equal to the spin-channel *t*-LMF, so no changes have been made to the code. But the closed shell case can be used for testing the implementation by performing an open-shell calculation on a closed shell system as both calculations should give the same values.

Step 4: Fock matrix evaluation: a separate Fock matrix for the common *t*-LMF has been

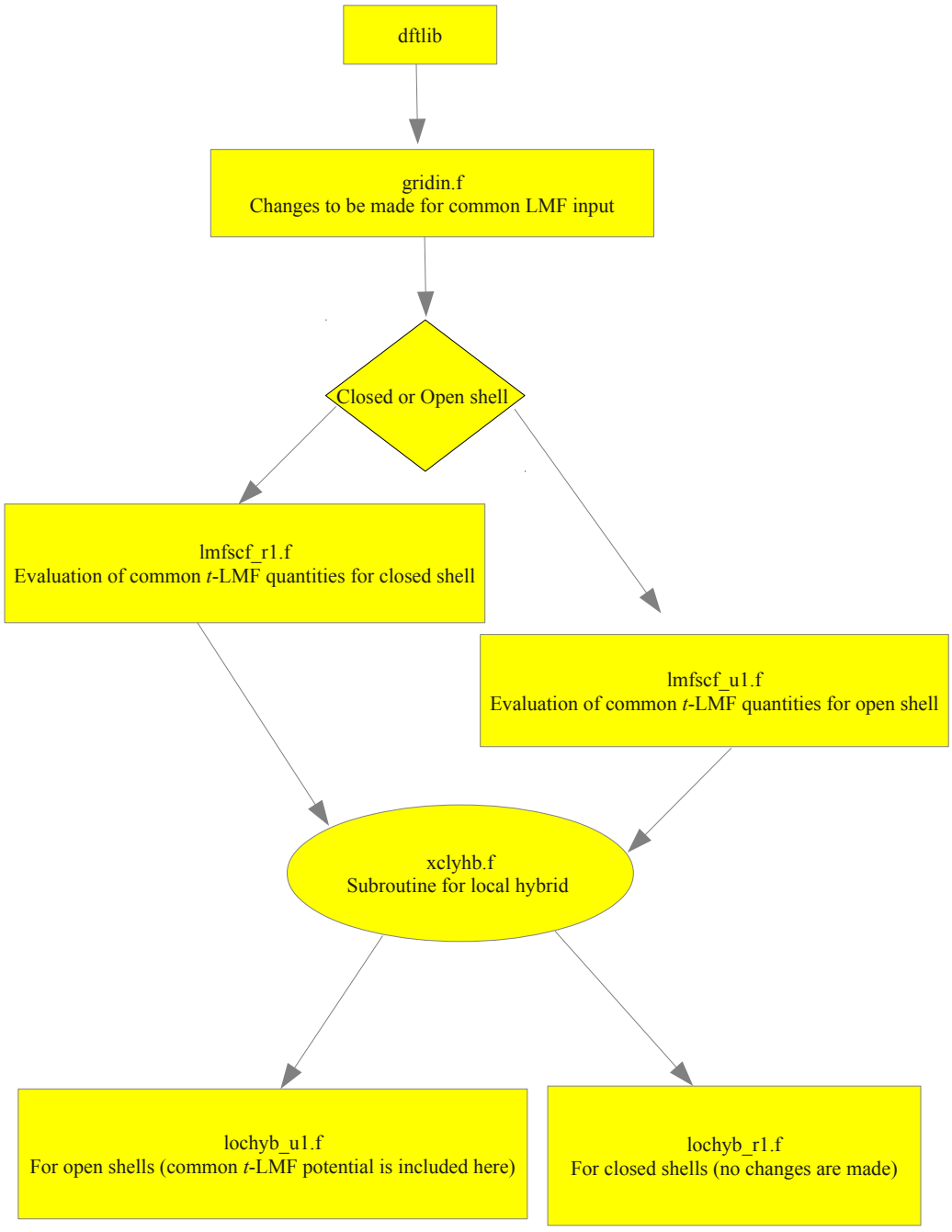

Figure 3.1: Flowchart for the SCF implementation of common t-LMF. The subroutines lmfscf-r1.f, lmfscf-u1.f, xclyhb.f, lochyb-u1.f, and lochyb-r1.f are the ones added for the purpose of local hybrids (in TBM5.10 local version developed for local hybrid functionals).

included along with the existing spin-channel LMFs. The file modified for this purpose is lochyb_ u1.f.

3.1.1 Testing

For any correct SCF implementation, the final SCF energy should always be lower than that of first iteration energy. For this initial test, SCF calculations have been performed on the G2-1 test set and the energy differences have been obtained (between final SCF and first iteration energies). The energy differences clearly show that the first criterion is satisfied. Further tests of the implementation have been carried out by performing computations on the atomic systems like helium, beryllium, neon, and calcium. For these atoms, both closed and open-shell cases, the final SCF energies have been found to be exactly the same (upto 6 decimal digits).

3.2 Post-SCF implementation of a new local mixing function

A new local hybrid functional has been developed by the Kümmel and coworkers [25] which is one-electron self-interaction free and has the correct asymptotic behaviour. The new local hybrid is expressed as

$$E_{XC}^{lh} = \int [\varepsilon_X^{exx}(\mathbf{r}) + f(\mathbf{r})(\varepsilon_X^{sl}(\mathbf{r}) - \varepsilon_X^{exx}(\mathbf{r}))]d\mathbf{r} + E_C^{sl}, \tag{3.8}$$

where the local mixing function f(**r**) is given as

$$f(\mathbf{r}) = \frac{1 - \frac{\tau_W(\mathbf{r})}{\tau(\mathbf{r})}\zeta^2(\mathbf{r})}{1 + ct^2(\mathbf{r})}. \tag{3.9}$$

The LMF can be reformulated (in relation to the eq.2.) and denoted as z-LMF

$$a(\mathbf{r}) = 1 - f(\mathbf{r}). \tag{3.10}$$

Here the terms are the usual von Weizäcker kinetic energy density $\tau_W(\mathbf{r})$, the local kinetic energy density $\tau(\mathbf{r})$, and the spin polarization $\zeta(\mathbf{r})$. The quantity $t^2(\mathbf{r})$, based on the reduced density gradient defined as

$$t^2(\mathbf{r}) := \frac{\left(\frac{\pi}{3}\right)^{1/3} a_o |\nabla\rho(\mathbf{r})|^2}{16\Phi^2(\zeta(\mathbf{r}))\rho^{7/3}(\mathbf{r})}, \tag{3.11}$$

where a_0 is the Bohr radius and the quantity $\Phi(\zeta(\mathbf{r})) = \frac{1}{2}[(1+\zeta)^{2/3} + (1-\zeta)^{2/3}]$. The LMF aims to fulfil the high density limit as $t^2 \to \infty$ and also, the LMF do not consider two spatially identical orbitals with opposite spins as a one-orbital region which meant that the one-electron and one-spin-orbital regions are clearly defined. There is a difference between the one-electron and one-spin-orbital regions and strictly these two regions do not coincide as the interacting system and KS system has only the total electron density in common. The value of LMF goes to 1 when $\tau(\mathbf{r}) \to \tau_{\mathbf{W}}(\mathbf{r})$ for one-spin-orbital densities. The above LMF has only one free parameter c, which affects the amount of exact-exchange used in a calculation and the freedom of varying this parameter can be used to explore the properties of the functional.

3.2.1 Self-interaction (SI) corrected correlation functional

Together with the LMF, a self-interaction corrected correlation functional has also been proposed:

$$E_C^{sl} = \int [1 - d(\mathbf{r})]\varepsilon_C^{LSDA}(\mathbf{r})d\mathbf{r}, \tag{3.12}$$

where the quantity $d(\mathbf{r})$ is defined as

$$d(\mathbf{r}) = \frac{\tau_W(\mathbf{r})}{\tau(\mathbf{r})}\zeta^2(\mathbf{r}). \tag{3.13}$$

The correlation functional is one-electron SI-free, ensures the correct asymptotic behaviour at $|\mathbf{r}| \to \infty$, and for regions of slowly varying density reduces to LSDA [25]. The functional is completely one-electron self-interaction free when $d(\mathbf{r})$ tends to 1, thereby reducing the XC functional only to exact-exchange term. This term cancels the Hartree repulsion avoiding the unwanted local correlation for one-orbital regions.

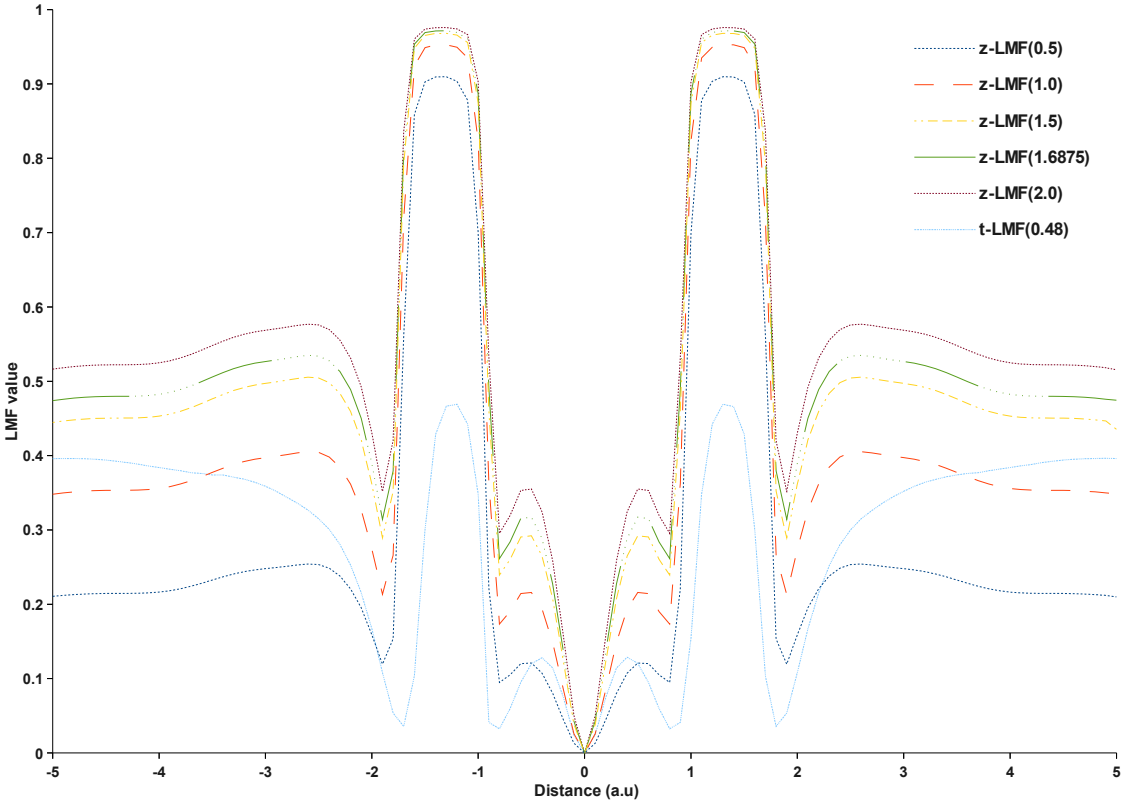

Figure 3.2: z-LMFs behaviour plotted along the bond axis in the F_2 Molecule (in each case the LMF parameter c value is given in parenthesis). F atomic nuclei are positioned at -1.34 and 1.34 on the x-axis at equilibrium distance.

Details

The implementation of z-LMF and the related self-interaction corrected correlation has been carried out in a local version of Turbomole program in post-SCF manner. Earlier the Kümmel group had fitted the free parameter for each system (only for a set of diatomic molecules) using techniques like D-fitting (dissociation energy) and E-fitting (experimental total energy). Reoptimization of the free parameter using the weighted minimization of MAEs for the AE6-BH6 atomisation energies and reaction barrier test sets (for polyatomic molecules) gives the free parameter value 1.6875 with the MAE 5.0984 kcal/mol.

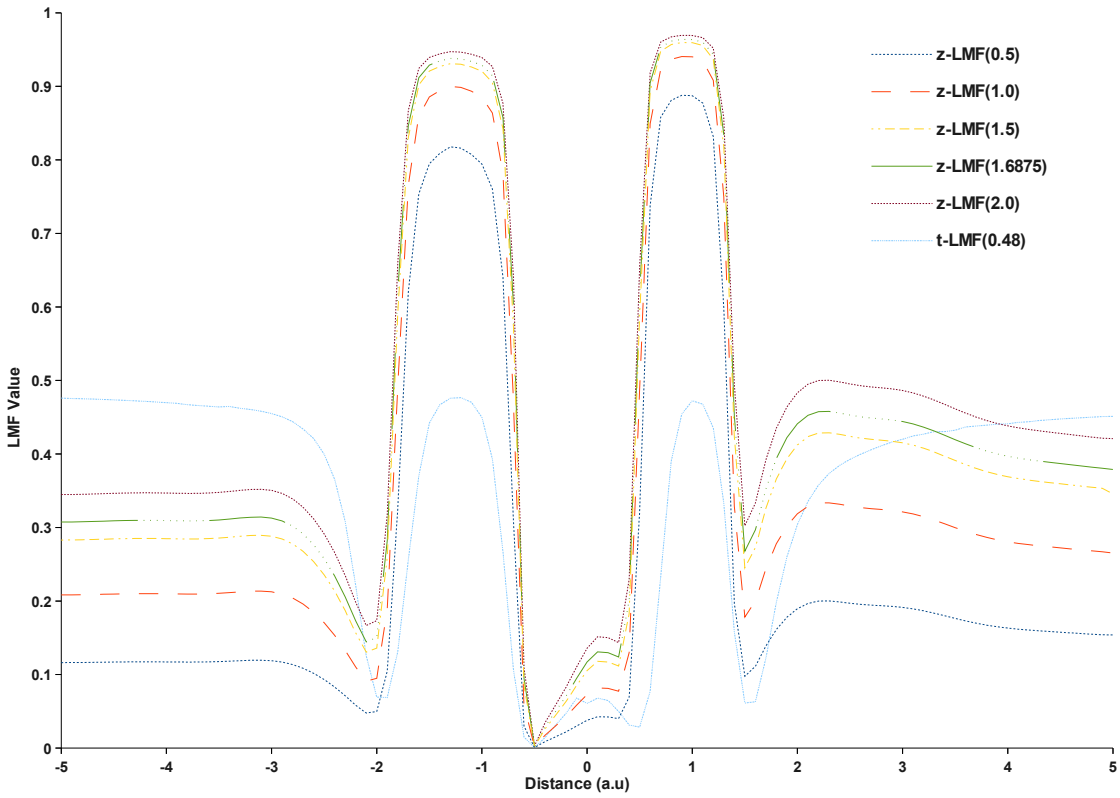

Figure 3.3: z-LMFs behaviour plotted along the bond axis in the CO Molecule (in each case the LMF parameter c value is given in parenthesis). Carbon and oxygen atomic nuclei are positioned at -1.24 and 0.93 on the x-axis at equilibrium distance.

z-LMF with different free parameters have been plotted (1D-plots along the bonding axis) for molecules F_2, and CO, to study the LMF behaviour in different regions of space. The LMF plots for all the three molecules are shown in Figures 3.2-3.4. z-LMFs (with different c parameters) attain maximum values closer to 1 near the nuclei regions. For the F_2 molecule, all LMFs have pronounced local maxima in the bonding regions whereas, this is not the case for the CN molecule. In case of the CO molecule, local maxima are found in the bonding region for all the LMFs (linear proportionality dependence with the z-LMF parameter). The LMF plots clearly indicate that large z-LMF parameter (c), is required for better description in the bonding regions. Finally all the z-LMFs approach the value 1 asymptotically (asymptotes around 12 a.u not shown in the plots) [25, 92].

3.3 A strongly correlated local hybrid

Based upon Becke's development of a real-space strong corrrelation model (B13+strgC) [Sec.2.6], construction of a local hybrid functional with a strong correlation correction has

been carried out. The general form of a typical local hybrid functional is given as

$$E_{XC}^{lh} = E_{X}^{lh} + E_{dynC}^{sl}. \tag{3.14}$$

The local hybrid exchange term is expressed as

$$E_{X}^{Lh} = \sum_{\sigma=\alpha,\beta} \int [a_{\sigma}(\mathbf{r})\varepsilon_{X,\sigma}^{exx}(\mathbf{r}) + (1 - a_{\sigma}(\mathbf{r}))\varepsilon_{X,\sigma}^{sl}(\mathbf{r})]d\mathbf{r}, \tag{3.15}$$

and the quantity E_{dynC}^{sl} represents any suitable semi-local correlation functional which takes care of the dynamical correlation. The terms in the local hybrid exchange are the semi-local exchange energy density $\varepsilon_{X,\sigma}^{sl}(\mathbf{r})$, exact-exchange energy density $\varepsilon_{X,\sigma}^{exx}(\mathbf{r})$, and $a_{\sigma}(\mathbf{r})$ is a suitable local mixing function (LMF). On reformulation of the local hybrid exchange energy expression, we have

$$E_{X}^{Lh} = E_{X}^{exx} + \sum_{\sigma=\alpha,\beta} \int [(1 - a_{\sigma}(\mathbf{r}))(\varepsilon_{X,\sigma}^{sl}(\mathbf{r}) - \varepsilon_{X,\sigma}^{exx}(\mathbf{r}))]d\mathbf{r}, \tag{3.16}$$

where the static correlation may be defined as

$$E_{statC}^{Lh} = \sum_{\sigma=\alpha,\beta} \int [(1 - a_{\sigma}(\mathbf{r}))(\varepsilon_{X,\sigma}^{sl}(\mathbf{r}) - \varepsilon_{X,\sigma}^{exx}(\mathbf{r}))]d\mathbf{r}. \tag{3.17}$$

Formally the above static correlation term only includes parallel-spin contributions. Switching from spin-channel LMFs to common LMFs (which contains cross-spin terms) allows to mimic better some of the opposite-spin static correlation. The formal static correlation of local hybrids with common LMFs is given by

$$E_{statC}^{Lh} = \int [(1 - a(\mathbf{r})) \sum_{\sigma=\alpha,\beta} (\varepsilon_{X,\sigma}^{sl}(\mathbf{r}) - \varepsilon_{X,\sigma}^{exx}(\mathbf{r}))]d\mathbf{r}. \tag{3.18}$$

On comparison with the B13 model, E_{statC}^{Lh} replaces E_{statC}^{B05}, whereas a general E_{dynC}^{sl} replaces the particular semi-local E_{dynC}^{B88}. The strong-correlation corrected local hybrid functional is expressed as

$$E_{XstrgC}^{Lh} = E_{XC}^{lh} + \Delta E_{strgC}^{Lh}. \tag{3.19}$$

The formulation of a strong-correlation correction is analogous to the B13 model, except that the correlation contributions are not separated in the same fashion as in the B13 model. Moreover in the B13 model only potential energy contributions are employed. Allowing different weights for the static and dynamic correlation energy densities, and

after transformation of the potential energy density terms using the "adiabatic connection" formula [22], the correction term is given by:

$$\Delta E^{Lh}_{strgC} = \sum_{n=2}^{N} \tilde{c}_n \int \tilde{x}^n(\mathbf{r}) \tilde{\varepsilon}^{Lh}_C(\mathbf{r}) d\mathbf{r}, \tag{3.20}$$

where

$$\tilde{x}(\mathbf{r}) = \frac{\varepsilon^{Lh}_{statC}(\mathbf{r})}{\varepsilon^{Lh}_{statC}(\mathbf{r}) + d\varepsilon^{sl}_{dynC}(\mathbf{r})},\ \tilde{\varepsilon}^{Lh}_C(\mathbf{r}) = \varepsilon^{Lh}_{statC}(\mathbf{r}) + d\varepsilon^{sl}_{dynC}(\mathbf{r}),\ d = \frac{a_{statC}}{a_{dynC}},\ \text{and}\ \tilde{c}_n = \frac{c_n}{a_{statC}}. \tag{3.21}$$

The above expression is the final form of a strong-correlation correction with two parameters d and $\tilde{c}_n$ (needed to be optimised based on further studies).

3.3.1 Implementation details

The implementation of a strong-correlation correction for local hybrid functionals has been carried out in a local version of the Turbomole program in post-SCF manner. Two new sub-routines (for closed- and open-shell cases) have been added consisting of all the terms needed for the strong-correlation correction. Detailed discussion on computations and results with this type of functional are provided in Chapter 6.

Chapter 4

Assessment of *s-d* Transfer Energies for 3*d*-Transition-Metal Atoms

s-d Transfer energies serve as a good benchmark for the XC approximations in DFT [Sec.2.7]. Preliminary tests (post-SCF calculations) had been carried out using local hybrid functionals with different local mixing functions (normal and spin-polarised) [93] as they are expected to provide a reasonable balance between non-dynamical correlation and minimisation of self-interaction errors. While post-SCF computations usually are not too far from self-consistent ones, in the present case self-consistent (SCF) computations are important as *s-d* transfer energies turn out to be very sensitive to the orbitals used. Therefore SCF computations with local hybrids have been carried out on 3*d*-transition-metal atoms for the excitation energies, using the formalisms discussed earlier [Sec.2.7]. Previously, extensive studies have been carried out on the performance of B3LYP functional for the excitation energies [23, 77, 87]. These studies suggest that the B3LYP reproduces the qualitative features of experimental trends and also hint that for good estimation of *s-d* transfer energies considerable amount of exact-exchange (EXX) is needed which can provide a balanced description of *s* and *d* orbitals. Therefore computations have also been carried out with the B3LYP functional for comparison purposes.

All computations have been carried out using local versions of Turbomole program modified (TBM5.10 by Hilke Bahmann and Alexei Arbuznikov) for local hybrid implementations [91]. Results obtained using LDA based local hybrid functionals with different LMFs such as *t*-LMF, *s*-LMF, *r*-LMF, and common *t*-LMF using a numerically evaluated

potential are reported here [Sec.2.4.1]. Three different local hybrids,namely LRSR1, LRSR2, and LRSR3 [Sec.2.4.2], constructed using a range-separated LSDA correlation functional with partial self-interaction correction and common *t*-LMF have also been tested [58]. In all these computations quadruple zeta valence plus polarization (QZVP) quality basis sets have been used.

4.1 Furche-Perdew formalism

For the FP formalism, values of Mean signed errors (MSE) and mean average errors (MAE) obtained for different functionals are tabulated (Tables 4.1 and 4.2). The experimental values are corrected for relativistic effects [23, 80, 93] to allow comparison with the present nonrelativistic computations (reference values).

Atom	Excitations	Reference Values	B3LYP	*t*-LMF (0.48)	*s*-LMF (0.22)	*r*-LMF (1.1275,0.01625)
Ca	$d^0s^2(^1S)$ - $d^1s^1(^3D)$	2.44	1.88	1.77	1.64	1.78
Sc	$d^1s^2(^2D)$ - $d^2s^1(^4F)$	1.33	0.68	0.47	0.34	0.50
Ti	$d^2s^2(^3F)$ - $d^3s^1(^5F)$	0.69	0.22	-0.13	-0.28	-0.09
V	$d^3s^2(^4F)$ - $d^4s^1(^6D)$	0.11	-0.16	-0.72	-0.85	-0.68
Cr	$d^4s^2(^5D)$ - $d^5s^1(^7S)$	-1.17	-1.44	-2.05	-2.15	-1.97
Mn	$d^5s^2(^6S)$ - $d^6s^1(^6D)$	1.97	1.48	1.38	1.35	1.45
Fe	$d^6s^2(^5D)$ - $d^7s^1(^5F)$	0.65	0.18	0.05	-0.15	0.13
Co	$d^7s^2(^4F)$ - $d^8s^1(^4F)$	0.17	-0.09	-0.32	-0.60	-0.16
Ni	$d^8s^2(^3F)$ - $d^9s^1(^3D)$	-0.33	-0.31	-0.72	-0.99	-0.48
Ni	$d^9s^1(^3D)$ - $d^{10}(^1S)$	1.57	1.73	1.55	1.37	1.76
Cu	$d^9s^2(^2D)$ - $d^{10}s^1(^2S)$	-1.85	-1.86	-2.25	-2.50	-1.94
MSE			-0.30	-0.60	-0.76	-0.48
MAE			0.33	0.60	0.76	0.51

Table 4.1: *s-d* Transfer energies (eV) using the Furche-Perdew formalism. The experimental values are corrected for relativistic effects. Here different local hybrid functionals are represented by the LMFs with the values of LMF parameters in parenthesis.

Atom	Excitations	Reference Values	common *t*-LMF (0.534)	LRSR1	LRSR2	LRSR3
Ca	$d^0s^2(^1S)$ - $d^1s^1(^3D)$	2.44	1.80	2.14	2.14	2.14
Sc	$d^1s^2(^2D)$ - $d^2s^1(^4F)$	1.33	0.47	0.80	0.78	0.72
Ti	$d^2s^2(^3F)$ - $d^3s^1(^5F)$	0.69	-0.08	0.19	0.18	0.22
V	$d^3s^2(^4F)$ - $d^4s^1(^6D)$	0.11	-0.66	-0.36	-0.30	-0.37
Cr	$d^4s^2(^5D)$ - $d^5s^1(^7S)$	-1.17	-2.01	-1.78	-1.31	-1.43
Mn	$d^5s^2(^6S)$ - $d^6s^1(^6D)$	1.97	1.50	1.59	1.56	1.65
Fe	$d^6s^2(^5D)$ - $d^7s^1(^5F)$	0.65	0.08	0.24	0.23	0.30
Co	$d^7s^2(^4F)$ - $d^8s^1(^4F)$	0.17	-0.22	-0.26	-0.27	-0.24
Ni	$d^8s^2(^3F)$ - $d^9s^1(^3D)$	-0.33	-0.59	-0.70	-0.69	-0.68
Ni	$d^9s^1(^3D)$ - $d^{10}(^1S)$	1.57	1.69	1.52	1.50	1.53
Cu	$d^9s^2(^2D)$ - $d^{10}s^1(^2S)$	-1.85	-2.16	-2.20	-2.20	-2.19
MSE			-0.52	-0.40	-0.35	-0.35
MAE			0.54	0.40	0.35	0.35

Table 4.2: *s-d* Transfer energies (eV) using the Furche-Perdew formalism. The experimental values are corrected for relativistic effects. LRSR1, LRSR2, and LRSR3 are three different local hybrids constructed using the range-separated LSDA correlation functional and the common *t*-LMF.

The results obtained clearly show that B3LYP is the best performing functional among the tested ones with MAE and MSE values -0.30 eV and 0.33 eV respectively. Studies on the performance of B3LYP functional for the *s-d* transfer energies suggest that even though errors are large, the experimental trends are remarkably well reproduced [87, 94, 95]. But

in the case of V and Co atoms, even the sign of computed excitation energies is predicted to be opposite to that of the experimental ones. MSEs and MAEs obtained using different local hxbrids are larger in comparison to the ones obtained with B3LYP functional. The main source of errors for these functionals is the wrong prediction of the ground state in Ti, V, and Co atoms. For other atoms such as Cr, Ni($^3D - {}^1S$), and Cu, the computed values have the same sign as the experimental ones but suffer from overestimation (more positive or more negative values than the experimental ones). The MSEs and MAEs obtained using local hybrids with range-separated correlation functionals are very close in magnitude to the B3LYP ones. Local hybrid functionals constructed with range-separated LSDA correlation give much better values than B3LYP for cases such as Ca, Sc, Mn, Fe, and Ni($^3D - {}^1S$). This could be due to the self-interaction reduction in the short-range correlation which gives larger *s* and *d* orbital separations [23]. However in the case of Ca, Sc, Mn, and Fe atoms for all the functionals considered, there is an underestimation on an average of 0.5 eV. Also all the tested functionals fail to predict the correct ground state for V and Co atoms. This could be mainly due to presence of several low-lying states which needs very good simulation of non-dynamical correlation (NDC) by the XC approximations. One approach of solving this problem is by performing computations using local hybrids constructed with more advanced exchange and correlation functionals [29] which are expected to be needed for proper handling of simulation of the NDC and reduction in the SIE. There are also broken-symmetry approaches developed for suspect multi-determinant states which are utilized for the *s-d* transfer energy computations and discussed in detail below.

4.2 Broken-symmetry approaches

The functionals tested are the same as those tested for the Furche-Perdew formalism. Full minimisation of the wavefunction has been carried out with C_1 symmetry constraint. In addition to the excitations considered for the Furche-Perdew formalism, five more excitations involving the IMD states of Cr, Fe, Co, and Ni atoms have also been considered (Table 4.3) [24]. Experimental values are corrected for the relativistic effects [80, 81, 96] and the spin-orbit couplings are averaged out using the degeneracy-weighted formula [95]. Due to the relativistic correction the reference value of Ni($d^8s^2(^3F) - d^9s^1(^1D)$) transition differs (goes from 0.3 eV to -0.05 eV) from the one reported in ref.[24].

Atom	Excitations	Reference Values
Ca	$d^0s^2(^1S)$ - $d^1s^1(^3D)$	2.42
Sc	$d^1s^2(^2D)$ - $d^2s^1(^4F)$	1.30
Ti	$d^2s^2(^3F)$ - $d^3s^1(^5F)$	0.66
V	$d^3s^2(^4D)$ - $d^4s^1(^6D)$	0.07
Cr	$d^4s^2(^5D)$ - $d^5s^1(^7S)$	-1.20
Cr	$d^4s^2(^5D)$ - $d^5s^1(^5S)$	-0.27
Mn	$d^6s^2(^4D)$ - $d^6s^1(^6D)$	1.93
Fe	$d^6s^2(^5D)$ - $d^7s^1(^5F)$	0.61
Fe	$d^6s^2(^5D)$ - $d^7s^1(^3F)$	1.24
Co	$d^7s^2(^4F)$ - $d^8s^1(^4F)$	0.11
Co	$d^7s^2(^4F)$ - $d^8s^1(^2F)$	0.58
Ni	$d^8s^2(^3F)$ - $d^9s^1(^3D)$	-0.38
Ni	$d^9s^1(^3D)$ - $d^{10}(^1S)$	1.49
Ni	$d^8s^2(^3F)$ - $d^9s^1(^1D)$	-0.05
Ni	$d^9s^1(^1D)$ - $d^{10}(^1S)$	1.21
Cu	$d^9s^2(^2D)$ - $d^{10}s^1(^2S)$	-1.90

Table 4.3: *s-d* Transfer energies (eV) for states including the IMD excitations. The reference values are corrected for relativstic effects and the spin-orbit couplings are averaged out.

4.2.1 Variational method

Computations have been carried out for all the excitations given in Table 4.3. The list also includes excitations involving the IMD states for the atoms Cr, Fe, Co, and Ni. For verifying the lowest-energy solutions, calculations have been performed starting with several different initial guesses. The excitation energies are tabulated below.

Atom	Excitations	Reference Values	B3LYP	*t*-LMF (0.48)	*s*-LMF (0.22)	*r*-LMF (1.1275,0.01625)
Ca	$d^0s^2(^1S)$ - $d^1s^1(^3D)$	2.42	1.91	1.67	1.64	1.68
Sc	$d^1s^2(^2D)$ - $d^2s^1(^4F)$	1.30	0.73	0.52	0.34	0.33
Ti	$d^2s^2(^3F)$ - $d^3s^1(^5F)$	0.66	0.22	-0.13	-0.28	-0.09
V	$d^3s^2(^4D)$ - $d^4s^1(^6D)$	0.07	-0.22	-0.77	-0.85	-0.73
Cr	$d^4s^2(^5D)$ - $d^5s^1(^7S)$	-1.20	-1.45	-2.04	-2.15	-1.97
Cr	$d^4s^2(^5D)$ - $d^5s^1(^5S)$	-0.27	-0.66	-0.92	-0.98	-0.77
Mn	$d^6s^2(^4D)$ - $d^6s^1(^6D)$	1.93	1.51	1.39	1.35	1.45
Fe	$d^6s^2(^5D)$ - $d^7s^1(^5F)$	0.61	0.27	0.02	-0.12	0.17
Fe	$d^7s^2(^5D)$ - $d^7s^1(^3F)$	1.24	0.70	0.62	0.32	0.56
Co	$d^7s^2(^4F)$ - $d^8s^1(^4F)$	0.11	-0.09	-0.32	-0.60	-0.16
Co	$d^8s^2(^2F)$ - $d^8s^1(^4F)$	0.58	0.19	-0.20	-0.33	0.25
Ni	$d^8s^2(^3F)$ - $d^9s^1(^3D)$	-0.38	-0.39	-0.78	-0.94	-0.56
Ni	$d^9s^1(^3D)$ - $d^{10}(^1S)$	1.49	1.82	1.62	1.77	1.84
Ni	$d^8s^2(^3F)$ - $d^9s^1(^1D)$	-0.05	-0.26	-0.62	-0.76	-0.38
Ni	$d^9s^1(^1D)$ - $d^{10}(^1S)$	1.21	1.68	1.46	1.62	1.66
Cu	$d^9s^2(^2D)$ - $d^{10}s^1(^2S)$	-1.90	-1.87	-2.22	-2.50	-1.95
MSE			-0.23	-0.53	-0.64	-0.41
MAE			0.34	0.58	0.73	0.51

Table 4.4: *s-d* Transfer energies (eV) using the variational approach.The reference values are corrected for relativistic effects and spin-orbit couplings are averaged out. Here different local hybrid functionals are represented by the LMFs with the values of LMF parameters in parenthesis.

Atom	Excitations	Reference Values	common *t*-LMF (0.534)	LRSR1	LRSR2	LRSR3
Ca	$d^0s^2(^1S)$ - $d^1s^1(^3D)$	2.42	1.79	1.80	1.80	1.84
Sc	$d^1s^2(^2D)$ - $d^2s^1(^4F)$	1.30	0.73	0.86	0.84	0.72
Ti	$d^2s^2(^3F)$ - $d^3s^1(^5F)$	0.66	0.11	0.19	0.18	0.22
V	$d^3s^2(^4D)$ - $d^4s^1(^6D)$	0.07	-0.49	-0.42	-0.43	-0.37
Cr	$d^4s^2(^5D)$ - $d^5s^1(^7S)$	-1.20	-1.74	-1.69	-1.68	-1.63
Cr	$d^4s^2(^5D)$ - $d^5s^1(^5S)$	-0.27	-0.80	-0.77	-0.79	-0.80
Mn	$d^6s^2(^4D)$ - $d^6s^1(^6D)$	1.93	1.46	1.59	1.56	1.62
Fe	$d^6s^2(^5D)$ - $d^7s^1(^5F)$	0.61	0.24	0.25	0.30	0.30
Fe	$d^7s^2(^5D)$ - $d^7s^1(^3F)$	1.24	0.73	0.50	0.50	0.53
Co	$d^7s^2(^4F)$ - $d^8s^1(^4F)$	0.11	-0.31	-0.26	-0.27	-0.24
Co	$d^8s^2(^2F)$ - $d^8s^1(^4F)$	0.58	-0.02	0.04	0.03	0.04
Ni	$d^8s^2(^3F)$ - $d^9s^1(^3D)$	-0.38	-0.79	-0.76	-0.76	-0.68
Ni	$d^9s^1(^3D)$ - $d^{10}(^1S)$	1.49	1.54	1.58	1.57	1.53
Ni	$d^8s^2(^3F)$ - $d^9s^1(^1D)$	-0.05	-0.65	-0.62	-0.63	-0.62
Ni	$d^9s^1(^1D)$ - $d^{10}(^1S)$	1.21	1.40	1.45	1.43	1.44
Cu	$d^9s^2(^2D)$ - $d^{10}s^1(^2S)$	-1.90	-2.23	-2.20	-2.20	-2.19
MSE			-0.43	-0.39	-0.40	-0.38
MAE			0.46	0.43	0.44	0.42

Table 4.5: *s-d* Transfer energies (eV) using the variational approach. The experimental values are corrected for relativistic effects and the spin-orbit couplings are averaged out. LRSR1, LRSR2, and LRSR3 are three different local hybrids constructed using the range-separated LSDA correlation functional and the common *t*-LMF [ref. Sec.2.4.2.].

The results obtained are very similar to the Furche-Perdew formalism for all the excitations involving NSD states. This is due to both methodologies having the same procedure for the NSD states except for the symmetry difference (O_h VS C_1) used for computations. In case of excitations involving the IMD states, for the Cr atom all functionals yielded significantly too negative values whereas in the case of the Fe-atom IMD states, the trend is reversed. For the Co atom, B3LYP and the *r*-LMF values obtained are closer to the experimental ones whereas the other functionals (*t*-LMF, *s*-LMF, and common *t*-LMF) give values with opposite sign. In the case of Ni, local hybrids with range-separated functionals and common *t*-LMF show better results than the B3LYP functional for the Ni($(^1D) - (^1S)$) excitation, but in the case of the Ni($(^3F) - (^1D)$) excitation B3LYP outperforms all other functionals. Out of all possible excitations involving the IMD states, the Co atom is the most complicated case (*t*-LMF, *s*-LMF, and the common *t*-LMF do not predict the correct order of states). In general for the IMD states, the variational method gives results which are farther from the experimental ones than the broken-symmetry methods discussed below.

4.2.2 Weighted-average broken-symmetry approach (WABS)

For WABS calculations only those atoms with excitations involving IMD states have been considered. Several computations have been carried out with different possibilities for both the NSD and IMD states to ensure the lowest-energy solutions. The results are tabulated below.

Atom	Excitations	Reference Values	B3LYP	*t*-LMF (0.48)	*s*-LMF (0.22)	*r*-LMF (1.1275,0.01625)
Cr	$d^4s^2(^5D)$ - $d^5s^1(^5S)$	-0.27	-0.51	-0.70	-0.62	-0.52
Fe	$d^7s^2(^5D)$ - $d^7s^1(^3F)$	1.24	0.86	0.84	0.71	0.75
Co	$d^8s^2(^2F)$ - $d^8s^1(^4F)$	0.58	0.34	0.27	0.23	0.47
Ni	$d^8s^2(^3F)$ - $d^9s^1(^1D)$	-0.05	-0.12	-0.45	-0.54	-0.19
Ni	$d^9s^1(^1D)$ - $d^{10}(^1S)$	1.21	1.55	1.28	1.42	1.46
MSE			-0.12	-0.29	-0.30	-0.15
MAE			0.25	0.32	0.39	0.25

Table 4.6: *s-d* Transfer energies (eV) using the WABS method. The experimental values are corrected for relativistic effects and the spin-orbit couplings are averaged out. Here different local hybrid functionals are represented by the LMFs with the values of LMF parameters in parenthesis.

Atom	Excitations	Reference Values	common *t*-LMF (0.534)	LRSR1	LRSR2	LRSR3
Cr	$d^4s^2(^5D)$ - $d^5s^1(^5S)$	-0.27	-0.61	-0.64	-0.62	-0.63
Fe	$d^7s^2(^5D)$ - $d^7s^1(^3F)$	1.24	0.99	0.67	0.67	0.69
Co	$d^8s^2(^2F)$ - $d^8s^1(^4F)$	0.58	0.17	0.20	0.20	0.19
Ni	$d^8s^2(^3F)$ - $d^9s^1(^1D)$	-0.05	-0.49	-0.48	-0.48	-0.51
Ni	$d^9s^1(^1D)$ - $d^{10}(^1S)$	1.21	1.25	1.30	1.29	1.33
MSE			-0.28	-0.33	-0.33	-0.33
MAE			0.30	0.37	0.36	0.38

Table 4.7: *s-d* Transfer energies (eV) using the WABS method.The reference values are corrected for relativistic effects and the spin-orbit couplings are averaged out. LRSR1, LRSR2, and LRSR3 are three different local hybrids constructed using the range-separated LSDA correlation functional and the common *t*-LMF [ref. Sec.2.4.2.].

The results obtained using the WABS formalism clearly show an improvement over the variational method (comparing only with excitations involving the IMD states from the variational method). The B3LYP and *r*-LMF functionals, exhibit the lowest MAEs and MSEs, and all the other tested functionals also have the correct sign. That is, for the Co-atom excitation, local hybrids with *t*-LMF, *s*-LMF, and common *t*-LMF exhibit change in the order of states compared to the variational method. In case of the Ni excitations, the trend is very similar to the variational method, but the values are improved.

4.2.3 Reinterpreted broken-symmetry approach (RBS)

This approach is mainly important in the case of Fe, Co, and Ni atoms, due to different orbitals for the NSD and PSCF states. In case of the Cr atom both the NSD and PSCF states have the same set of orbitals. The results are tabulated below.

Atom	Excitations	Reference Values	B3LYP	*t*-LMF (0.48)	*s*-LMF (0.22)	*r*-LMF (1.1275,0.01625)
Cr	$d^4s^2(^5D)$ - $d^5s^1(^5S)$	-0.27	-0.52	-0.73	-0.62	-0.58
Fe	$d^7s^2(^5D)$ - $d^7s^1(^3F)$	1.24	0.94	0.93	0.58	0.66
Co	$d^8s^2(^2F)$ - $d^8s^1(^4F)$	0.58	0.31	0.22	0.18	0.32
Ni	$d^8s^2(^3F)$ - $d^9s^1(^1D)$	-0.05	-0.20	-0.59	-0.74	-0.48
Ni	$d^9s^1(^1D)$ - $d^{10}(^1S)$	1.21	1.63	1.42	1.65	1.75
MSE			-0.11	-0.29	-0.33	-0.21
MAE			0.28	0.38	0.51	0.42

Table 4.8: *s-d* Transfer energies (eV) using the RBS method. The experimental values are corrected for relativistic effects and the spin-orbit couplings are averaged out. Here different local hybrid functionals are represented by the LMFs with the values of LMF parameters in parenthesis.

Atom	Excitations	Reference Values	common *t*-LMF (0.534)	LRSR1	LRSR2	LRSR3
Cr	$d^4s^2(^5D)$ - $d^5s^1(^5S)$	-0.27	-0.62	-0.66	-0.63	-0.64
Fe	$d^7s^2(^5D)$ - $d^7s^1(^3F)$	1.24	0.86	0.71	0.70	0.68
Co	$d^8s^2(^2F)$ - $d^8s^1(^4F)$	0.58	0.13	0.16	0.14	0.13
Ni	$d^8s^2(^3F)$ - $d^9s^1(^1D)$	-0.05	-0.61	-0.59	-0.59	-0.60
Ni	$d^9s^1(^1D)$ - $d^{10}(^1S)$	1.21	1.37	1.42	1.40	1.43
MSE			-0.32	-0.33	-0.34	-0.34
MAE			0.38	0.42	0.41	0.43

Table 4.9: *s-d* Transfer energies (eV) using the RBS method. The experimental values are corrected for relativistic effects and the spin-orbit couplings are averaged out. LRSR1, LRSR2, and LRSR3 are three different local hybrids constructed using the range-separated LSDA correlation functional and the common *t*-LMF [ref. Sec.2.4.2.].

In this procedure, the excitation energies for Cr do not vary much from the WABS results due to the presence of same set of orbitals for the NSD and PSCF states. In case of Fe, the results do change, but very slightly (on the order of 0.05-0.1 eV) for all the functionals due to energetically very close IMD and PSCF states for Fe. For the Co atom, the results are underestimated in comparison to the WABS approach due to the energy difference between the IMD and PSCF states. In the case of Ni, the excitation energies are overestimated (more negative in case of $d^8s^2(^3F) - d^9s^1(^1D)$ and more positive in case of $d^9s^1(^1D) - d^{10}(^1S)$ excitations) due to the slightly wider energy gap between the

IMD and PSCF states. The reason for Co and Ni atomic states having a wide energy gap is the spin-flip which creates PSCF states with very high energies. Studies by Truhlar and co-workers [24] reported that certain functionals can increase the energy gap by 50-100 kcal/mol, and therefore broken-symmetry approaches should not applied to these kind of systems.

4.3 Conclusions

The Furche-Perdew formalism invokes a complicated symmetry-constrained approach for the balanced description of non-dynamical correlation for multi-determinantal states. In this formalism the B3LYP performs somewhat better than the local hybrid functionals studied here. However, the results obtained using local hybrids with range-separated correlation (along with common *t*-LMF) are comparable to those of the B3LYP, due to large EXX admixture. For atomic systems Ti, V, and Co, the Furche-Perdew formalism fails to predict the correct order of the states due to their multi-determinantal ground state character. For Ca, Sc, Mn, and Fe atom cases, all functionals tested using this formalism underestimate these values by 0.5 eV on an average.

The variational method gives results very similar to the Furche-Perdew formalism for excitations involving NSD states. Along with the B3LYP functional, good results have been obtained using local hybrids with range-separated correlation functionals and the common *t*-LMF. Similar to the Furche-Perdew formalism, the major discrepancies arise in the case of the Co atom for all tested functionals (the sign of the excitation energies is wrongly predicted). For the IMD excitations, the variational method gives values with large errors.

Broken-symmetry approaches offer another way of dealing with the non-dynamical correlations in multi-determinantal cases. In these approaches, for excitations involving IMD states, results obtained using the WABS approach are better in comparison to the variational approach. The values for the Fe atom excitations are still underestimated (0.3 eV). In case of Co, the results are very much improved and B3LYP predicts a value closer to the experimental ones. Local hybrids with range-separated correlation perform better than the B3LYP functional for the Ni($d^9s^1(^1D) - d^{10}(^1S)$) excitation.

Finally computations have been carried out using the RBS approach where an artificial

state is obtained (denoted as PSCF) by flipping the spin of the singly occupied orbital in the IMD state. This makes sure that both the IMD and PSCF states have the same orbitals. The results obtained are very similar to the results from the WABS approach except for Co and Ni, as expected due to the different orbitals involved. As explained above, the RBS and the WABS methods have different orbitals for NSD states only for Fe and Co cases. In this sense both methods are quite similar, except that the RBS is physically more justified than the WABS. The above studies suggest that the RBS and WABS approaches are very important for resolving broken-symmetry problems and should be applied for appropriate cases. Also further development of local hybrids with more refined exchange and correlation functionals [29] will be advantageous for the computation of *s*-*d* transfer energies of the transition-metal atoms.

Chapter 5

Evaluation of Fractional Charge Behaviour for Local Hybrid Functionals

The concept of fractional charges in DFT has been introduced to discuss the stepwise-linearity of the total energy for the exact functional [Sec.2.5]. Fractional charges can be observed in ensembles or open systems where electrons can be exchanged with the environment [17, 18, 97]. Fractional charges in DFT provide an efficient assessment for the delocalisation error of the XC functional. Delocalisation error is the tendency of the XC functional to over delocalise the added charge resulting in the convex behavior of the total energy. Such a delocalisation resulting in the convex behaviour corresponds to the deviation from the stepwise-linearity of the energy. This is also related to the self-interaction error (SIE), central to DFT with approximate XC functionals [12, 46, 98]. The SIE for one-electron is defined exactly, but there is an ambiquity regarding its definition for the many-electron case. A many-electron self-interaction free functional can be understood as one which gives not only exact linearity of the total energy between integer numbers but also accurate energies at the integer numbers [12, 66, 99]. The SIE of density functionals is responsible for problems in the computation of band gaps, reaction barriers, and charge-transfer excitation energies. The other exact condition related to stepwise-linearity condition is the ionisation potential (IP) theorem [28, 74]. This states that the highest occupied KS eigenvalue should be equal to the negative of the ionisation potential. This requires the correct asymptotic behavior of the XC potential i.e. $V_{xc} \rightarrow -\frac{1}{r}$ as $r \rightarrow \infty$. Unfortunately, many density functional approximations do not satisfy the above mentioned

conditions and these deficiencies are connected to common failures of density functional approximations [67, 100, 101].

Previously, local hybrid functionals and range-separated local hybrids have been tested for stepwise-linearity of the energy to assess delocalisation errors [102]. Performance of these functionals for delocalisation errors (also referred to as integrated many-electron self-interaction errors) has been found to be satisfactory. In this perspective, assessement of other local hybrid functionals (constructed using common *t*-LMF and range-separated correlation functionals [56–58]) for the stepwise-linearity of the ground state and its extension to low-lying excited states have been carried out in this chapter. Implications of stepwise-linearity on the fundamental band gap, derivative discontinuity, and the IP theorem have already been explained [Sec.2.5]. For further assessment, studies related to the fundamental band gaps computed using the energy differences (integer gap) and the derivative differences (derivative gap) are also carried out. In the last section, validation of the IP theorem is performed by studying the behaviour of frontier orbital energies with regard to the fractional electron numbers [68, 103].

5.1 Tests of systems for fractional electron number

Computations have been carried out with fractional electron numbers for the assessment of stepwise-linearity of the ground and lowest-energy excited states for different spin/spatial symmetry. A local version of Turbomole program (modified for local hybrid implementations) have been used for carrying out all the computations [91, 104]. Atomic systems like carbon, oxygen, vanadium, and copper have been considered for testing. The $\mathbf{CH_2}$ molecule (both the triplet and singlet states), which has been studied extensively using highly correlated methods [67, 105], is also considered for testing. Local hybrid functionals based on LSDA exchange and VWN correlations along with *t*-LMF (with LMF parameters 0.48, 0.70, and 1.0), *s*-LMF(0.22), *r*-LMF(1.1275,0.01625), and common *t*-LMF with LMF parameter value 0.534 (denoted as com-*t*-LMF(0.534)) [Sec.2.4.1] have been tested. Local hybrid functionals constructed using LSDA exchange and range-separated correlation functional (denoted as LRSR1, LRSR2, LRSR3 depending on the parameters) along with the common *t*-LMF have also been assessed [Sec.2.4.2]. Recently proposed self-interaction-free local hybrid functional using Kümmel-LMF (denoted as *z*-LMF(1.6785) in the Figures) along with the self-interaction corrected correlation functional also been as-

sessed for fractional charge behaviour [Sec.3.2] [25]. Self-consistent (SCF) computations have been performed (except in the case of local hybrid with z-LMF and self-interaction corrected correlation [Sec.3.2]) using a numerical potential with no spherical symmetry constraint. Basis sets aug-cc-pV5Z have been used in case of the atomic systems and the QZVP (uncontracted) basis sets for the $\mathbf{CH}_2$ molecule. The energies for each system have been computed by varying the electron number in steps of 0.1. Always the spin orbital with highest energy (HOMO) is occupied fractionally [76]. For every tested functional, the exact behaviour has been constructed by straight-line interpolation of the energy values obtained at integer points. Deviations from the stepwise-linearity of energy for different functionals have been plotted against the electron number of the system. The computational procedure is elaborated using the carbon atom as test case.

5.1.1 Carbon

The ground-state electronic configuration is $1s^2 2s^2 2p^2$, corresponding to an open shell triplet (^3P). C_1 symmetry is used in all computations on the carbon atom. Starting with the neutral carbon atom, the number of electrons is varied such that it results in an anionic (^2S) and a cationic (^2P) state. The plots for the ground-state energy difference versus the electron number for different functionals are shown in Figures 5.1 and 5.2. The figures clearly show that all the tested functionals exhibit almost a straight line behaviour going from the electron number 5 to 6. From neutral atom to anion all density functionals shows convex behaviour whereas the HF method displays concave behaviour.

Deviation values obtained are the true measure of delocalisation error for the tested functionals. They are shown in Figures 5.3 and 5.4. The plots clearly show that local hybrid with t-LMF(1.0) gives the minimum deviation from the exact behaviour. This is due to 100 exact-exchange admixture in the exchange energy which balances out the localisation and delocalisation behaviours. As stated earlier HF shows the opposite behaviour to the DFT functionals. There is also a clear trend of deviations getting lower as the average amount of exact-exchange admixture increases. Usually the magnitude of deviations are larger in the cationic part (even though they show almost straight line behaviour) in comparison with the values for 6 to 7 due to large energy differences (magnitude of IP values are generally greater than the EA values). Local hybrid functionals with t-LMF(0.70), s-LMF(0.22), and the ones with range-separated correlation functional (LRSR1, LRSR2, LRSR3) give deviations very close to each other (with the curves sometimes even overlapping). Among

the functionals using range-separated correlation, LRSR3 is the one with low deviation values due to the large prefactor for the *t*-LMF and full eliminination of self-interaction in the short-range correlation functional [Sec.2.4.2].

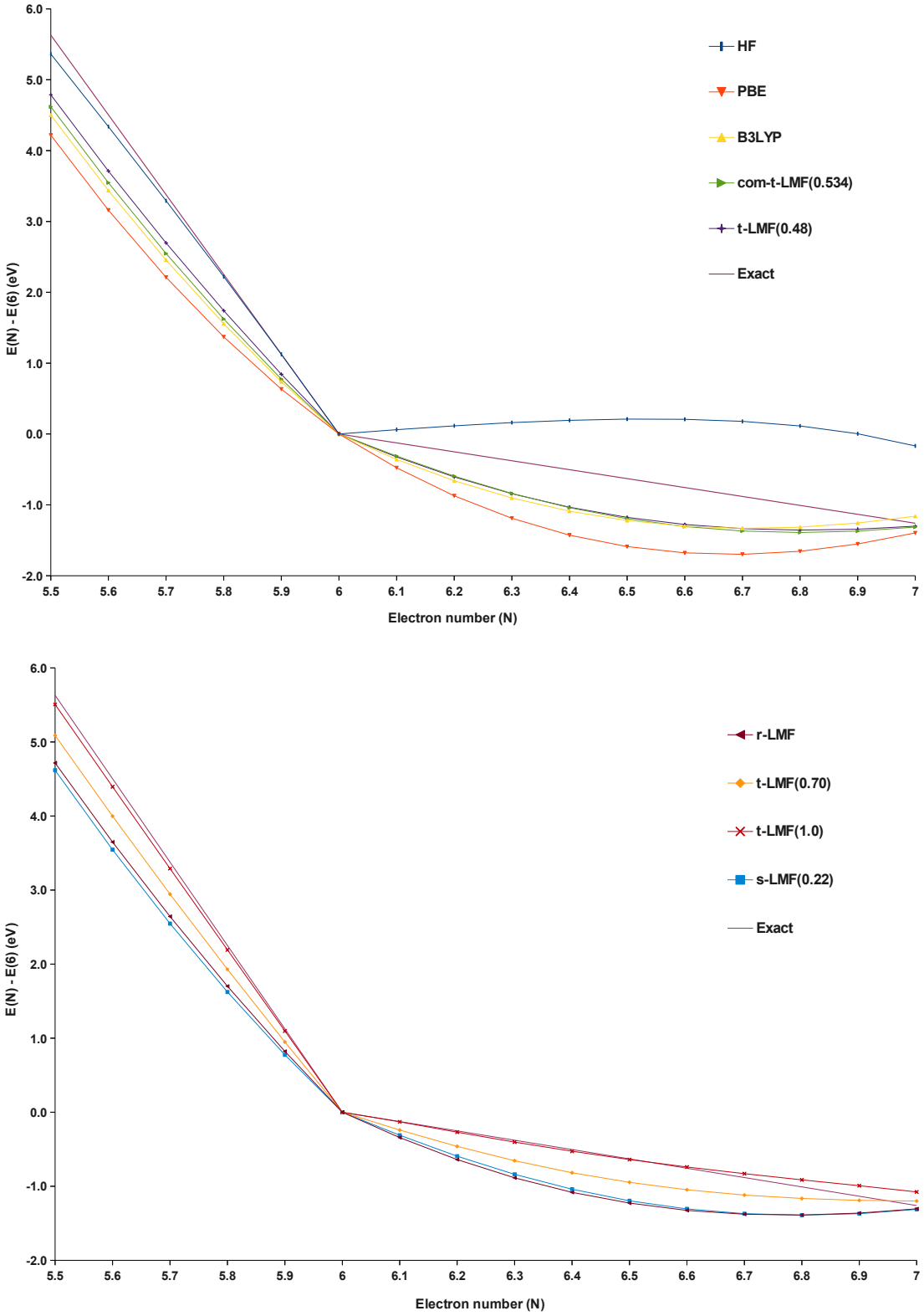

Figure 5.1: Electronic energies of carbon (^3P) versus electron number. The exact curve is based on the experimental IP and EA values.

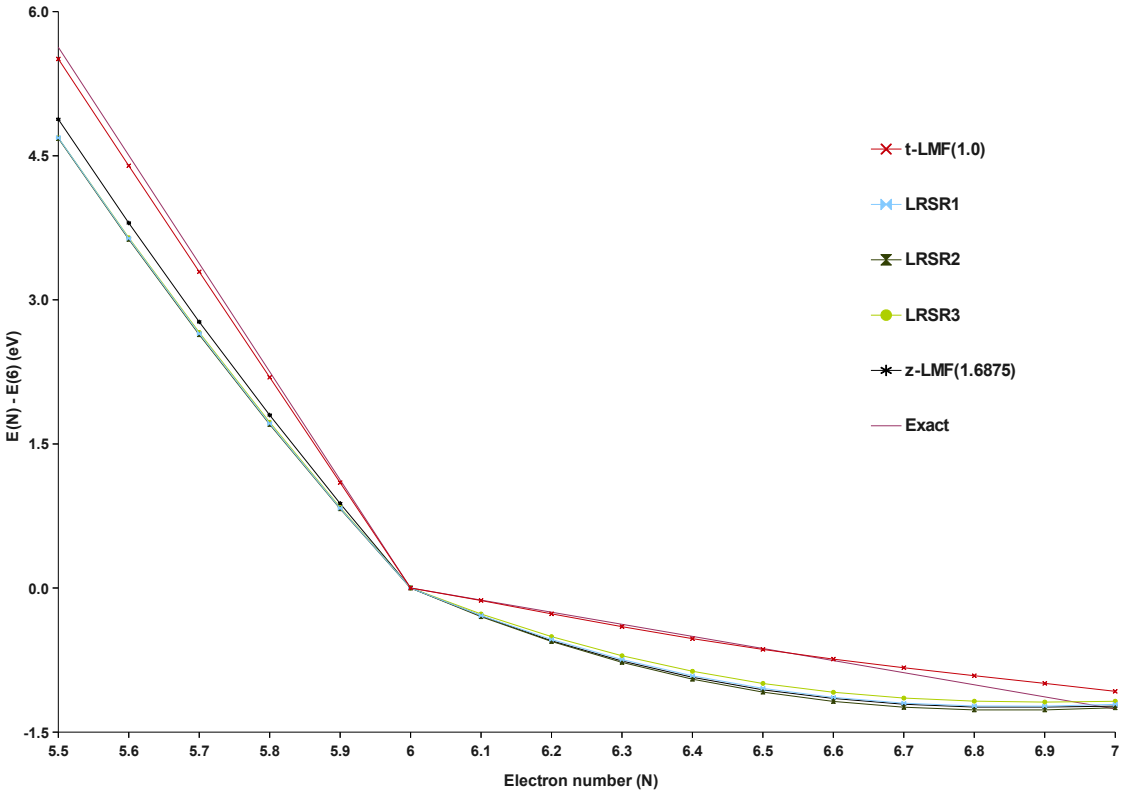

Figure 5.2: Electronic energies of carbon (^3P) versus electron number. The exact curve is based on the experimental IP and EA values.

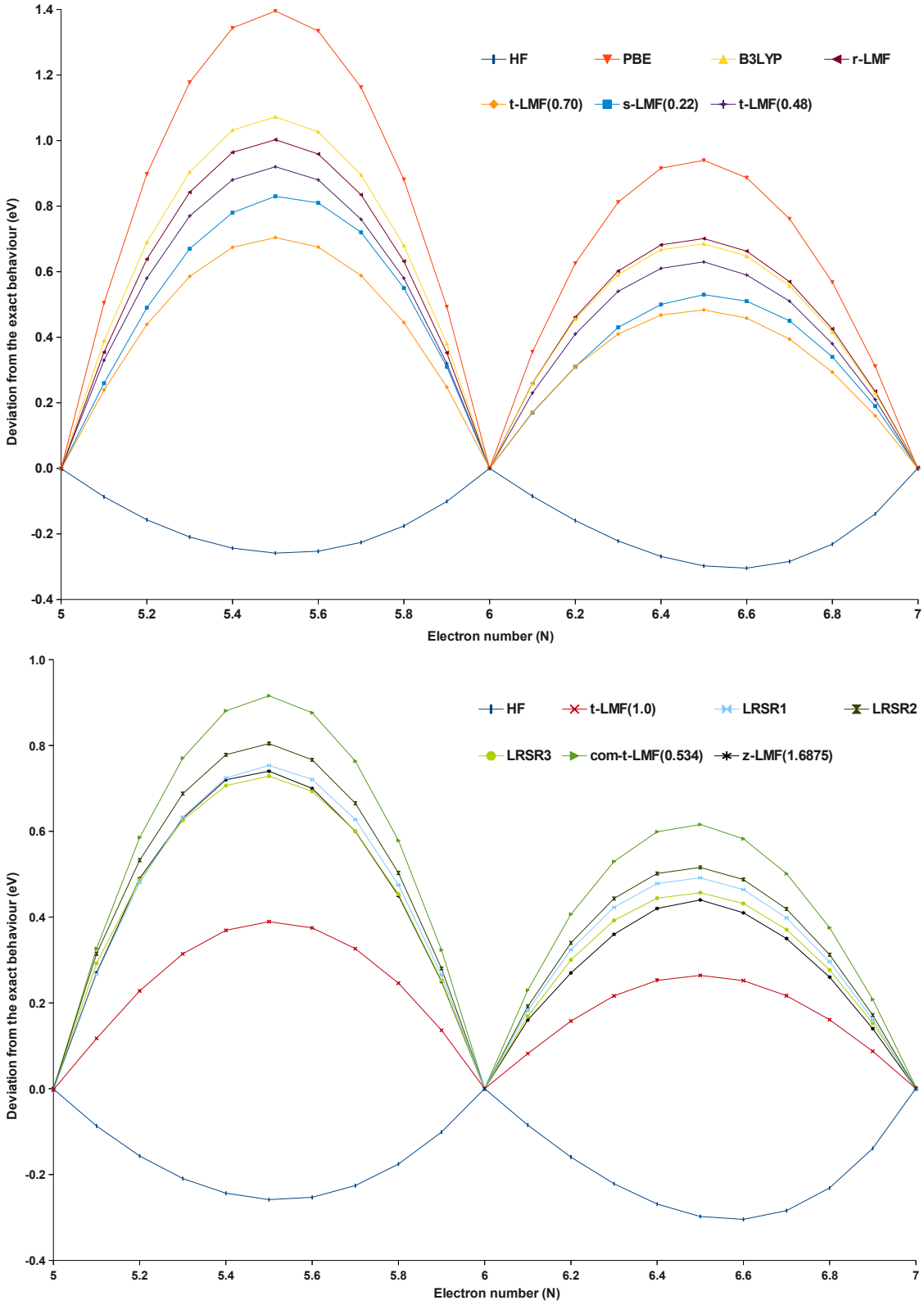

Figure 5.3: Deviation from the exact straight-line energy dependence with different functionals for carbon (^3P). The values are computed assuming correct energies for a given functional at integer values.

In case of the carbon atom, the two unpaired electrons in $2p$ orbitals can spin-pair giving rise to a low-lying singlet excited state (^1D). Ionisation of this singlet (^1D) results in the doublet state cation (^2P) and addition of an electron will result in the formation of a doublet anionic state (^2S). Computations similar to the ground-state carbon (^3P) have been carried out and the deviations from the exact behaviour are plotted in Figure.5.4. Deviation plots for the singlet state also show a very similar trend to that of the triplet case. The local hybrid functional with *t*-LMF(1.0) gives the smallest deviations followed by *t*-LMF(0.70). Local hybrid functionals with range-separated correlation functionals containing the self-interaction reduction in short-range correlation also show very good results (among them minimum deviations by LRSR3 functional with full self-interaction elimination in correlation functional). The *z*-LMF with self-interaction corrected correlation also shows deviations closer to the local hybrids with range-separated correlation functionals.

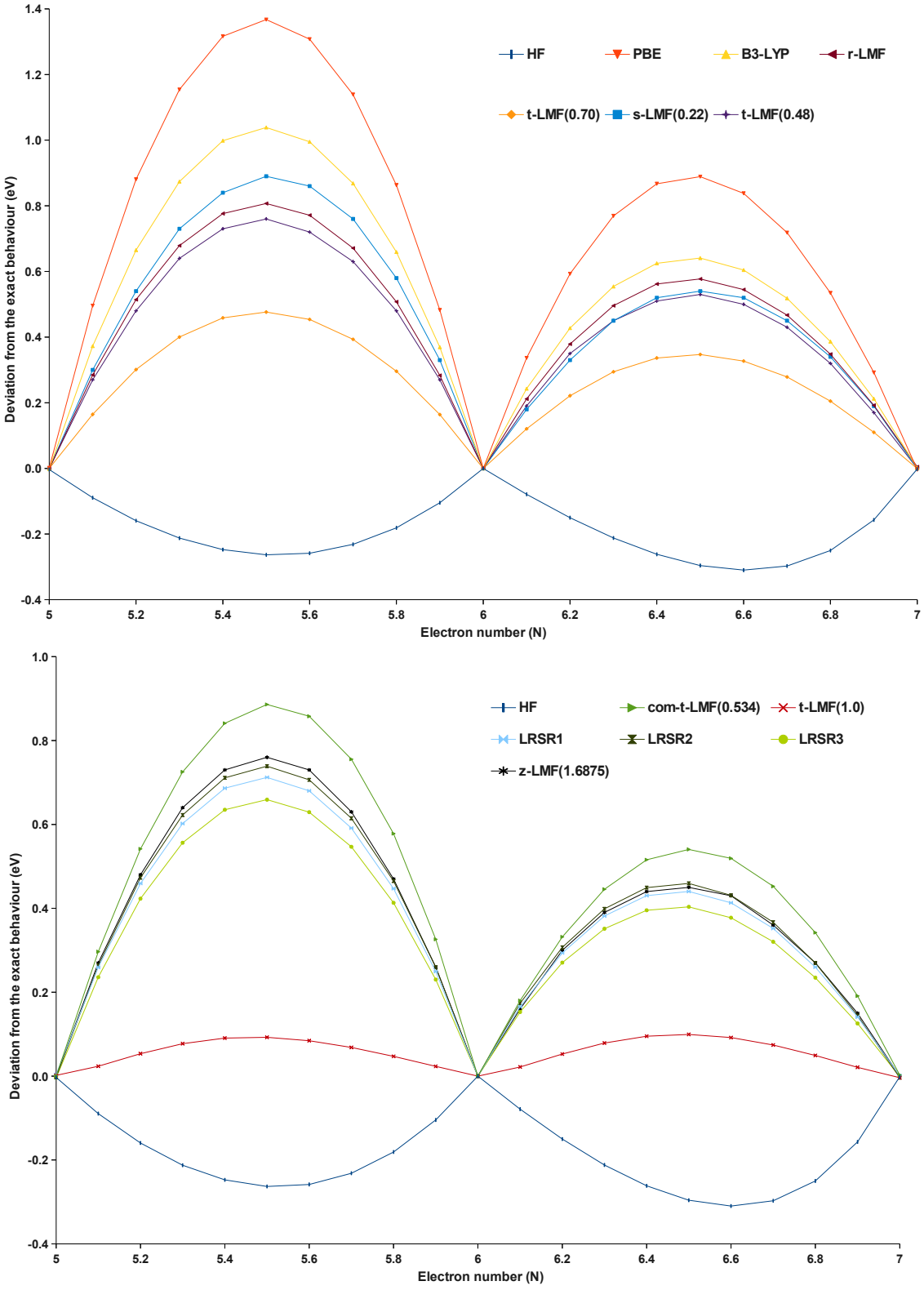

Figure 5.4: Deviation from the exact straight-line energy dependence with different functionals for carbon (^1D). The values are computed assuming correct energies for a given functional at integer values.

5.1.2 Oxygen

The oxygen atom has a triplet (^3P) ground state and a low-lying singlet excited state (^1D). Removal of an electron from the triplet state results in a quartet state (^4S) cation and from the singlet state it results in a doublet-state (^2D) cation. Addition of an electron to both the singlet and triplet state results in a doublet-state (^2P) anion. Further addition of an electron to the triplet ground state results in a singlet-state (^1S) dianion with fully filled $2p$-orbitals. For all computations C_1 symmetry is used. Plots of deviations from the exact straight-line behaviour for the triplet and singlet states are shown in Figures 5.5 and 5.6. In the case of triplet, going from cation to neutral atom, the *t*-LMF(1.0) gives deviations close to zero already approaching the numerical noise in the calculations. The z-LMF shows deviations which are lower than the values for local hybrids with range-separated correlation. From neutral atom to anion, the *t*-LMF with parameters 0.7 and 1 show less deviations in comparison with the other tested functionals. In case of singlet excited-state (^1D), the qualitative trends are very much similar to the triplet ones with minimum deviations given by local hybrids with the *t*-LMF(1.0) followed by z-LMF(1.6875) and *t*-LMF(0.70) respectively.

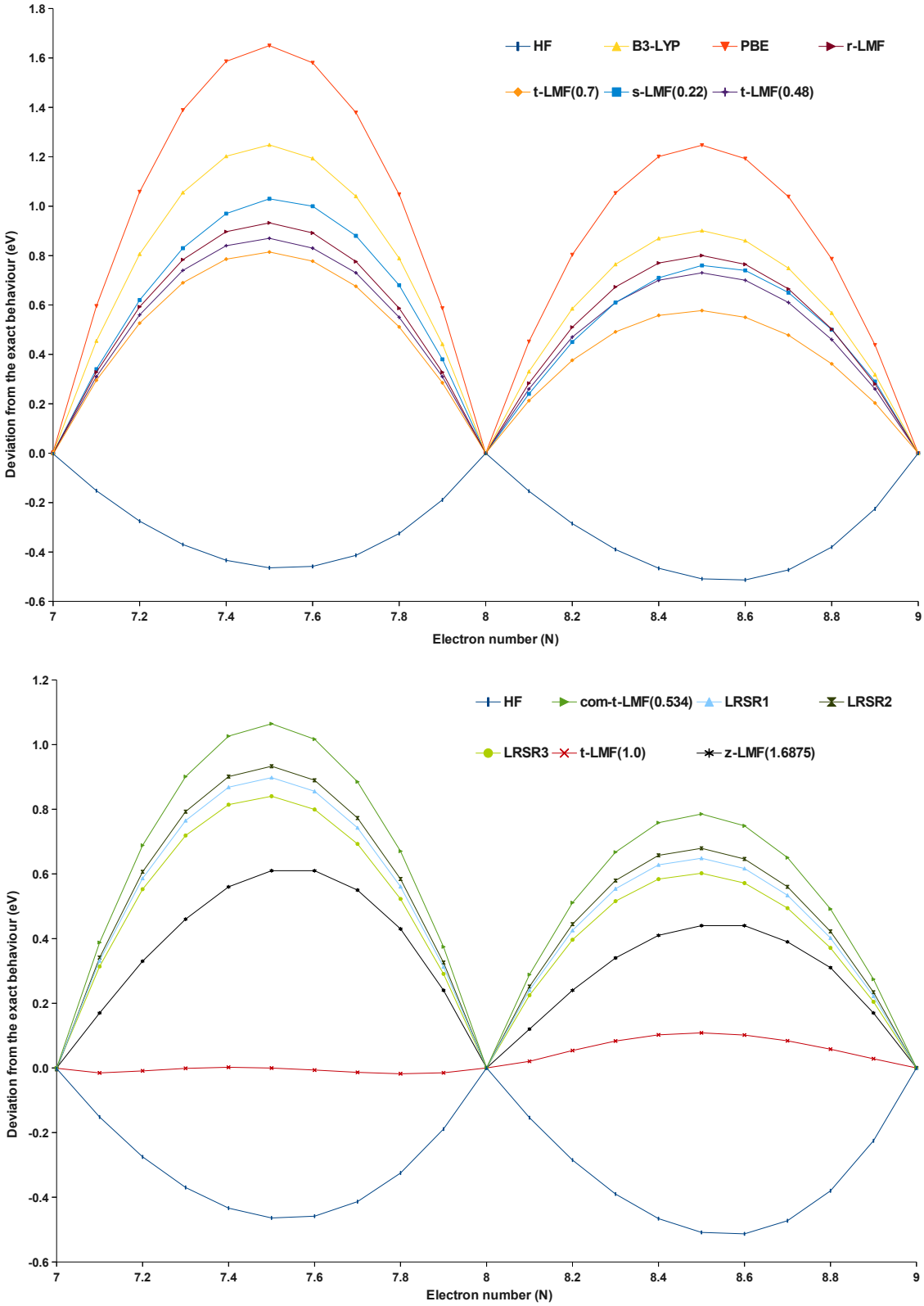

Figure 5.5: Deviation from the exact straight-line energy dependence with different functionals for oxygen (^3P). The values are computed assuming correct energies for a given functional at integer values.

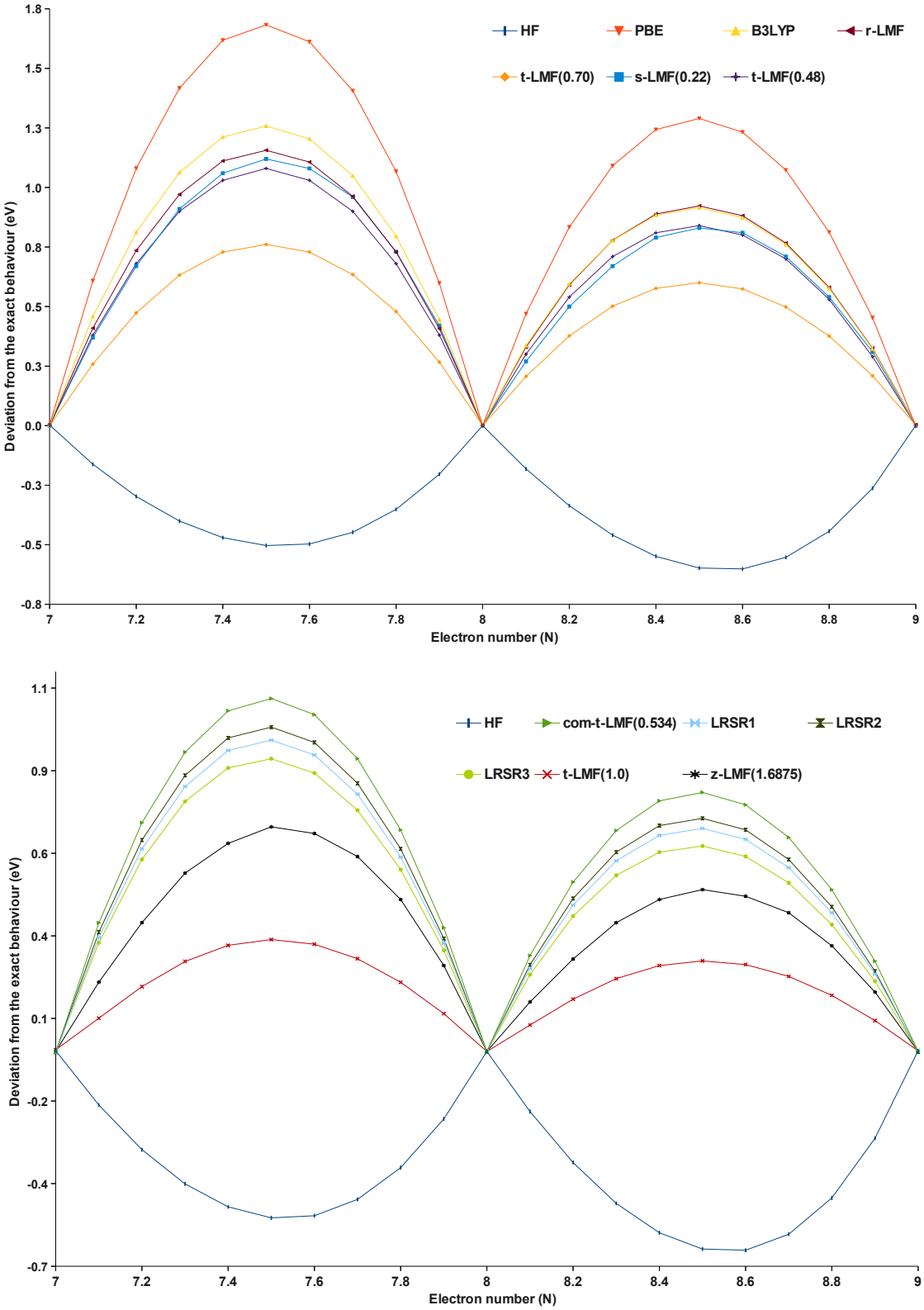

Figure 5.6: Deviation from the exact straight-line energy dependence with different functionals for oxygen (^1D). The values are computed assuming correct energies for a given functional at integer values.

5.1.3 Vanadium

The ground-state (^4F) has an electronic configuration [Ar]$4s^2 3d^3$ with several low-lying electronially excited states. Therefore the low-lying state (^6D) with an electronic configuration of [Ar]$4s^1 3d^4$ is also considered for computations. In case of the ground-state, varying the electron number results in a cation (^5F), and an anion (^5D). The low-lying excited state (^6D) can give rise to two different cationic as well as anionic states. Different cationic states $3d^4(^5D)$ or $4s^1 3d^3(^5F)$ arise depending on the removal of electron from either an $4s$ or $3d$ orbital. Similarly, addition of an electron to either a $4s$ or $3d$ orbital results in the anionic states $4s^2 3d^4(^5D)$ or $4s^1 3d^5(^7S)$. In case of vanadium, all computations have been carried out using O_h symmetry. The results are shown in Figures 5.7 to 5.9. For the ground-state (^4F) going from the electron number 22 to 23, HF shows the usual localisation error with deviation values close to zero. Surprisingly, the *s*-LMF(0.22) gives almost similar deviations as the *t*-LMF(1.0 followed by the *z*-LMF(1.6875). For the low-lying excited state (^6D), Figure 5.8 shows deviations obtained by addition/removal of 4*s*-electron and Figure 5.9 shows deviations obtained when an 3*d*-electron is added or removed from the (^6D) state.

Usually the magnitude of deviations is larger going from the cation to the neutral atom, but here many functionals show larger deviations in the anionic part. This is mainly due to functionals giving overestimated energy values for anions. In all these cases, the minimum deviations are shown by either *t*-LMF(1.0) or *z*-LMF(1.6875) with interchanging curves. The unclear trends for behaviour of different local hybrids are due to the many-electron SIE with the 3*d*-electrons invovled. Specially, the asymmetric behaviour of *z*-LMF can be due to the explicit inclusion of spin-polarisation which changes the functional behaviour from nonlocal to purely local [99, 106].

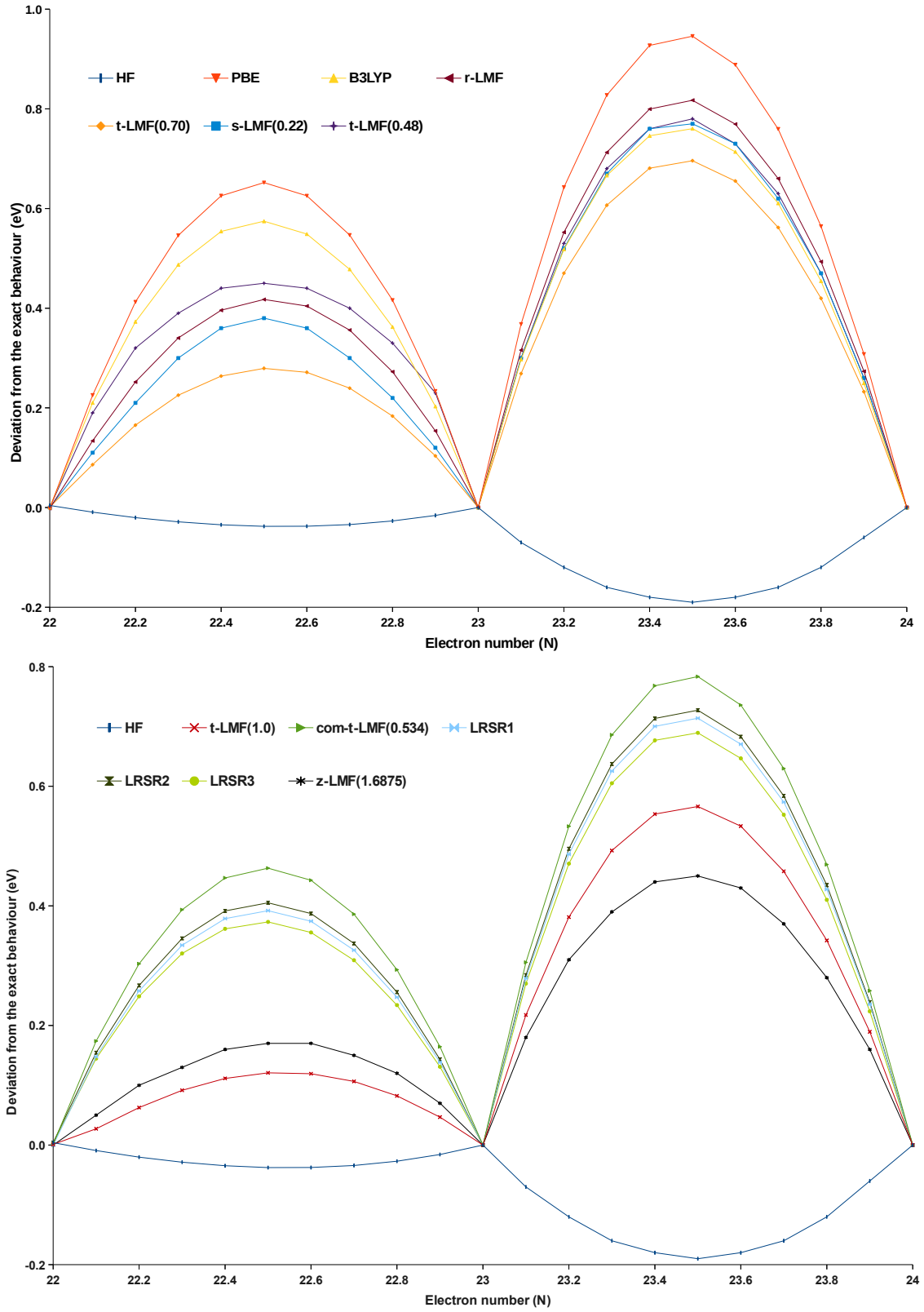

Figure 5.7: Deviation from the exact straight-line energy dependence with different functionals for vanadium (^4F). The values are computed assuming correct energies for a given functional at integer values.

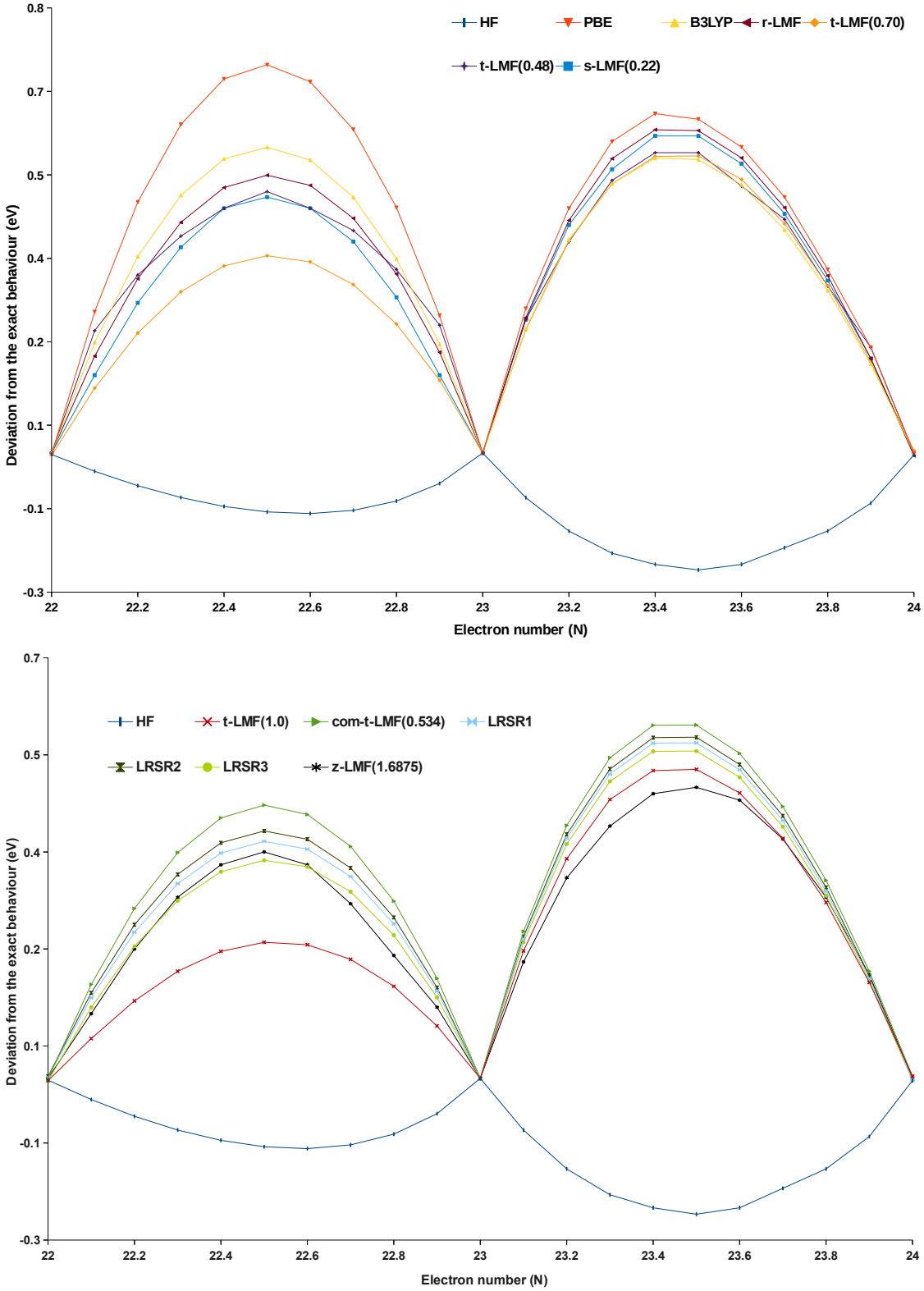

Figure 5.8: Deviation from the exact straight-line energy dependence with different functionals for vanadium (^6D). Here the cationic and anionic state configurations are $3d^4(^5D)$ and $4s^2 3d^4(^5D)$ respectively. The values are computed assuming correct energies for a given functional at integer values.

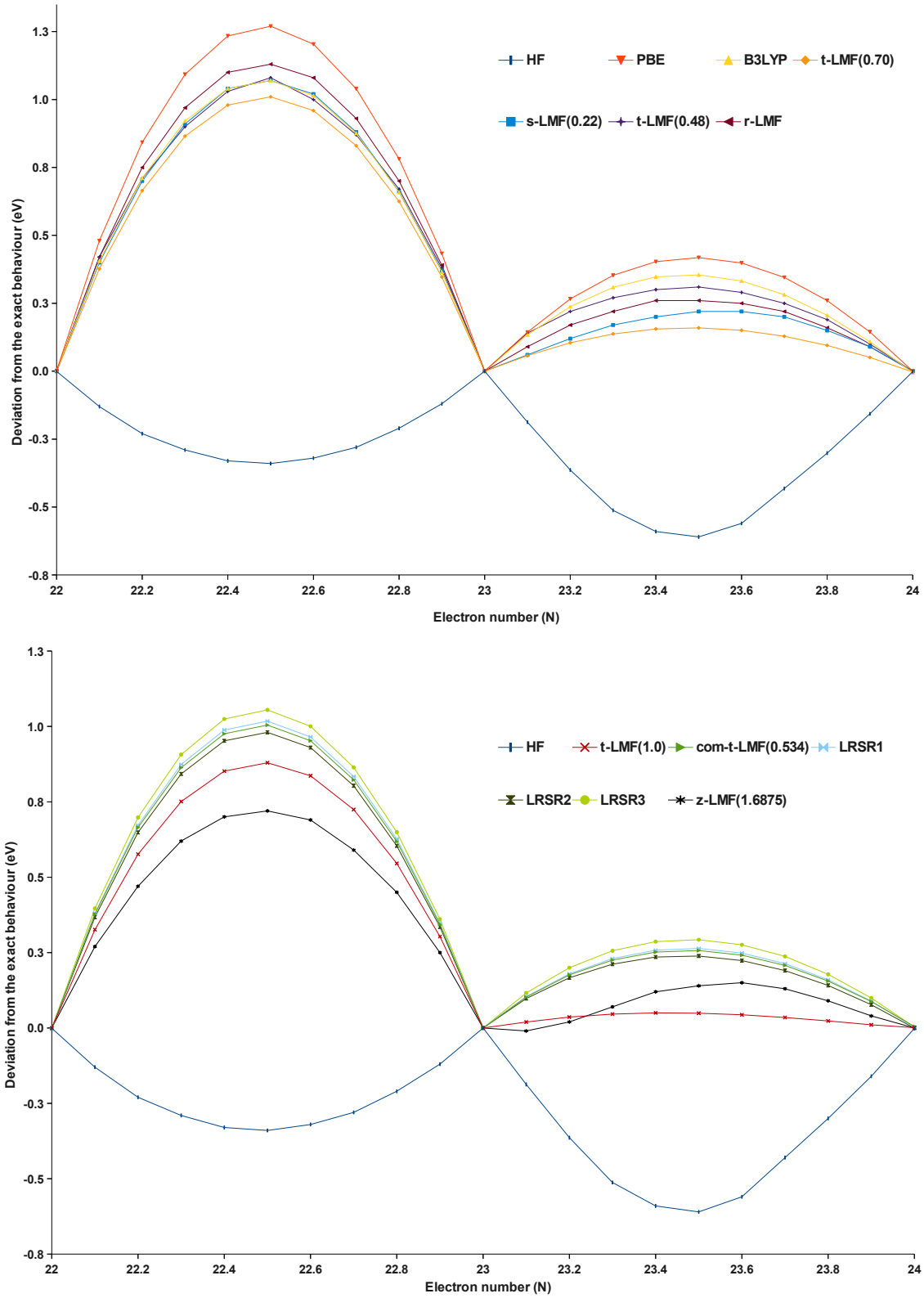

Figure 5.9: Deviation from the exact straight-line energy dependence with different functionals for vanadium (^6D). Here the cationic and anionic state configurations are $4s^1 3d^3 (^5F)$ and $4s^1 3d^5 (^7S)$ respectively. The values are computed assuming correct energies for a given functional at integer values.

5.1.4 Copper

The ground-state is a doublet (^2S) with the electronic configuration [Ar]$4s^1 3d^{10}$. Copper also has a low-lying doublet state (^2D) with configuration [Ar]$4s^2 3d^9$. The doublet ground-state on ionisation gives a singlet (^1S) with $3d^{10}$ configuration. Addition of an electron to the doublet-state results in the formation of a singlet (^1S) with the configuration [Ar]$3d^{10}4s^2$. The low-lying excited state (^2D) on ionisation results in a triplet state (^3F) with configuration [Ar]$4s^2 3d^8$ and upon electron addition gives a fully filled singlet state (^1S). Computations involving the copper atom have been performed using O_h symmetry. The results are shown in Figures 5.10 to 5.11. For the ground-state (^2S), the results clearly show that the *t*-LMF(1.0) is the one with minimum deviation followed closely by the *t*-LMF(0.70) and *z*-LMF(1.6875).

In case of low-lying doublet (^2D) state, the best performing functional is *z*-LMF(1.6875) followed closely by *t*-LMF(1.0). Addition of an electron to both the ground and low-lying doublet states results in the same singlet (^1S) state. Even then the tested functionals do not show the same trend (the deviation values are larger for the excited state) due to different set of orbitals getting filled fractionally i.e $4s$ or $3d$ orbitals respectively for ground and excited states .

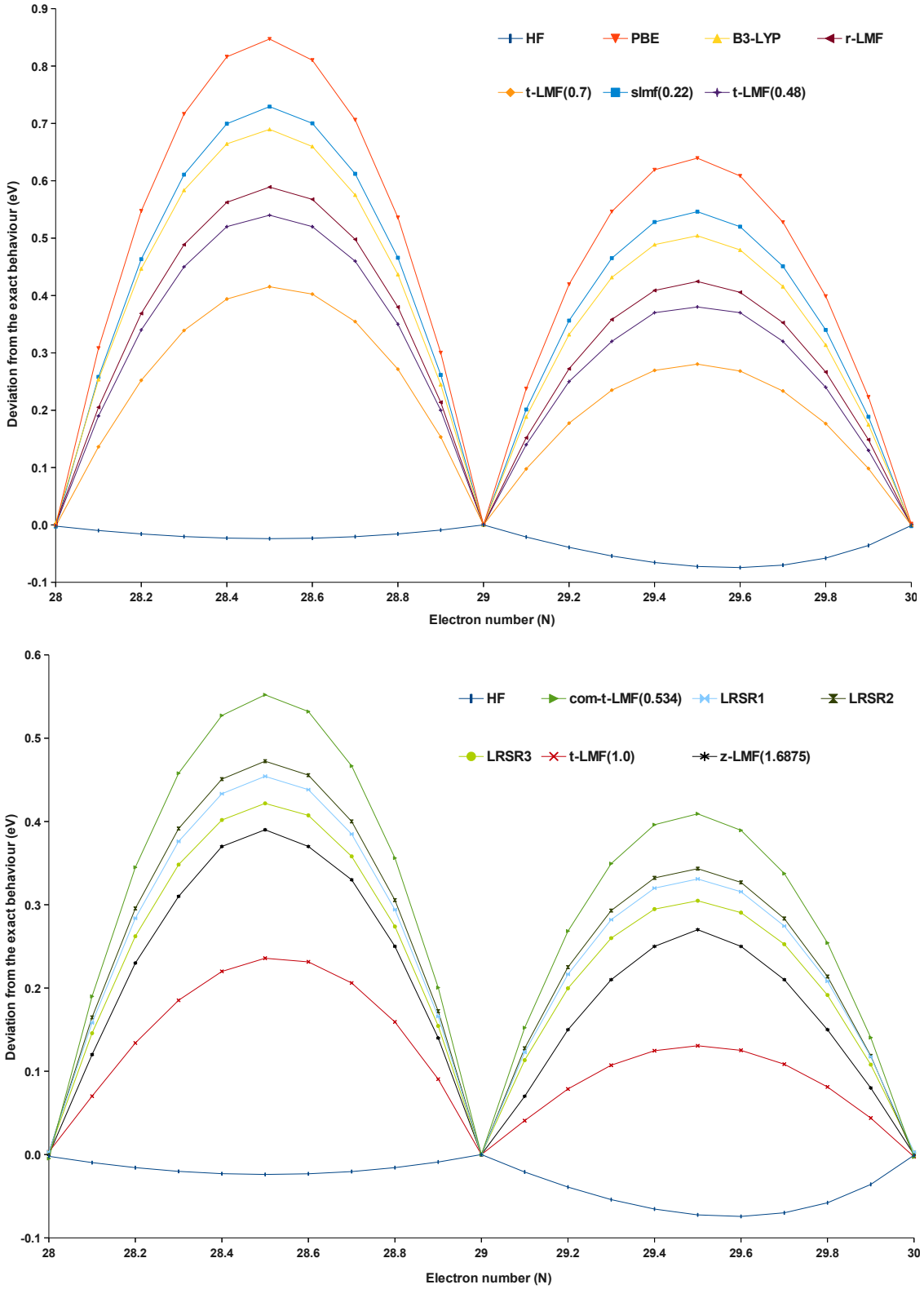

Figure 5.10: Deviation from the exact straight-line energy dependence with different functionals for copper (^2S). The values are computed assuming correct energies for a given functional at integer values.

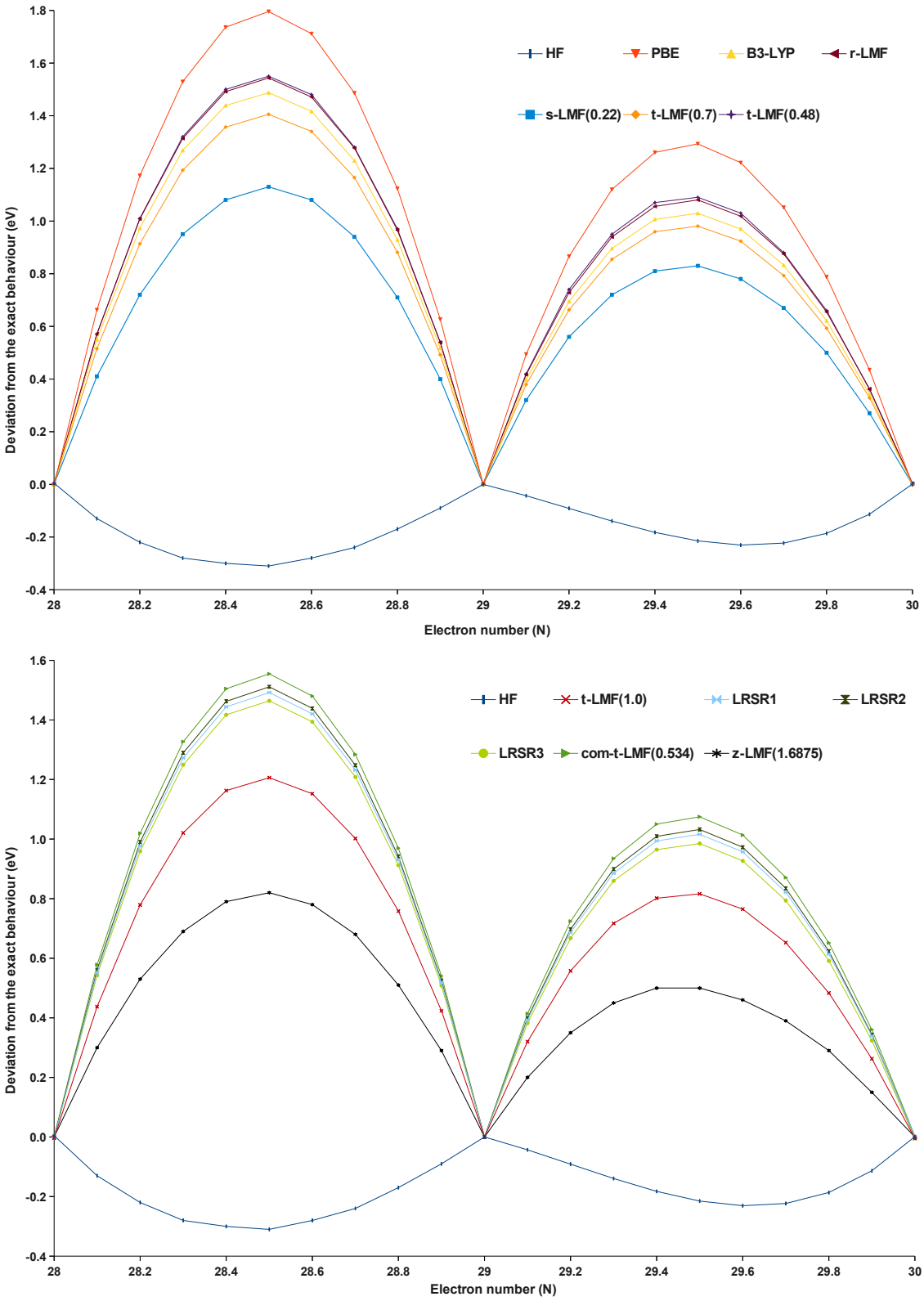

Figure 5.11: Deviation from the exact straight-line energy dependence with different functionals for copper (^2D). The values are computed assuming correct energies for a given functional at integer values.

5.1.5 The CH_2 molecule

In case of the $\mathbf{CH_2}$ molecule, the two non-bonding electrons on the carbon atom can share an $a1$ orbital forming a singlet (1-A1) state and a triplet (3-B1) state depending on the occupation of the $a1$ and $b1$ orbitals. Both the singlet and triplet states on ionisation gives the same cationic (2-A1) state and on electron addition gives the same anionic (2-B1) state. The energy difference between these two states is very much dependent on the structure (bond angle of **H-C-H**) [105]. Depending on the **H-C-H** bond angle, the highest eigenvalue orbital for singlet and triplet can be any of these a1(α), b1(α), and a1(β) orbitals. For simplifying the structural complications, geometry with **H-C-H** bond angle 131° has been considered for both singlet and triplet cases. For the triplet (3-B1) state, fraction of an electron is removed from the $b1(\alpha)$ orbital to form a cation and for anion formation the fraction of an electron is added to $a1(\beta)$ orbital. Similarly for the singlet case the fraction of electron is removed from the a1(β) orbital for the cation case and for anion formation electron is added to the $b1(\alpha)$ orbital. The results are shown in Figures 5.12 and 5.13.

In the case of triplet (3-B1), the *t*-LMF(1.0) shows minimum deviation with an oscillatory behaviour going from neutral molecule to anion. This could be due to the full EXX admixture resulting in localisation rather than delocalisation. The deviation plots for the singlet state (1-A1) clearly shows that *t*-LMF(1.0) has a minimum deviation followed closely by *t*-LMF(0.7). Local hybrid functional with range-separated correlations also show results closer to the *t*-LMF(0.7) for both the singlet and triplet states. For the singlet state, deviations are very large for the *z*-LMF(1.6875) due to the overestimated energy values in between integers (this is due to the numerical instabilities of post-SCF computations and closely spaced orbital energies).

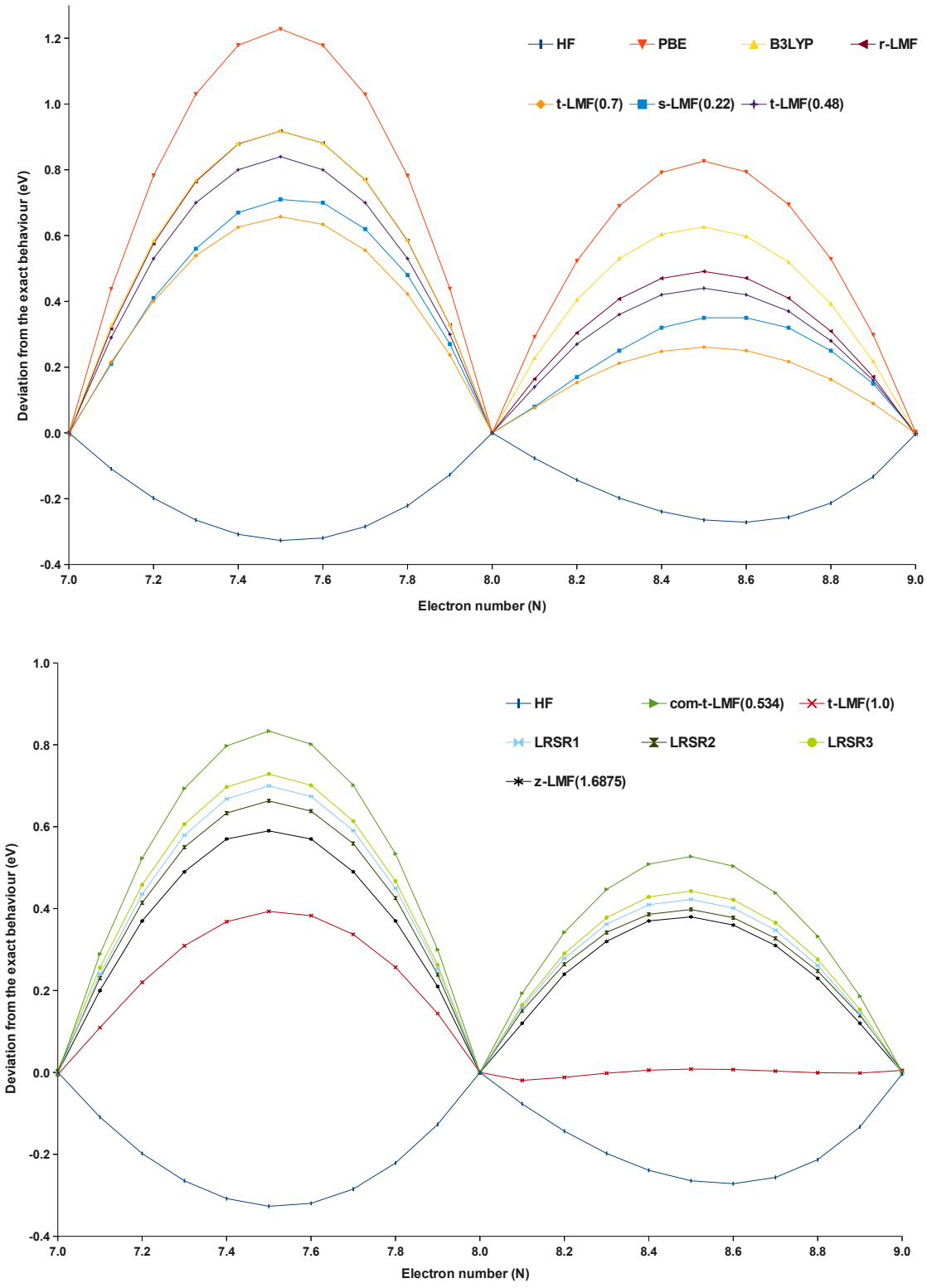

Figure 5.12: Deviation from the exact straight-line energy dependence with different functionals for CH_2 (3-B1). The values are computed assuming correct energies for a given functional at integer values.

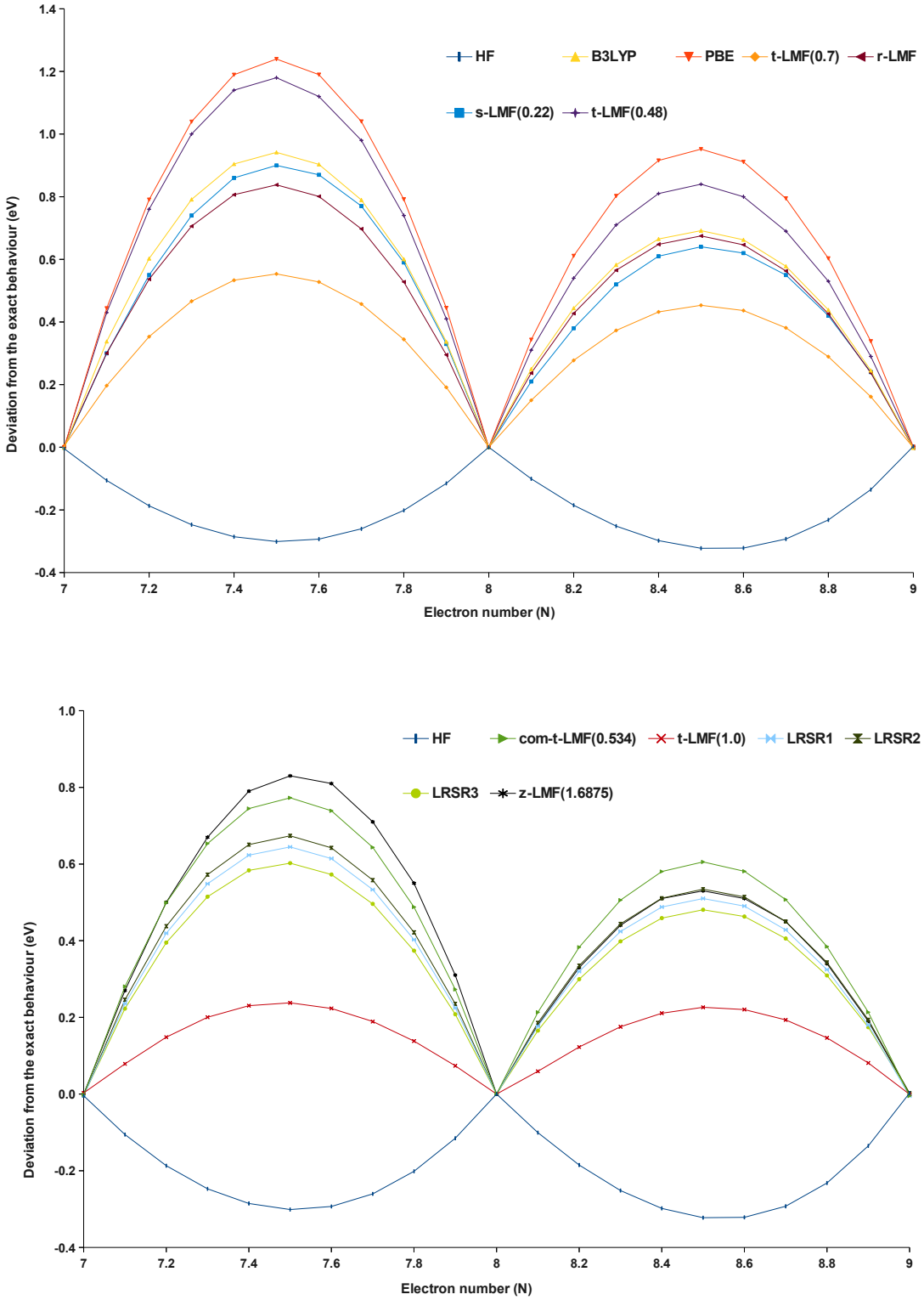

Figure 5.13: Deviation from the exact straight-line energy dependence with different functionals for $\mathbf{CH_2}$ (1-A1).The values are computed assuming correct energies for a given functional at integer values.

Assessment of local hybrids for fractional electron number clearly show good estimates for the delocalisation errors. But the above deviations from stepwise-linearity reveal to a large extent only the one-electron SIE, which is a specific manifestation of many-electron SIE. In this scenario, studies related to the fundamental band gaps, IPs, and EAs computed using the energy differences and derivative differeneces with different local hybrid functionals are carried out for greater understanding of the many-electron SIE problem.

5.2 The fundamental band gap problem

The fundamental band gap of any system is given by the difference between the ionisation potential (IP) and electron affinity (EA) [17, 27, 28, 67, 68, 103]. These two are related to the fundamental processes of electron addition (EA) and removal (IP) which are themselves computed as energy differences (referred to as the integer gap) [Eq.2.37]. The band gap can also be computed as the derivative difference (derivative discontinuity at N_0)between left and right derivative of the energy at integer electron number. The expressions for the left and right derivatives of the energy are given by,

$$\left.\frac{\delta E}{\delta N}\right|_{N_0-\delta} = \frac{E(N_0) - E(N_0-\delta)}{\delta} = -IP, N_0 - 1 < N \leq N_0, \tag{5.1}$$

$$\left.\frac{\delta E}{\delta N}\right|_{N_0+\delta} = \frac{E(N_0+\delta) - E(N_0)}{\delta} = -EA, N_0 - 1 < N \leq N_0, \tag{5.2}$$

This derivative difference can be expressed as the difference between the KS eigenvalues corresponding to the HOMO and LUMO. However, the above band gap lacks an important contribution, derivative discontinuity expressed as the difference in the XC potentials [Sec.2.5]. For exact functional the derivative gap and the integer gap should be the same. Computations are carried out on carbon (^3P), oxygen (^3P), and the $\mathbf{CH_2}$ (3-B1) molecule (basis sets and symmetry constraints remain the same as in tests for fractional charge behaviour). For derivative difference computations, the value of δ chosen is 0.001 [103]. The results are tabulated below (Tables 5.1 to 5.3).

Carbon (^3P)						
	E^{int}	IP	EA	E^{deriv}	IP	EA
HF	10.35	10.80	0.45	12.65	11.95	-0.71
PBE	9.94	11.54	1.60	0.53	6.10	5.58
B3LYP	10.16	11.46	1.30	3.06	7.25	4.20
t-LMF(0.48)	10.05	11.65	1.60	3.82	8.02	4.20
t-LMF(0.70)	10.11	11.63	1.52	6.05	8.90	2.85
t-LMF(1.0)	10.20	11.61	1.41	7.93	10.13	2.20
s-LMF(0.22)	10.08	11.60	1.52	3.76	7.62	3.86
r-LMF	10.05	11.61	1.60	3.28	7.73	4.45
com-*t*-LMF(0.534)	10.04	11.60	1.56	4.35	8.25	3.90
LRSR1	10.04	11.49	1.46	5.09	8.57	3.48
LRSR2	10.03	11.52	1.49	4.87	8.48	3.61
LRSR3	10.02	11.45	1.42	5.44	8.72	3.28
z-LMF(1.6875)	10.00	11.23	1.23	6.06	8.82	2.76
Expt.	10.00	11.26	1.26	10.00	11.26	1.26

Table 5.1: IP, EA, and the fundamental band gap values (in eV) using the energy differences and derivative differences for carbon (^3P).

Oxygen (^3P)						
	E^{int}	IP	EA	E^{deriv}	IP	EA
HF	12.73	12.02	-0.71	16.55	14.19	-2.35
PBE	12.62	14.06	1.44	1.13	7.57	6.45
B3LYP	12.72	14.03	1.31	4.16	9.15	4.99
t-LMF(0.48)	12.51	13.89	1.37	6.36	10.52	4.16
t-LMF(0.70)	12.61	14.02	1.41	9.16	11.99	2.83
t-LMF(1.0)	12.81	13.82	1.01	13.01	14.05	1.04
s-LMF(0.22)	12.49	13.77	1.28	5.73	9.51	3.78
r-LMF	12.48	13.85	1.37	5.82	10.25	4.43
com-*t*-LMF(0.534)	12.51	14.01	1.50	5.49	10.05	4.56
LRSR1	12.44	13.80	1.36	6.30	10.36	4.06
LRSR2	12.43	13.84	1.41	6.04	10.25	4.22
LRSR3	12.38	13.69	1.31	6.67	10.49	3.82
z-LMF(1.6875)	12.75	13.45	0.70	8.81	10.71	1.90
Expt.	12.15	13.61	1.46	12.15	13.61	1.46

Table 5.2: IP, EA, and the fundamental band gap values (in eV) using the energy differences and derivative differences for oxygen (^3P).

The band gaps computed using the energy differences are very close to the experimental ones for all the tested functionals. In all the test cases, the IP values computed using different functionals are very close to the experimental values. The EA values computed are also in good agreement with the experimental ones except for the $\mathbf{CH_2}$ molecule, where the values obtained are somewhat underestimated for all functionals.

CH_2 (3-B1)						
	E^{int}	IP	EA	E^{deriv}	IP	EA
HF	11.25	9.72	-1.3	11.15	8.81	-2.35
PBE	10.46	10.59	0.13	5.74	9.07	3.33
B3LYP	10.28	10.38	0.10	6.73	9.34	2.61
t-LMF(0.48)	10.56	10.64	0.07	7.28	8.85	1.58
t-LMF(0.70)	10.64	10.60	-0.04	7.99	8.52	0.53
t-LMF(1.0)	10.76	10.41	-0.21	8.97	8.09	-0.88
s-LMF(0.22)	10.60	10.61	0.01	7.08	8.15	1.07
r-LMF	10.53	10.61	0.09	7.00	8.71	1.71
com-*t*-LMF(0.534)	10.29	10.53	0.24	7.38	9.61	2.23
LRSR1	10.24	10.41	0.17	7.61	9.58	1.96
LRSR2	10.24	10.37	0.13	7.55	9.60	2.06
LRSR3	10.25	10.45	0.20	7.73	9.57	1.85
z-LMF(1.6875)	10.40	10.23	-0.17	7.82	7.71	-0.11
Expt.	9.78	10.40	0.62	9.78	10.40	0.62

Table 5.3: IP, EA, and the fundamental band gap values (in eV) using the energy differences and derivative differences for **CH_2** (3-B1).

Results obtained using the derivative differences approach are very poor in comparison to the values obtained using energy differences for all test cases. Some of the local hybrid functionals with *r*-LMF or *s*-LMF show appreciatively underestimated values for both the IPs and EAs. The errors can be a rough estimate for the missing derivative discontinuity of the approximate functional [Sec.2.5.3]. Local hybrids with *t*-LMF(0.7) and *t*-LMF(1.0) IP exhibit values which are in reasonable agreement with the experimental ones. There is a clear trend of IP and EA values obtained closer to the experimental as the amount of EXX increases in the functional. Usually the derivative values for the EA are severely underestimated or overestimated /off the mark in comparison to experimental ones, leading to large errors in the band-gap calculations. In principle, fractional electron numbers should only affect the frontier orbital energies (neglecting the orbital relaxations) [76, 107]. Therefore studies on the behaviour of frontier orbital energies versus the electron number for different local hybrid functionals are presented in the next section (*z*-LMF has not been assessed due to the post-SCF implementation).

5.3 Frontier orbital energies versus electron number: the IP theorem

In exact KS-DFT, the IP theorem states that the ionisation potential equals the exact KS eigenvalue corresponding to the highest occupied molecular orbital of a system at N_0, an integer number of electrons [Sec.2.5]. The IP theorem is the DFT version of Koopmans' theorem [71, 74, 108]. In general, Koopmans' theorem for HF theory gives meaning to all occupied and unoccupied orbitals whereas the IP theorem gives only precise meaning for a single KS-eigenvalue, corresponding to the HOMO [27, 69, 109]. Studies carried out by Wang and co-workers [68] show that the for the exact functional, the eigenvalue of the lowest unoccupied molecular orbital (LUMO) in DFT is equal to the electron affinity (EA) value. The stepwise-linearity condition of the energy implies that the following equations hold

$$\varepsilon_f = \varepsilon_{HOMO} = -IP, N_0 - 1 < N \leq N_0, \tag{5.3}$$

$$\varepsilon_f = \varepsilon_{LUMO} = -EA, N_0 \leq N < N_0 + 1. \tag{5.4}$$

This jump in the orbital eigenvalues is connected to the discontinuity of the XC potential [28, 67, 68].

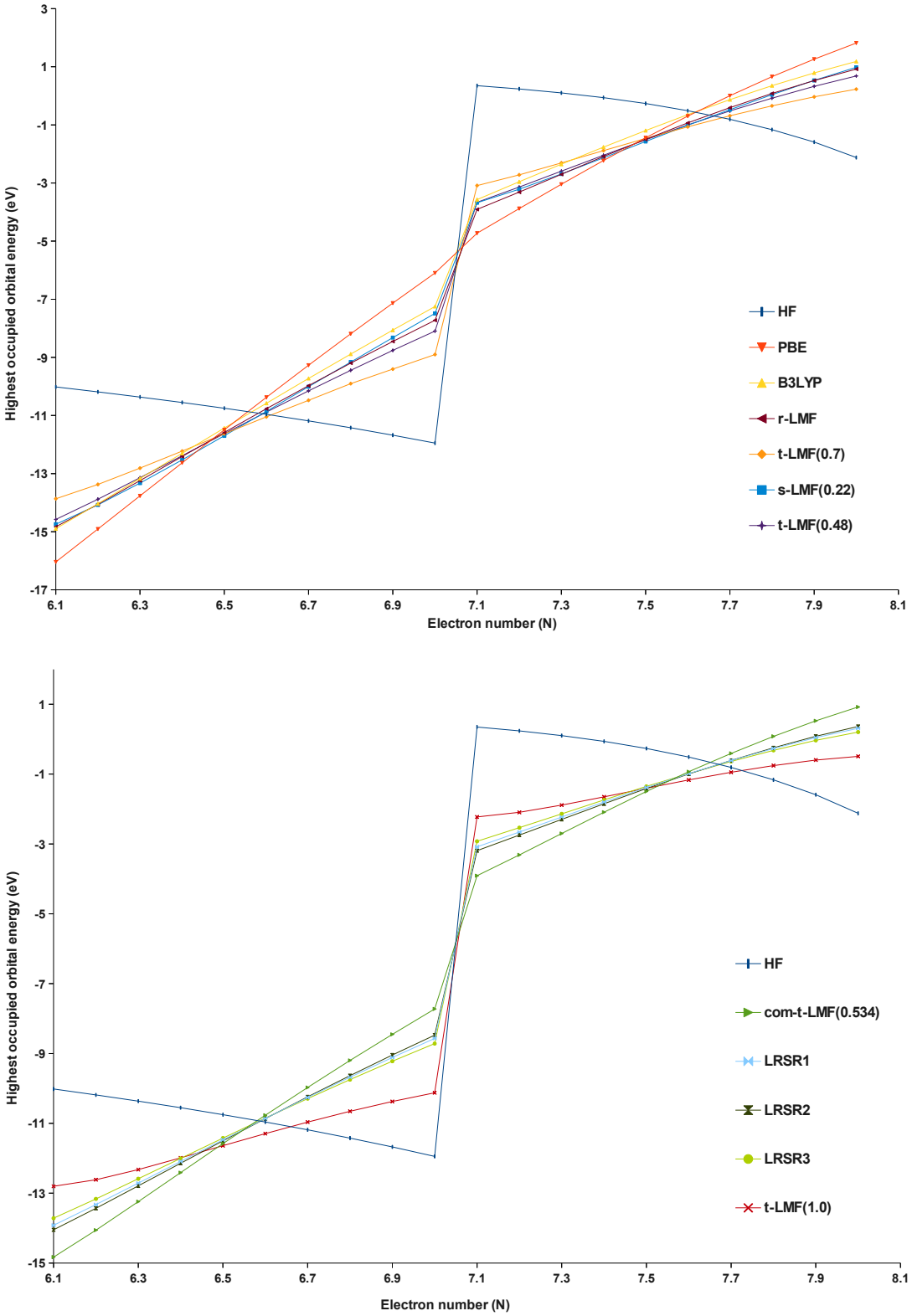

Figure 5.14: Frontier orbital energies of carbon (^3P) versus the electron number. All functionals except for PBE clearly show the shift in eigenvalues on crossing the integer number.

Plots of the frontier orbital energies versus the electron number for carbon (^3P),

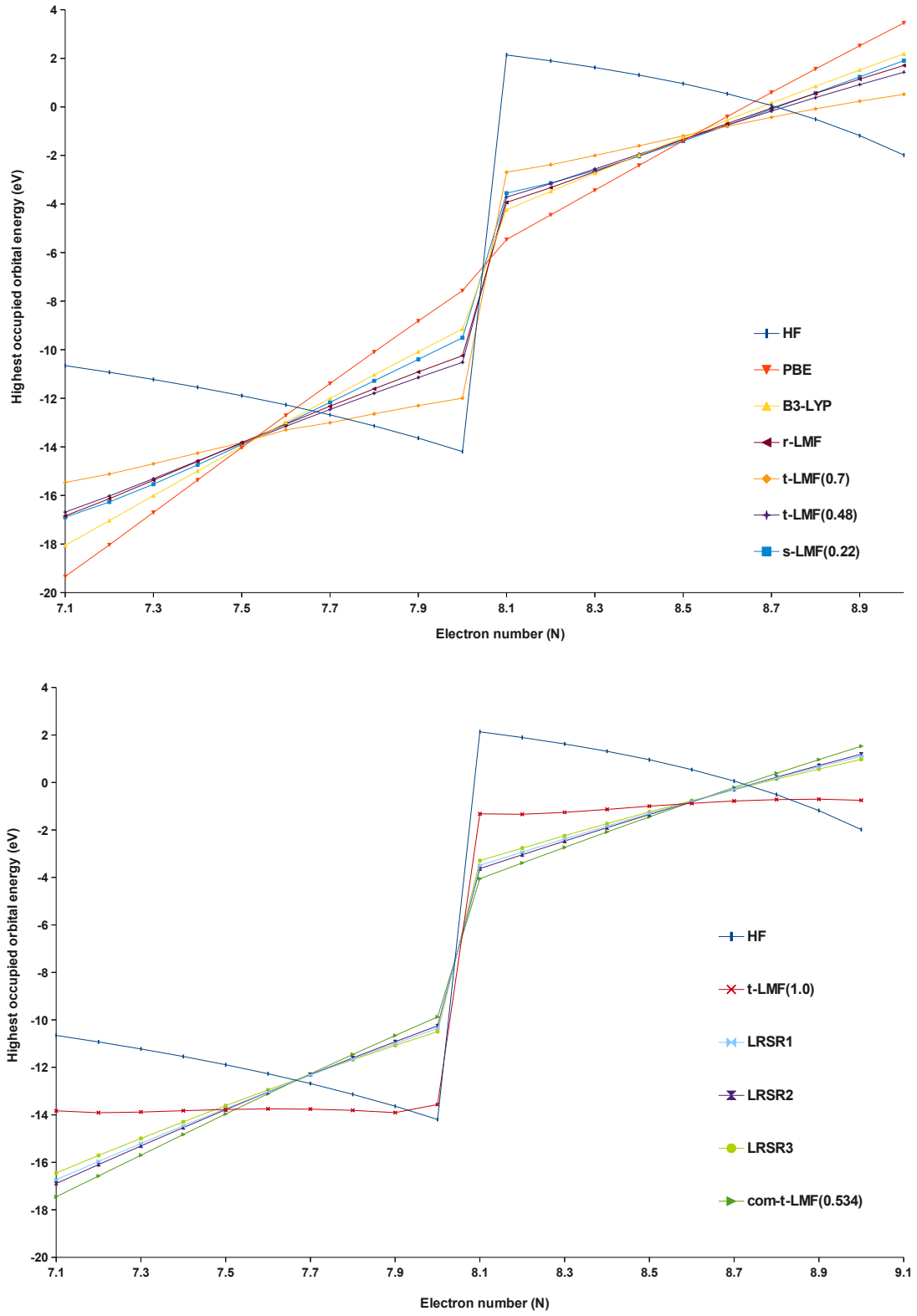

Figure 5.15: Frontier orbital energies of oxygen (^3P) versus the electron number. All functionals except for PBE clearly show the shift in eigenvalues on crossing the integer number.

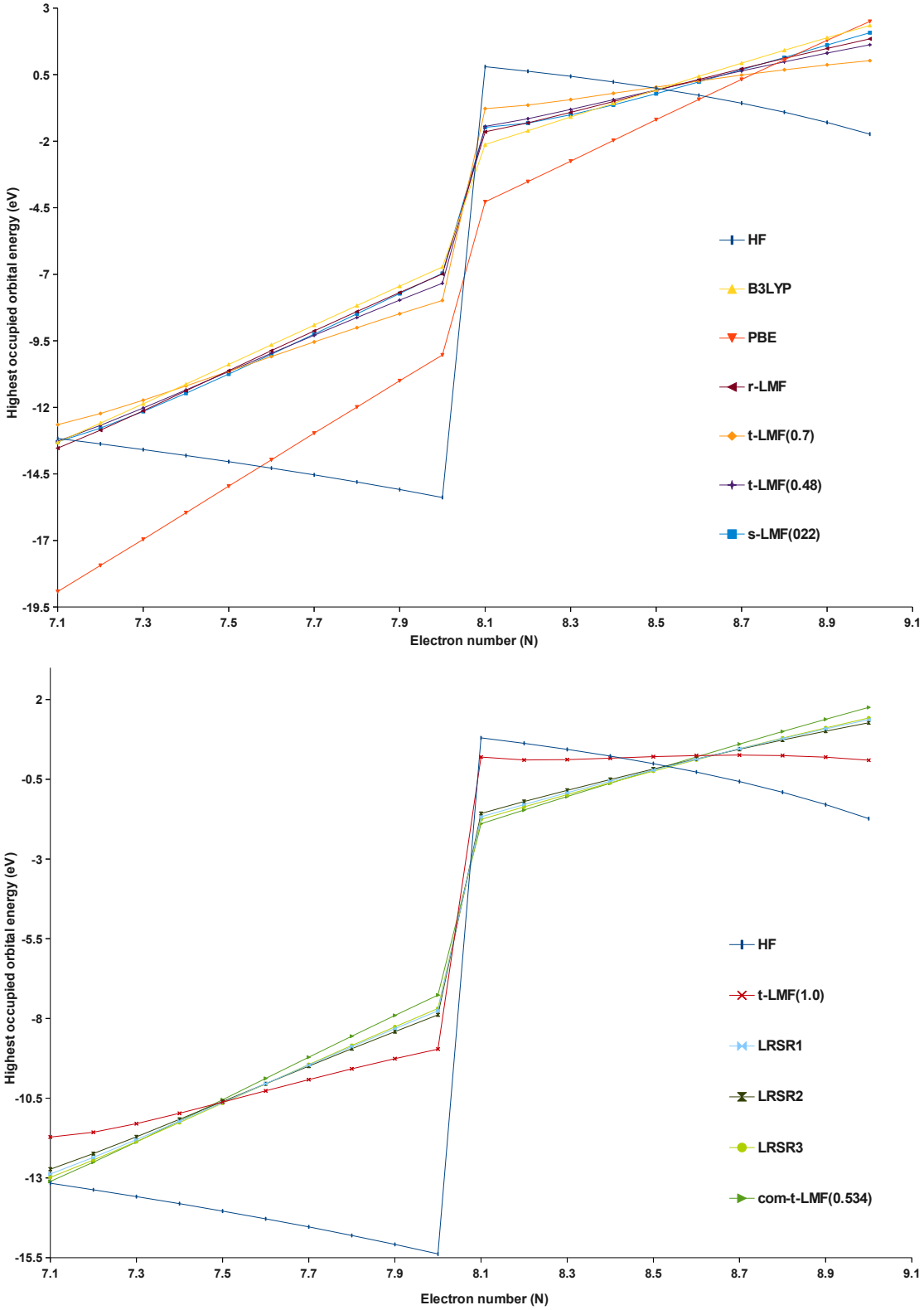

Figure 5.16: Frontier orbital energies of CH_2 (3-B1) versus the electron number. All functionals clearly show the shift in eigenvalues on crossing the integer number with HF giving more accurate one.

oxygen (^3P), and $\mathbf{CH}_2$ (3-B1) are shown in Figures 5.12 to 5.15, respectively. The main observation of these studies is the jump in the orbital eigenvalues as they cross the integer number of electrons and constancy of the orbital eigenvalues in between the integers [27, 68]. All tested functionals, except for PBE (is almost continuous) exhibit the necessary discontinuity in the eigenvalues on crossing the integer number of electrons, more so with larger exact-exchange admixture. In all the test cases, the HF frontier orbital energies decrease between integers with increase of fractional electron numbers, whereas the DFT approximations mostly show an increase. The local hybrid with *t*-LMF(1.0) also exhibits the best constancy between integer occupations. Local hybrid functionals with range-separated correlation also exhibit a reasonable discontinuity but a nonnegligible increase in the orbital eigenvalues in between integers. The situation is very similar for *t*-LMF(0.7). These studies clearly indicate that for proper description of IPs and EAs using orbital eigenvalues, a large amount of EXX admixture along with the discontinuity contributions from the correlation part is necessary [25, 28, 110, 111].

5.4 Conclusions

An assessment of local hybrid functionals for the stepwise linearity of the ground and low-lying excited states in atomic and molecular systems has been carried out. Apart from several local hybrid functionals, standard functionals and methods such as the HF, PBE, and B3LYP have also been used for comparison purposes. Further studies on the energy derivatives and frontier-orbital eigenvalues have also been carried out for understanding the many-electron self-interaction errors. Evaluations for the stepwise-linearity condition clearly suggest that local hybrids do exhibit reduced delocalisation errors due to the EXX admixtures, compared to standard DFAs. The results obtained clearly show that in general the local hybrid with an unscaled *t*-LMF exhibits best performance in most of the cases. This has to be seen in the context of inferior performance for thermochemistry, compared to some of the other local hybrids with lower EXX admixture. Results obtained using the *z*-LMF are in many cases comparable to the best performing functionals (with some numerical noise possibily SCF computations could improve the results). Local hybrids with range-separated correlation functionals (LRSR1, LRSR2, LRSR3) show improved performance compared to the simplest early local hybrids, due to their larger overall EXX admixture. Studies related to the computation of fundamental band gaps,

IPs, and EAs using the energy and derivative differences also showed similar performance for local hybrid functionals. Finally, studies on the behaviour of frontier orbital energy eigenvalues versus fractional electron numbers (satisfaction of the IP theorem) clearly show the missing discontinuity contributions (to what extent depends on the functional) and the close relationship between SIE of the functionals and the orbital eigenvalues.

Chapter 6

Evaluation of Static Correlation Error for Local Hybrid Functionals in Atoms

Assessment of local hybrid functionals for fractional spin behaviour is as relevant as the evaluation of those for fractional charges. Fractional spins can arise in the case of systems with near and absolute degeneracies, and may also be considered as ensembles of integer spin-states. The exact condition of spin constancy has been established by Wang and co-workers [20]. Deviation from this exact behaviour is know as static correlation error or fractional spin error [Sec.2.5]. Fractional spins are very crucial in the simulation of non-dynamical (also know as strong or static) correlation [112]. Within the single-determinant KS scheme, proper treatment of strong correlations remains a challenging problem [100]. For this reason, many approaches have been proposed to incorporate the non-dynamical correlation and extend the true KS-DFT beyond a single-determinant methodology [113–117]. Quite recently, Becke proposed a density functional based on his B13 model with strong-correlation correction for atoms [22, 26]. Construction of a local hybrid functional based on this model along with strong-correlation corrections has already been discussed [Sec.3.3]. In this chapter assessment of local hybrid functionals for static correlation errors along with the detailed analysis of the results obtained are carried out.

6.1 Performance of local hybrids for strong-correlation test sets

One way of testing for strong correlation performance is to consider, for a given atom, if the usual spin-polarised or free-atom (FA) configuration has the same energy as the spin-depolarised atom configuration (SDP) [26]. Difference between the computed energies of these configurations are a measure of the static correlation error [Sec.2.6]. Computations have been performed using local hybrid functionals (LSDA based ones with common *t*-LMF and range-separated correlation functional) with and without the strong-correlation correction [Sec.3.3]. Errors are also obtained using standard methods such as the HF, PBE, and B3LYP. All computations have been performed in a post-SCF (PSCF) manner using the LSDA orbitals (for the convenience of comparison with results from B13 and B13(XstrgC) models which used numerical post-LSDA) on open-shell atomic systems from hydrogen (H) to fluorine (F) [22, 26]. Errors and mean absolute errors (MAE) (in kcal/mol) are reported in Table 6.1. Intial tests have been carried out using only one strong-correlation correction term with parameters $\tilde{c}_2$ = 0.526 and d = 1.

Error values obtained for local hybrids are very close to the B13 values. Unfortunately, performance of local hybrids with the strong-correlation corrections is very poor in comparison to the B13 (XstrgC) model. In some test cases, for local hybrids with strong-correlation correction, the error values are larger in magnitude due to underestimated spin-depolarised (SDP) configuration energies (too negative). The B13 (XstrgC) model included two strong-correlation correction terms, the second and third order giving almost similar error values. Including the third order correction to local hybrids deteriorate the results further (values are not shown in tables as in many cases unphysical total energies have been obtained). In the local hybrid formalism, key ingredients for the simulation of non-dynamical correlation are the exact-exchange and the semi-local exchange energy densities [58]. The local hybrids used for Table 6.1 do not account for calibration of exchange-energy densities and thus feature ill-defined non-dynamical correlation energy terms. Therefore, in the following local hybrid functionals based on advanced exchange and correlation functionals (GGA-based local hybrids), along with calibrated exchange-energy densities have been utilised for the strong-correlation test sets as they can improve the definition of non-dynamical correlation energy [29, 118]. In the next section, detailed discussions on calibration of exchange-energy densities along with strong-correlation tests

are carried out.

Table 6.1: Errors and mean absolute errors (MAE) obtained using different local hybrid functionals for strong-correlation tests. The values for B13 and B13 (XstrgC) models are used for comparison.

	H	Li	B	C	N	O	F	MAE [a]
HF	90.6	36.3	69.0	185.6	354.4	252.1	129.6	159.7
PBE	25.7	6.7	11.5	34.1	71.9	73.4	9.7	33.3
B3LYP	33.7	9.9	21.6	60.6	121.0	41.7	32.6	45.9
B13	37.0	9.0	23.7	67.8	133.6	97.1	48.6	59.5
B13 (XstrgC)	2.4	-2.4	2.9	6.0	8.7	12.2	10.9	6.5
Lh-LSDA [b]	52.1	15.8	31.5	79.0	147.4	92.4	39.3	65.4
Lh-LSDA-SIR-SRc [c]	58.0	17.4	35.3	88.1	163.3	119.2	45.7	75.4
Lh-LSDA (XstrgC) [d]	101.7	-1.9	53.9	-5.9	-19.1	-9.5	-21.5	30.5
Lh-LSDA-SIR-SRc (XstrgC)	40.7	14.1	40.9	151.2	91.1	-436.1	-187.6	137.4

[a] Values in kcal/mol

[b] Lh-LSDA: Eq.2.17 with common *t*-LMF and $b = 0.534$

[c] Lh-LSDA-SIR-SRc: Eq.2.21 with range-separation scheme erfgau, μ = 0.8, λ = 1.0, and b = 0.713.

[d] XstrgC (strong-correlation correction): Eq.3.20 with $\tilde{c}_2$ = 0.526 and d = 1

6.2 Calibration of exchange-energy densities

The exchange-energy densities are not uniquely defined in DFT. Any non-vanishing function which integrates to zero can alter the exchange-energy density while keeping the integrated energy constant. In the case of local hybrid functionals, this is not the case due to the local mixing function (LMF) which contributes to the integrated energy [29, 119]. The properties of the calibration function have been extensively studied along with their effect on the energy functional [40, 120]. Calibration functions containing only semi-local quantities may be obtained as divergence of a field, given by equation

$$\mathbf{G}_\sigma = \nabla.\mathbf{F}_\sigma, \tag{6.1}$$

where the expression for field F_σ is given by,

$$\mathbf{F}_\sigma = f(s_\sigma)\rho_\sigma^{-1/3}\nabla\rho_\sigma. \tag{6.2}$$

In the above expression the quantity s_σ is the dimensionless density gradient (Eq.2.25) and $f(s_\sigma)$, an appropriate damping function. The explicit form of the calibration function is expressed as

$$\mathbf{G}_\sigma = \rho_\sigma^{-1/3}\{f^{'}(s_\sigma)s_\sigma[\frac{\nabla\rho_\sigma.\nabla|\nabla\rho_\sigma|}{|\nabla\rho_\sigma|} - \frac{4}{3}\frac{|\nabla\rho_\sigma|^2}{\rho_\sigma}] + f(s_\sigma)[\nabla^2\rho_\sigma - \frac{1}{3}\frac{\nabla|\nabla\rho_\sigma|^2}{\rho_\sigma}]\}. \tag{6.3}$$

The calibration function with an appropriate damping function $f(s_\sigma)$, and its derivative are expressed as

$$f(s_\sigma) = {s_\sigma}^p \exp(-\eta s_\sigma^2), \tag{6.4}$$

$$f^{'}(s_\sigma) = f(s_\sigma)(\frac{p}{s_\sigma} - 2\eta s_\sigma), \tag{6.5}$$

where p is the power factor and η is the Gaussian decay exponent. The formulation of a GGA-based local hybrid with calibration function (CF) and common *t*-LMF

$$\begin{aligned} E_{XC}^{lh-GGA-cG} = \sum_{\sigma=\alpha,\beta}\int \left[\varepsilon_{X,\sigma}^{exx}(\mathbf{r}) + (1-a(\mathbf{r}))(\varepsilon_{X,\sigma}^{DFT}(\mathbf{r}) - \varepsilon_{X,\sigma}^{exx}(\mathbf{r}) + a_X\Delta\varepsilon_{X,\sigma}^{GGAx} + cG_\sigma(\mathbf{r}))\right]\mathrm{d}\mathbf{r} \\ + E_C^{LSDA} + a_C\Delta E_C^{GGAc}, \end{aligned} \tag{6.6}$$

where the quantities $\Delta\varepsilon_{X,\sigma}^{GGAx}$ and ΔE_C^{GGAc} are gradient corrections to exchange and correlation, respectively, with coefficients a_X and a_C [29, 118, 119]. Based on the above framework for local hybrids with GGA functionals and calibrated exchange-energy densities, three different functionals have been considered for testing. They are outlined as

1. Lh-LSDA-cG: Local hybrid with LSDA exchange and correlation along with calibration function (Eq.6.7 with LMF parameter value b = 0.534, a_X = 0, a_C = 0, η = 0.096, and c-parameter = -0.00493).

2. Lh-PBE-cG: Local hybrid with PBE exchange and correlation along with calibration function (Eq.6.7 with LMF parameter value b = 0.455, a_X = 1.0, a_C = 1.0, η = 0.12, and c-parameter = -0.00364).

3. Lh-BLYP-cG: Local hybrid with Becke (B88) exchange and Lee-Yang-Parr (LYP) correlation along with calibration function (Eq.6.7 with LMF parameter value b = 0.404, a_X= 0.9, a_C = 0.81, η = 0.096, and c-parameter = -0.00630).

Results obtained using calibrated local hybrids are reported in Table 6.2 (error values in kcal/mol). Reduction in the static correlation error for these functionals can be expected due to the better description of non-dynamical correlation energies by the calibrated exchange-energy densities [29, 118]. Even then the error values for different calibrated local hybrids with strong-correlation correction are enormous in comparison to the B13 (XstrgC) model [22, 26]. The main reason for these large errors could be due to the spurious positive non-dynamical correlation (NDC) energy for atoms [121, 122]. For identifying the problems related to strong-correlation correction, detailed studies on the real-space grid quantities such as the non-dynamical and total correlation energy densities, strong-correlation parameter $\tilde{x}(r)$, and the integrated non-dynamical correlation (NDC) energies, are carried out on the test atoms.

	H	Li	B	C	N	O	F	MAE
B13	37.0	9.0	23.7	67.8	133.8	97.1	48.6	59.5
B13 (XstrgC)	2.4	-2.4	2.9	6.0	8.7	12.2	10.9	6.5
Lh-LSDA-cG	52.1	17.0	34.5	85.4	158.3	100.3	43.8	70.2
Lh-LSDA-cG (XstrgC)	101.7	-14.1	40.9	151.1	191.6	363.2	334.2	190.2
Lh-PBE-cG	52.4	7.4	32.2	79.4	147.6	70.5	41.7	61.6
Lh-PBE-cG (XstrgC)	59.1	-12.7	24.8	57.9	110.5	173.9	138.7	78.9
Lh-BLYP-cG	32.6	-5.6	32.6	79.7	145.9	93.9	41.1	60.1
Lh-BLYP-cG (XstrgC)	46.4	11.7	36.7	61.3	183.5	122.6	190.2	93.2

Table 6.2: Errors and mean absolute errors (MAE) obtained using advanced local hybrid functionals (GGA-based) with calibrated exchange-energy densities for strong-correlation tests. All the values are in kcal/mol.

6.3 Studies related to the non-dynamical correlation (NDC) energies of test-atoms

For understanding the shortcomings related to the local hybrids with strong-correlation correction, the integrated NDC energy contributions to the total energy for each test atom (both FA and SDP cases) have been computed using advanced functionals with and without calibrated exchange-energy densities. The results are shown in Tables 6.3 and 6.4. In case of free-atom (FA) configurations, the integrated NDC energy contributions are mostly positive for local hybrids with or without calibration function (except for oxygen and fluorine atoms: Lh-PBE-cG functional shows negative values). The values obtained for functionals with calibration are always lower than the one including the calibration function. For spin-depolarised (SDP) configurations, integrated NDC energy contributions are negative in all the test-atoms cases for Lh-PBE, Lh-PBE-cG, Lh-BLYP, and Lh-BLYP-cG functionals (Lh-LSDA and Lh-LSDA-cG show all positive values). The values become more negative in those cases where the calibration function has been included. These studies clearly indicate that the inclusion of calibration function for exchange-energy densities reduces significantly the positive non-dynamical correlation energy contributions.

Notably, however, the spurious positive NDC energies for LSDA-based local hybrids are so large that calibration cannot correct for this very much. This is due to the generally

underestimated exchange energies at LSDA level.

Functional	H		Li		B		C	
	FA	SDP	FA	SDP	FA	SDP	FA	SDP
Lh-LSDA	12.28	-15.12	71.86	57.60	155.06	121.27	200.26	103.59
Lh-LSDA-cG	12.28	-15.12	68.55	53.89	143.87	108.66	185.51	85.74
Lh-PBE	1.77	-30.81	6.94	-9.88	13.13	-25.15	13.38	-90.36
Lh-PBE-cG	1.77	-30.81	5.17	-11.33	8.62	-30.44	5.55	-99.07
Lh-BLYP	2.12	-33.67	9.54	-7.46	19.40	-17.57	23.39	-84.07
Lh-BLYP-cG	2.12	-33.67	5.93	-13.15	4.50	-32.25	9.38	-93.73

Table 6.3: Integrated NDC energy contributions to the total energy (in kcal/mol) for first-row atoms: both free-atom (FA) and spin-depolarised (SDP) cases.

Functional	N		O		F	
	FA	SDP	FA	SDP	FA	SDP
Lh-LSDA	247.87	59.54	296.25	145.55	343.47	255.82
Lh-LSDA-cG	229.60	35.18	275.23	118.12	316.46	225.64
Lh-PBE	16.21	-186.26	8.85	-150.08	6.72	-89.66
Lh-PBE-cG	6.14	-198.61	-2.06	-165.03	-15.86	-107.63
Lh-BLYP	27.96	-180.27	22.71	-140.21	17.84	-75.52
Lh-BLYP-cG	13.48	-204.58	8.88	-162.53	3.69	-93.54

Table 6.4: Integrated NDC energy contributions to the total energy in (kcal/mol) for first-row atoms: both free-atom (FA) and spin-depolarised (SDP) cases.

The main reason for the shortcomings of the local hybrids with strong-correlation correction is not the positive value of integrated NDC energies itself, but rather the positive NDC energy densities in certain regions of space. The dimensionless strong-correlation parameter $\tilde{x}(r)$, being ratio of NDC energy-density to the sum of the NDC and dynamical correlation energy-densities, must interpolate smoothly between weakly-correlated to strongly-correlated cases (i.e. values from 0 to 1 in certain regions of space) [22, 26]. Divergences occur in the strong-correlation parameter ($\tilde{x}(r)$ does not smoothly interpolate between 0 to 1) in regions of space where the value of total correlation energy-density is close to 0 (sum of the NDC and dynamical correlation energy-densities). This behaviour is clearly visible in the plots (Figure 6.1) for the strong-correlation parameter $\tilde{x}(r)$ value along the grid points studied for the carbon atom (both FA and SDP configurations).

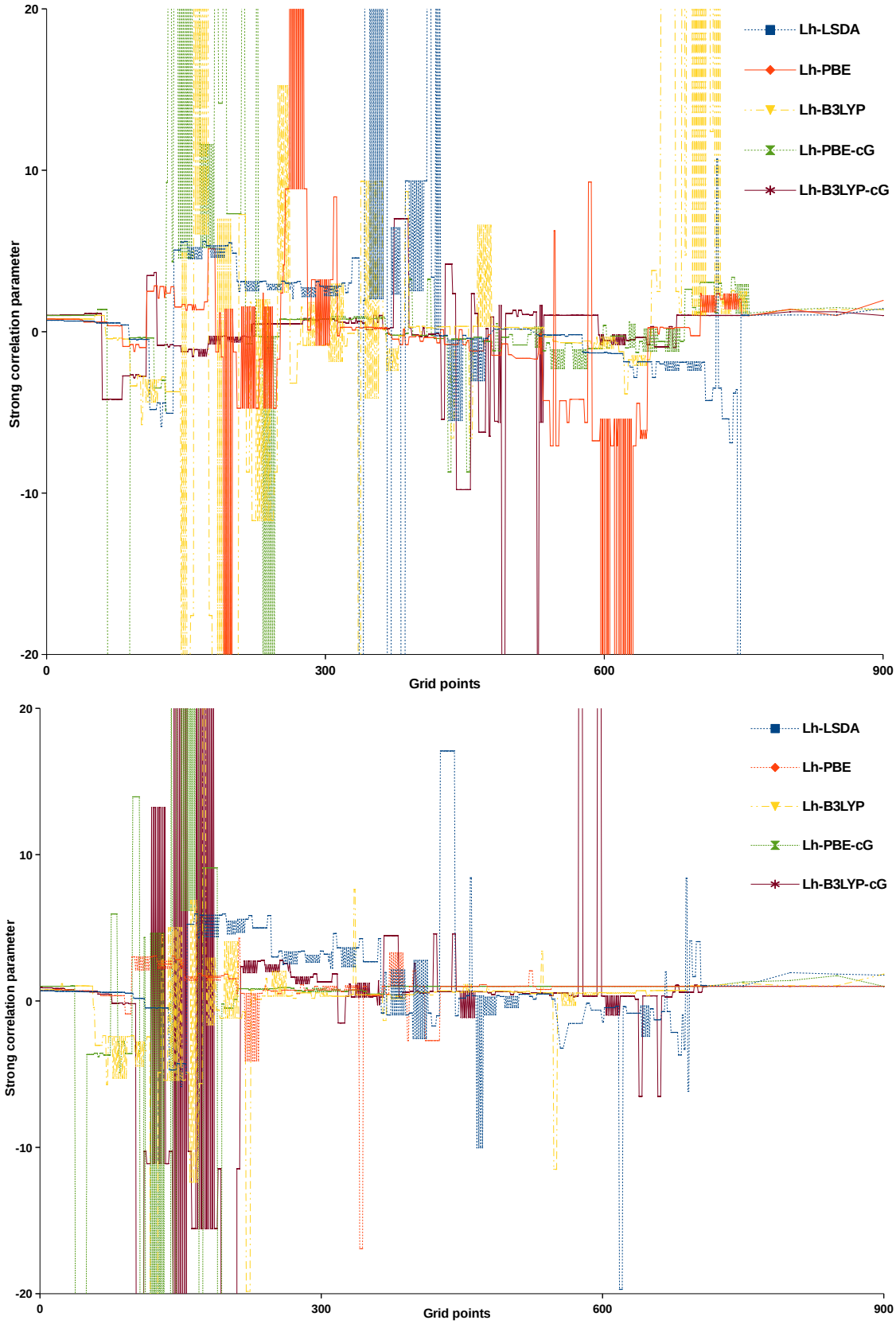

Figure 6.1: Strong-correlation parameter $\tilde{x}(r)$ value along the grid points for the carbon atom.

6.4 Conclusions

The values obtained for static correlation errors using local hybrids (LSDA based ones) along with strong-correlation correction (only to second order) are not satisfactory in comparison to that of the B13 (XstrgC) model. Advanced local hybrids (GGA-based) with calibrated exchange-energy densities along with strong-correlation correction have also been tested as they provide an improved definition for the non-dynamical correlation energy. Even with these calibrated local hybrid functionals the desired results have not been obtained. For a deeper understanding of problems related to the strong-correlation correction model, integrated NDC energy contributions to the total energy for test-atoms have been analysed. Further investigation into the real-space quantities such as the total correlation energy densities, and strong-correlation parameter $\tilde{x}(r)$, reveal the divergences (strong-correlation parameter $\tilde{x}(r)$ not being bound within 0 to 1) in the model due to spurious positive NDC energy densities. The positive sign of NDC energy density is a fundamental problem which requires more precise methodology and deeper understanding for the simulation of non-dynamic/static correlation in KS-DFT. Therefore the construction of a strong-correlation parameter $\tilde{x}(r)$ which interpolates smoothly from uncorrelated to strongly correlated i.e with values in the range [0, 1] in real space, is highly necessary for the development of strongly-correlated local hybrid functionals based on the ideas of the B13(XstrgC) model.

Chapter 7

Summary and Outlook

The main scope of this work has been the assessment of local hybrid functionals for fundamental properties of the exact functional. The stepwise linearity of the energy for ground and low-lying excited states, the IP theorem, and the spin-constancy conditions have been assessed using different local hybrid functionals. Key understandings have been obtained regarding the failures of local hybrid functionals upon assessment for the above properties.

The fractional-charge behaviour of different local hybrid functionals (including local hybrids with range-separated correlation functionals along with common t-LMF) have been evaluated for the assessement of self-interaction errors (both one- and many- electron SIE). The Kümmel-LMF (denoted as z-LMF) along with one-electron self-interaction elimination in the correlation part (implemented in a post-SCF manner) also been assessed for the stepwise-linearity behaviour. Closer investigation of the results clearly indicate that the local hybrids with 100 exact-exchange admixture (EXX) (t-LMF(1.0)) show minimum deviation from the stepwise-linearity. Detailed studies on the results obtained for IPs, EAs, and the band gap values using the energy and their derivatives differences reiterated similar trends to that of fractional charge behaviour. Assessment of the IP theorem clearly shows that the local hybrid functionals possess the desired derivative discontinuity but lack the required amount of correlation contribution, thereby resulting in errors.

Fractional spins play a very crucial role in understanding the static correlation error. Based on the ideas of Becke's B13 (XstrgC) strong-correlation model, translated into the local hybrid framework, local hybrids with strong-correlation correction have been implemented in a post-SCF manner. Evaluation of static correlation errors for local

hybrid functionals have been carried out using strong-correlation test sets. Local hybrids (LSDA based with common *t*-LMF and range-separated correlation functionals) gave error values very similar to that of global hybrids (B3LYP). Upon inclusion of strong-correlation correction (only to second order), obtained results did not show any significant improvement and even deteriorated in many cases. Even GGA-based local hybrids with calibrated exchange-energy densities along with strong-correlation correction also did not provide the desired results. The main reason for the failures are positive static correlation energy densities leading to divergences in the strong-correlation model ($\tilde{x}(r)$ parameter being ratio of static correlation to the total correlation energy-densities is not within [0,1] range). This points towards future improvements of local hybrids needed as basis for strong-correlation models.

Computation of *s*-*d* transfer energies for 3*d*-metal atoms using different local hybrid functionals gave good estimates of the self-interaction errors and problems with an inaccurate description of non-dynamical correlation. Within the Furche-Perdew (FP) formalism, local hybrids with range-separated correlation functionals (along with common *t*-LMF) produced results which are comparable to those of the B3LYP. Major discrepancies arose in case of atoms such as Ti, V, and Co, due to the failure of formalism to predict the correct order of the states which are multi-determinantal in character. Broken-symmetry approaches namely, the weighted average broken symmetry (WABS) and the re-interpreted broken symmetry (RBS) approaches have been used for the cases involving inherently multi-determinantal (IMD) states in the Cr, Fe, Co, and Ni atoms. For the IMD excitations, results obtained using the WABS and the RBS approaches for local hybrids were found to be very similar. Local hybrids with range-separated correlation functionals showed better performance than B3LYP for some excitations involving IMD states.

Development of XC funtionals satisfying the exact conditions is highly desirable for the simulation of systems of interest in chemistry and condensed-matter physics. Fallacies of DFT methodology in regard to the strongly correlated systems, Mott insulators, and band gaps in general, are related to the violation of exact functional properties by the density functionals. Fulfilment of stepwise-linearity of total energy (related to many-electron self-interaction error) without any explicit corrections to the local hybrid functionals is highly appealing (ensuring that the developed local hybrids do exhibit the desired derivative discontinuity). This would in turn be very beneficial, as such local hybrids can retain the previous advantages and also have better applicability for wider range of properties. It

is expected that improved local mixing functions including suitable ingredients, as well as the proper calibration of the employed exchange-energy densities, will provide the necessary improvements. Satisfaction of the IP theorem is also an important condition which dictate the performance of XC functional for several electronic properties. While a number of local hybrids have now been tested for exact conditions and *s*-*d* transfer energies of 3*d*-metal atoms, such tests should also be performed for the coming generations of functionals, in particular when suitable, advanced calibration functions are used, e.g. the most recent ones based on successive partial integration steps. Finally, the successful construction of strongly-correlated local hybrid functionals will be of great importance for solving the static correlation (strong correlation) problem in DFT.

Bibliography

[1] W. Kohn, Rev. Mod. Phys. **71**, 1253 (1999).

[2] P. Hohenberg and W. Kohn, Phys. Rev. **136**, B864 (1964).

[3] R. G. Parr and W. Yang, *Density-Functional Theory of Atoms and Molecules* (Oxford Science Publications, 1989).

[4] J. P. Perdew, K. Burke, and M. Ernzerhof, Phys. Rev. Lett. **77**, 3865 (1996).

[5] J. P. Perdew, Phys. Rev. Lett. **55**, 1665 (1985).

[6] D. C. Langreth and M. Mehl, Phys. Rev. B **28**, 1809 (1983).

[7] A. D. Becke, J. Chem. Phys. **98**, 5648 (1993).

[8] A. D. Becke, J. Chem. Phys. **98**, 1372 (1993).

[9] J. P. Perdew, J. A. Chevary, S. H. Vosko, K. A. Jackson, M. R. Pederson, D. J. Singh, and C. Fiolhais, Phys. Rev. B **46**, 6671 (1992).

[10] O. A. Vydrov and G. E. Scuseria, J. Chem. Phys. **121**, 8187 (2004).

[11] L. A. Curtiss, K. Raghavachari, P. C. Redfern, and J. A. Pople, J. Chem. Phys. **106**, 1063 (1997).

[12] Y. Zhang and W. Yang, J. Chem. Phys. **109**, 2604 (1998).

[13] J. Jaramillo, G. E. Scuseria, and M. Ernzerhof, J. Chem. Phys. **118**, 1068 (2003).

[14] M. Kaupp, H. Bahmann, and A. V. Arbuznikov, J. Chem. Phys. **127**, 194102 (2007).

[15] A. V. Arbuznikov, H. Bahmann, and M. Kaupp, J. Phys. Chem.. A **113**, 11898 (2009).

[16] T. M. Maier, H. Bahmann, and M. Kaupp, J. Chem. Theory Comput. **11**, 4226 (2015).

[17] J. P. Perdew, R. G. Parr, M. Levy, and J. L. Balduz Jr, Phys. Rev. Lett. **49**, 1691 (1982).

[18] R. K. Nesbet, Phys. Rev. A **56**, 2665 (1997).

[19] Y. Zhang and W. Yang, in *Theoretical Chemistry Accounts* (Springer, 2000) pp. 346–348.

[20] A. J. Cohen, P. Mori-Sánchez, and W. Yang, J. Chem. Phys. **129**, 121104 (2008).

[21] J. P. Perdew and K. Schmidt, in *AIP Conference Proceedings* (Institute of Physics Publishing LTD, 2001) pp. 1–20.

[22] A. D. Becke, J. Chem. Phys. **138**, 074109 (2013).

[23] F. Furche and J. P. Perdew, J. Chem. Phys. **124**, 044103 (2006).

[24] S. Luo, B. Averkiev, K. R. Yang, X. Xu, and D. G. Truhlar, J. Chem. Theory Comput. **10**, 102 (2013).

[25] T. Schmidt, E. Kraisler, A. Makmal, L. Kronik, and S. Kümmel, J. Chem. Phys. **140**, 18A510 (2014).

[26] A. D. Becke, J. Chem. Phys. **138**, 161101 (2013).

[27] E. J. Baerends, O. V. Gritsenko, and R. Van Meer, Phys. Chem. Chem. Phys. **15**, 16408 (2013).

[28] T. Körzdörfer and S. Kümmel, Phys. Rev. B **82**, 155206 (2010).

[29] A. V. Arbuznikov and M. Kaupp, J. Chem. Phys. **141**, 204101 (2014).

[30] E. Schrödinger, Phys. Rev. **28**, 1049 (1926).

[31] M. Born and R. J. Oppenheimer, Ann. Physik **389**, 457 (1927).

[32] P.-O. Löwdin, Phys. Rev. **97**, 1474 (1955).

[33] N. S. Ostlund and A. Szabo, *Modern Quantum Chemistry: Introduction to Advanced Electronic Structure Theory* (Dover Publications, 1996).

[34] C. J. Cramer, *Essentials of Computational Chemistry: Theories and Models* (John Wiley & Sons, 2013).

[35] T. Helgaker, P. Jorgensen, and J. Olsen, *Molecular Electronic Structure Theory* (John Wiley & Sons, 2000).

[36] P. W. Atkins and R. S. Friedman, *Molecular Quantum Mechanics* (Oxford University Press, 2011).

[37] I. N. Levine, *Quantum Chemistry*, Vol. 6 (Pearson Prentice Hall, Upper Saddle River, New Jersey, 2009).

[38] W. Kohn and L. J. Sham, Phys. Rev. **140**, A1133 (1965).

[39] M. Levy and J. P. Perdew, Phys. Rev. A **32**, 2010 (1985).

[40] J. P. Perdew, V. N. Staroverov, J. Tao, and G. E. Scuseria, Phys. Rev. A **78**, 052513 (2008).

[41] P. A. M. Dirac, in *Mathematical Proceedings of the Cambridge Philosophical Society*, Vol. 26 (Cambridge University Press, 1930) pp. 376–385.

[42] D. M. Ceperley and B. Alder, Phys. Rev. Lett. **45**, 566 (1980).

[43] S. H. Vosko, L. Wilk, and M. Nusair, Can. J. Phys. **58**, 1200 (1980).

[44] J. P. Perdew and Y. Wang, Phys. Rev. B **46**, 12947 (1992).

[45] A. D. Becke, Phys. Rev. A **38**, 3098 (1988).

[46] J. P. Perdew and A. Zunger, Phys. Rev. B **23**, 5048 (1981).

[47] T. Tsuneda and K. Hirao, J. Chem. Phys. **140**, 18A513 (2014).

[48] T. Leininger, H. Stoll, H.-J. Werner, and A. Savin, Chem. Phys. Lett. **275**, 151 (1997).

[49] J. Toulouse, A. Savin, and H.-J. Flad, Int. J. Quantum Chem. **100**, 1047 (2004).

[50] O. A. Vydrov and G. E. Scuseria, J. Chem. Phys. **125**, 234109 (2006).

[51] I. C. Gerber and J. G. Angyán, Chem. Phys. Lett. **415**, 100 (2005).

[52] J. Heyd and G. E. Scuseria, J. Chem. Phys. **121**, 1187 (2004).

[53] A. V. Krukau, G. E. Scuseria, J. P. Perdew, and A. Savin, J. Chem. Phys. **129**, 124103 (2008).

[54] J. Heyd, G. E. Scuseria, and M. Ernzerhof, J. Chem. Phys. **118**, 8207 (2003).

[55] J. C. Slater, Phys. Rev. **81**, 385 (1951).

[56] A. V. Arbuznikov, M. Kaupp, and H. Bahmann, J. Chem. Phys. **124**, 204102 (2006).

[57] A. V. Arbuznikov and M. Kaupp, Chem. Phys. Lett. **440**, 160 (2007).

[58] A. V. Arbuznikov and M. Kaupp, J. Chem. Phys. **136**, 014111 (2012).

[59] A. V. Arbuznikov and M. Kaupp, J. Chem. Phys. **128**, 214107 (2008).

[60] M. Kaupp, A. Arbuznikov, and H. Bahmann, Zeitschrift für Physikalische Chemie **224**, 545 (2010).

[61] H. Bahmann, A. Rodenberg, A. V. Arbuznikov, and M. Kaupp, J. Chem. Phys. **126**, 011103 (2007).

[62] K. Theilacker, A. V. Arbuznikov, H. Bahmann, and M. Kaupp, J. Phys. Chem. A **115**, 8990 (2011).

[63] A. D. Becke, J. Chem. Phys. **122**, 064101 (2005).

[64] J. P. Perdew and Y. Wang, Phys. Rev. B **45**, 13244 (1992).

[65] D. N. Mermin, Phys. Rev. **137**, A1441 (1965).

[66] P. Mori-Sánchez, A. J. Cohen, and W. Yang, Phys. Rev. Lett. **100**, 146401 (2008).

[67] E. R. Johnson, W. Yang, and E. R. Davidson, J. Chem. Phys. **133**, 164107 (2010).

[68] W. Yang, A. J. Cohen, and P. Mori-Sánchez, J. Chem. Phys. **136**, 204111 (2012).

[69] J. P. Perdew and M. Levy, Phys. Rev. Lett. **51**, 1884 (1983).

[70] A. Seidl, A. Görling, P. Vogl, J. Majewski, and M. Levy, Phys. Rev. B **53**, 3764 (1996).

[71] I. Dabo, A. Ferretti, N. Poilvert, Y. Li, N. Marzari, and M. Cococcioni, Phys. Rev. B **82**, 115121 (2010).

[72] A. J. Cohen, P. Mori-Sánchez, and W. Yang, J. Chem. Phys. **126**, 191109 (2007).

[73] K. Burke, J. Chem. Phys. **136**, 150901 (2012).

[74] T. Tsuneda, J.-W. Song, S. Suzuki, and K. Hirao, J. Chem. Phys. **133**, 174101 (2010).

[75] W. Yang, Y. Zhang, and P. W. Ayers, Phys. Rev. Lett. **84**, 5172 (2000).

[76] J. F. Janak, Phys. Rev. B **18**, 7165 (1978).

[77] E. R. Johnson, R. M. Dickson, and A. D. Becke, J. Chem. Phys. **126**, 184104 (2007).

[78] C. W. Bauschlicher Jr, S. P. Walch, and H. Partridge, J. Chem. Phys. **76**, 1033 (1982).

[79] J. G. Harrison, J. Chem. Phys. **79**, 2265 (1983).

[80] K. Raghavachari and G. W. Trucks, J. Chem. Phys. **91**, 1062 (1989).

[81] N. B. Balabanov and K. A. Peterson, J. Chem. Phys. **125**, 074110 (2006).

[82] F. W. Kutzler and G. S. Painter, Phys. Rev. B **43**, 6865 (1991).

[83] J. Harris and R. Jones, J. Chem. Phys. **70**, 830 (1979).

[84] S. Yanagisawa, T. Tsuneda, and K. Hirao, J. Chem. Phys. **112**, 545 (2000).

[85] D. Rinaldo, L. Tian, J. N. Harvey, and R. A. Friesner, J. Chem. Phys. **129**, 164108 (2008).

[86] C. W. Bauschlicher Jr, J. Chem. Phys. **86**, 5591 (1987).

[87] T. V. Russo, R. L. Martin, and P. J. Hay, J. Chem. Phys. **101**, 7729 (1994).

[88] M. Nishino, S. Yamanaka, Y. Yoshioka, and K. Yamaguchi, J. Phys. Chem. A **101**, 705 (1997).

[89] R. L. Martin, Chem. Phys. Lett. **75**, 290 (1980).

[90] F. Weigend, Phys. Chem. Chem. Phys. **4**, 4285 (2002).

[91] "TURBOMOLE V5.10 2008, a development of University of Karlsruhe and Forschungszentrum Karlsruhe GmbH, 1989-2007, TURBOMOLE GmbH, since 2007; available from
`http://www.turbomole.com`.".

[92] T. Schmidt, E. Kraisler, L. Kronik, and S. Kümmel, Phys. Chem. Chem. Phys. **16**, 14357 (2014).

[93] H. Bahmann, *Implementation, Development and Assessment of Local Hybrid Density Functionals*, Ph.D. thesis, Julius-Maximilians-Universität Würzburg (2010).

[94] E. R. Johnson and A. D. Becke, Can. J. Chem. **87**, 1369 (2009).

[95] Y. Zhao and D. G. Truhlar, J. Chem. Phys. **124**, 224105 (2006).

[96] N. B. Balabanov and K. A. Peterson, J. Chem. Phys. **123**, 064107 (2005).

[97] A. Ruzsinszky, J. P. Perdew, G. I. Csonka, O. A. Vydrov, and G. E. Scuseria, J. Chem. Phys. **126**, 104102 (2007).

[98] O. A. Vydrov, G. E. Scuseria, and J. P. Perdew, J. Chem. Phys. **126**, 154109 (2007).

[99] T. Schmidt and S. Kümmel, Phys. Rev. B **93**, 165120 (2016).

[100] A. J. Cohen, P. Mori-Sánchez, and W. Yang, Chemical Reviews **112**, 289 (2011).

[101] Y. Zhang and W. Yang, Theor. Chem. Acc. **103**, 346 (2000).

[102] R. Haunschild, T. M. Henderson, C. A. Jiménez-Hoyos, and G. E. Scuseria, J. Chem. Phys. **133**, 134116 (2010).

[103] N. Q. Su, W. Yang, P. Mori-Sanchez, and X. Xu, J. Phys. Chem. A **118**, 9201 (2014).

[104] R. Ahlrichs, M. Bär, M. Häser, H. Horn, and C. Kölmel, Chem. Phys. Lett. **162**, 165 (1989).

[105] J. R. Flores and R. J. Gdanitz, J. Chem. Phys. **123**, 144316 (2005).

[106] P. De Silva and C. Corminboeuf, J. Chem. Phys. **142**, 074112 (2015).

[107] W. Yang, P. Mori-Sánchez, and A. J. Cohen, J. Chem. Phys. **139**, 104114 (2013).

[108] T. Koopmans, Physica **1**, 104 (1934).

[109] R. Armiento and S. Kümmel, Phys. Rev. Lett. **111**, 036402 (2013).

[110] C.-W. Tsai, Y.-C. Su, J.-D. Chai, and G.-D. Li, Phys. Chem. Chem. Phys. **15**, 8352 (2013).

[111] O. A. Vydrov and G. E. Scuseria, J. Chem. Phys. **122**, 184107 (2005).

[112] P. Mori-Sánchez, A. J. Cohen, and W. Yang, Phys. Rev. Lett. **102**, 066403 (2009).

[113] E. R. Johnson and J. Contreras-García, J. Chem. Phys. **135**, 081103 (2011).

[114] M. Fuchs, Y.-M. Niquet, X. Gonze, and K. Burke, J. Chem. Phys. **122**, 094116 (2005).

[115] F. Malet and P. Gori-Giorgi, Phys. Rev. Lett. **109**, 246402 (2012).

[116] A. Mirtschink, M. Seidl, and P. Gori-Giorgi, J. Chem. Theory Comput. **8**, 3097 (2012).

[117] P. Gori-Giorgi and M. Seidl, Phys. Chem. Chem. Phys. **12**, 14405 (2010).

[118] K. Theilacker, A. V. Arbuznikov, and M. Kaupp, Mol. Phys. **114**, 1118 (2016).

[119] T. M. Maier, M. Haasler, A. V. Arbuznikov, and M. Kaupp, Phys. Chem. Chem. Phys. (2016).

[120] J. P. Perdew and J. Tao, J. Mol. Struct.: THEOCHEM **943**, 19 (2010).

[121] K. Burke, F. G. Cruz, and K.-C. Lam, J. Chem. Phys. **109**, 8161 (1998).

[122] J. Nafziger and A. Wasserman, J. Chem. Phys. **143**, 234105 (2015).

Acknowledgement

I am very grateful to my advisor Prof. Dr. Martin Kaupp for giving me an opportunity to work in his research group. Special thanks go to Dr. Hilke Bahmann, Dr. Alexey Arbuznikov, and all other members of Prof. Kaupp's group for the enlightening discussions. Special mentions to Heidi Grauel, Nadine Rechenberg, Numerik Server staff, and TUbit staff for there excellent assistance and support.

I am also indebted to all my friends and acquaintances with whom I had interactions in all these years.

Finally and importantly, I would like to acknowledge the DAAD foundation for providing me the PhD scholarship and aiding me in every possible way during all these years.